DEPOSITIONAL PROCESSES: THEIR INFLUENCE ON THE MINERALOGY OF THE HATTERAS ABYSSAL PLAIN SEDIMENTS

A Thesis

Presented to

the Faculty of the Department of Geology

East Carolina University

In Partial Fulfillment

of the Requirements for the Degree

Master of Science in Geology

by

Mark W. Ayers

June 1979

DEPOSITIONAL PROCESSES: THEIR INFLUENCE ON THE MINERALOGY OF THE HATTERAS ABYSSAL PLAIN SEDIMENTS

by

Mark W. Ayers

APPROVED BY:

THESIS COMMITTEE

Pei-lin Tien

Dr. Pei-lin Tien, Supervising Professor

Scott W. Snyder

Dr. Scott W. Snyder

Richard L Mauger

Dr. Richard L. Mauger

Dr. Orrin H. Pilkey

CHAIRMAN OF THE DEPARTMENT OF GEOLOGY

C J Brown

Dr. Charles Q. Brown

DEAN OF THE GRADUATE SCHOOL

Joseph G. Boyette/cre

Dr. Joseph G. Boyette

TABLE OF CONTENTS

ABSTRACT v

ACKNOWLEDGMENTS vii

INTRODUCTION 1

GEOLOGIC SETTING 5

OCEAN CIRCULATION 8

SEDIMENTATION AND STRATIGRAPHY 13

MINERALOGY OF THE WESTERN NORTH ATLANTIC 18

ANALYTICAL TECHNIQUES 23

ANALYTICAL PRECISION 30

RESULTS 36

DISCUSSION AND SUMMARY 51

APPENDIX 1 - Sample Log 69

APPENDIX 2 - Analytical Procedure 75

APPENDIX 3 - Carbonate and Organic Carbon 76

APPENDIX 4 - Mineral Composition of the <2μ Fraction of the Surficial Sediments 80

APPENDIX 5 - Composition of the Whole Surface Samples 92

APPENDIX 6 - Mineral Composition of the <2μ Fraction of Subsurface Samples 102

APPENDIX 7 - Composition of Whole Subsurface Samples 111

REFERENCES CITED 122

ILLUSTRATIONS

figure		page
1.	Physiography of the Western North Atlantic . . .	2
2.	Core Locations and major sources of Turbidity Currents	7
3.	Cold-Deep Water Circulation of the Western North Atlantic	9
4.	Warm-Shallow Water Circulation of the Western North Atlantic.	11
5A.	Morphology of a Turbidity Current	16
5B.	Bouma's Sequences for Turbidite Deposition . . .	16
6.	Transportation of Clay Minerals on the Shelf . .	20
7.	Interpretation of the X-ray Diffraction Patterns	26
8.	Coarse Fraction Analysis	31
9.	Linear Correlation of Peak Intensity and Weight Percentage of the Carbonate Minerals	35
10.	Smectite Distribution off the Southeastern United States	52
11.	Illite Distribution off the Southeastern United States	53
12.	Kaolinite Distribution off the Southeastern United States	54
13.	Chlorite Distribution off the Southeastern United States	55
14.	Source Areas of Turbidites on the Hatteras Abyssal Plain	61
15A.	Flow in Turbidity Current Head	63

figure page

15B. Hypothetical Reconstruction of Turbidity Current Head 63

16. Schematic Representation of Fine Sediment Interchange 64

17. Abundance of Dolomite and Quartz in Hatteras Abyssal Plain Sediments 66

TABLES

Table page

1. Peaks Used in Whole Sample X-ray Diffraction Analysis 29

2. Precision of the Clay Mineral Analyses 33

3. Precision of the Powder Whole-Sample Analyses 34

4. Precision of the Weight Percent Organic Carbon Analyses 37

5. Average Percent Clay Minerals in $< 2\mu$ Samples 39

6. Average Percent Minerals in Whole Samples . . . 43

7. Average Carbonate and Organic Carbon in Whole Samples 45

ABSTRACT

The Hatteras Abyssal Plain, a major deep-sea basin, is located approximately 500 to 1000 km off the coast of the southeastern United States. Using X-ray diffraction techniques, twenty-six surface samples and seventy-one subsurface samples have been analyzed to determine the mineral content of the clay fraction (< 2μ) and of the whole sample. The clay mineral assemblage in the < 2 μ fractions consists of smectite, illite, kaolinite, and chlorite. Illite is always the most abundant mineral, averaging 75% (by weight); smectite averages 10%; chlorite averages 8%; and kaolinite averages 7%. The non-clay minerals, quartz and calcite, are also present in the < 2μ fraction of the samples. Mineral composition of the whole sample (as determined by X-ray diffraction of unoriented backpacked powder slides) consists of quartz, chlorite, muscovite, feldspar, calcite, dolomite, and aragonite.

Clay mineral suites of the hemipelagic and turbiditic sediment on the plain are identical. To explain the homogeneity of clay mineral assemblages, a model for the behavior of fine sediments in turbidity currents has been hypothesized. In the model, clay sized sediment is constantly being lost from the current and replaced by fine bottom sediment that is commonly incorporated through erosion. In this study, the greater abundance of silt sized

dolomite in the turbidites served as a tool for distinguishing fine-grained distal turbidites from hemipelagic sequences.

ACKNOWLEDGMENTS

I would like to express my sincere thanks to Drs. Pei-Lin Tien, Richard Mauger, and Scott Snyder of East Carolina University, and also to Dr. Orrin Pilkey of Duke University for assistance and guidance in the preparation of this thesis. I also wish to thank my wife Beth for her tireless assistance and encouragement.

This investigation was made possible by financial support provided by the East Carolina University Department of Geology and by Dr. Pilkey's National Science Foundation grant entitled "Collaborative Research on Sedimentation on the Hatteras Abyssal Plain" (#DES75-14416).

INTRODUCTION

The study area is restricted primarily to the Hatteras Abyssal Plain, a major flysch basin located from 500 to 1000 km off the coast of the southeastern United States. The Hatteras Abyssal Plain is an elongate north-south trending feature, about 900 km in length. The width varies from 150 to more than 300 km. The basin is characterized by a gentle south-sloping gradient (1:3000) and by low relief. Depths range from 5100 to 5450 m (Cleary and others, 1977). It is only one of several large abyssal plains that lie off the eastern continental margin of the United States (Figure 1).

Abyssal plains are the flattest physiographic features on earth (Bouma and Hollister, 1973). Their extremely smooth surfaces are interrupted only occasionally by abyssal hills and seamounts of volcanic origin. Seismic reflection profiles taken across abyssal plains reveal reflecting layers that are as flat and featureless as the surface.

With the exception of minor amounts of biogenic pelagic debris, the sediments of the abyssal plains are terrigenous in origin and are often deposited by density currents, such as debris flows and turbidity currents (Bouma and Hollister, 1973). Hemipelagic deposition is important in the deep-sea environment and is responsible for the slow

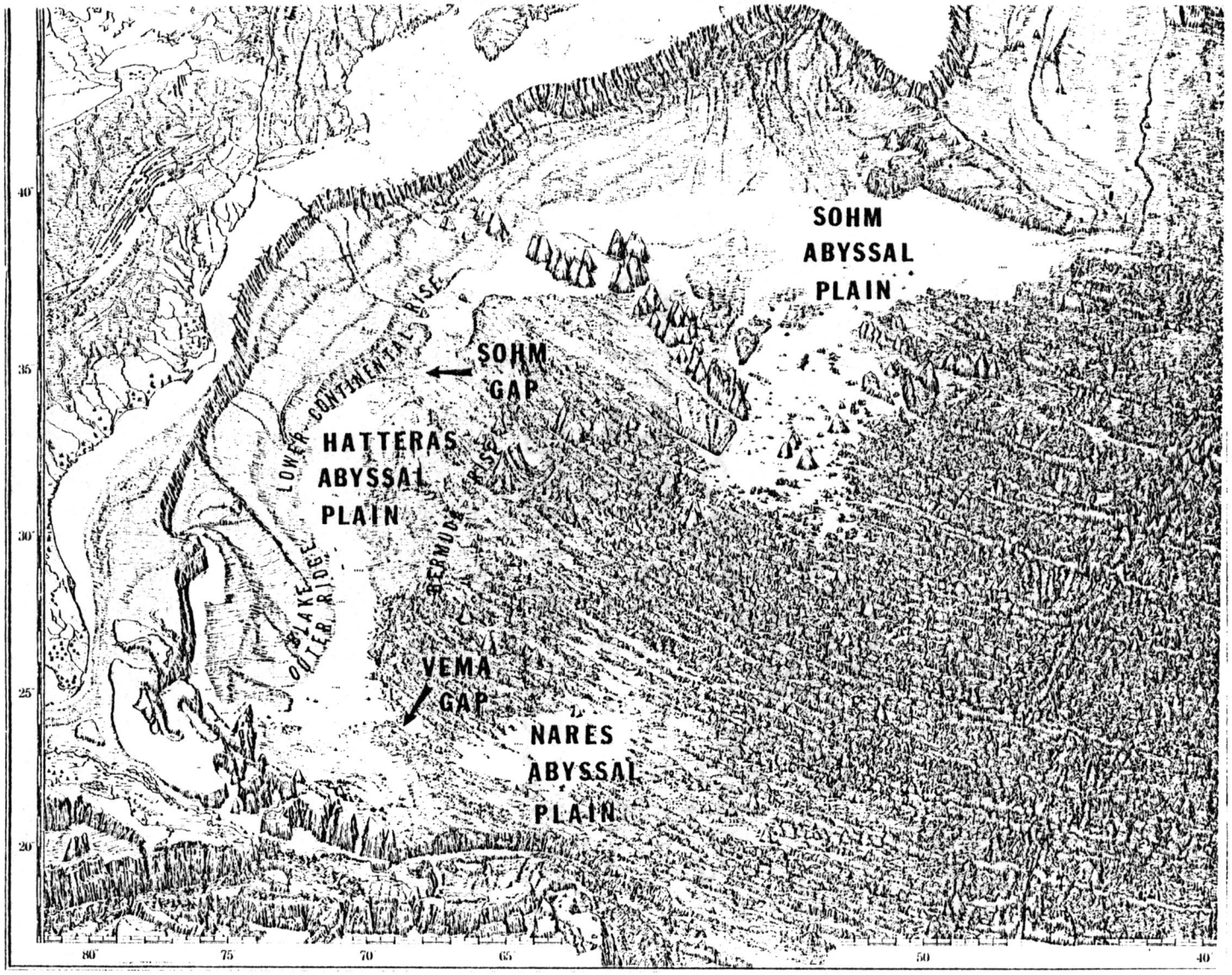

Figure 1. Physiography of the Western North Atlantic, showing the abyssal plains off the east coast of the United States (modified from Heezen and Tharp, 1968).

accumulation of silts and clays on the abyssal plains. Pelagic oozes are common in many deep-sea environments, but they are not common in the sedimentary sequences of the abyssal plains. In the abyssal plains, the normally dominant pelagic biogenic sediments are overwhelmed by the tremendous influx of terrigenous sediment.

The Hatteras Abyssal Plain has been the object of numerous studies. A detailed study of turbidite deposition on the Hatteras Abyssal Plain was first undertaken by Horn and others (1971). Recently, Cleary and others (1977) studied the three major points where turbidity currents enter the plain proper. Two of these, the Hatteras and the Wilmington Fans, have been described in detail (Cleary and Conolly, 1974a: Ayers and Cleary, in prep.). The "Black Shell Turbidite", which is believed to have been correlated over a larger area than any other turbidite, has been discovered on the Hatteras Abyssal Plain (Elmore, 1976). The provenance and composition of the deep-sea sands from the plain have been studied (Cleary and Conolly, 1974b). Trace elements in the abyssal sediments are being studied (Brown, personal communication, 1977). The sedimentary structures of the abyssal plain cores are being studied by Sparks (personal communication, 1977).

The distribution and mineralogy of sediments from the Hatteras Abyssal Plain have not been studied in detail. Samples studied previously to determine the clay mineralogy

contained mixtures of illite, smectite, chlorite, and kaolinite (Terlecky, 1966; Pevear, 1968).

The regional aspects of clay mineralogy along the continental margin of the eastern United States have been studied by Biscaye (1965), Hathaway (1972), Neileisel and Weaver (1967), Pevear (1972), Pierce (1971), Rex (1969), Terleckey (1966), Zemmels and others (1972), and Zimmerman (1972). Most of the above studies deal with the mineralogy of the clay fraction ($< 2\mu$) or the fine mud fraction ($< 20\mu$). Only the studies of Rex (1969) and Zemmels and others (1972) have described the mineralogy of the whole samples. Except for the studies by Zimmerman (1972), Pierce (1971), Rex (1969), and Zemmels and others (1972), the studies mentioned above have dealt with the areal distribution of clay minerals in the surface sediments. In my study, the mode of deposition, and the vertical and areal variations in the mineral content of the whole sample and the clay ($<2\mu$) fraction were determined in order to do the following:

1) To identify the authigenic and terrigenous minerals that occur in the Hatteras Abyssal Plain.

2) To map the areal and vertical distribution of minerals in the hemipelgaic muds.

3) To distinguish between hemipelagic sequences and fine distal turbidites, using mineral content.

4) To determine the provenance of the turbidites, using their mineral content.

GEOLOGIC SETTING

The Hatteras Abyssal Plain is situated off a tectonically stable margin. Yet, sedimentation in this basin is similar to that found in basins off tectonically more active margins. This similarity can apparently be attributed to sea level fluctuation during the Pleistocene Epoch (Cleary and others, 1977). Lowering of the sea level affected marine sedimentation in two ways. First, the sediment load in the rivers was increased by the lowering of the ultimate base level of the continental drainage system and by glacial erosion in the north. Secondly, rivers flowed to the present shelf break and consequently deposited their loads directly on the upper continental slope. The resulting rapid buildup of sediment on the steeper slope eventually led to numerous submarine avalanches which developed into turbidity currents. Turbidity currents then flowed to the basin floor and deposited their loads. In this manner, sedimentation on the Hatteras Abyssal Plain proceeded in much the same way as it would in a "flysch" basin off an active margin.

The Hatteras Abyssal Plain lies between the lower continental rise to the west and the Bermuda Rise to the east. The northernmost part of the lower continental rise, adjacent to the Hatteras Abyssal Plain, is characterized by a series of lower continental rise hills (Cleary and others,

1977). These hills are gentle sinuous features with an average relief of 50 meters (Ayers and Cleary, in preparation). The southwestern boundary of the plain is the Blake Outer Ridge, a feature with little local relief. To the east, the Bermuda Rise forms an abrupt border. The Bermuda Rise is best characterized as a group of abyssal hills of very high relief.

The Sohm and Nares Abyssal Plains are linked to the Hatteras by gaps through which a southward flow of turbidity currents has occurred (Figure 1). The Sohm Gap links the Sohm and Hatteras Abyssal Plains. This gap has a complicated physiography of high local relief, indistinct channels, closed depressions, and isolated hills (Pratt, 1965). To the south, the Vema Gap links the Nares and Hatteras Abyssal Plains. The Antilles Outer Ridge marks the southern limit of the Nares Abyssal Plain (Cleary and others, 1977).

There are three major sources of turbidity currents to the Hatteras Abyssal Plain (Cleary and others, 1977). All are in the northern half of the plain (figure 2). The Hudson Canyon terminates in the Sohm Gap area and is known to supply a large amount of material to the plain. Unfortunately, the complicated physiography in the gap makes it difficult to locate and define the exact terminus of the Hudson Canyon (Pratt, 1965). The Wilmington Canyon System crosses onto the plain via a broad fan at the base of the

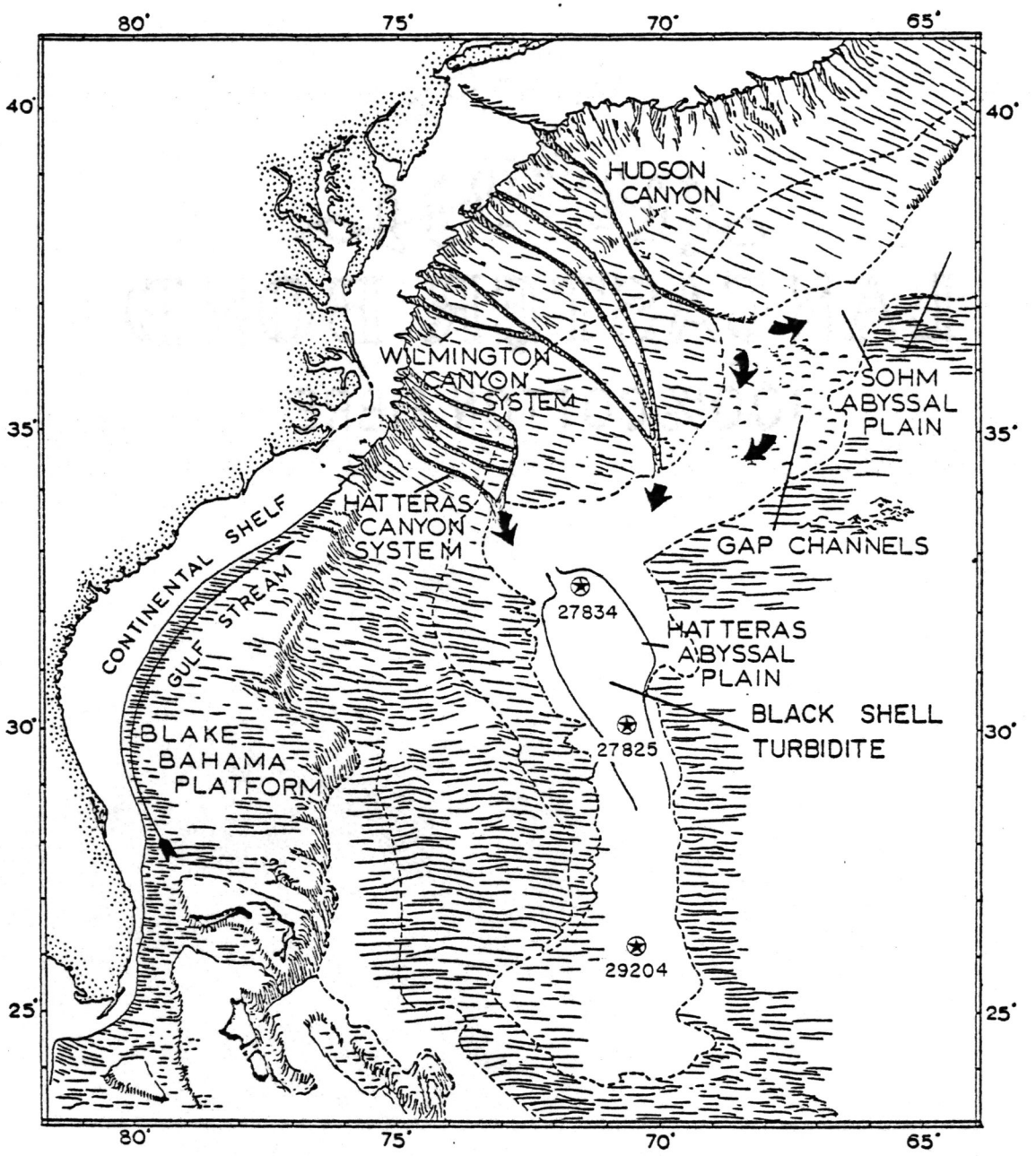

Figure 2. Core locations and major sources of turbidity currents on the Hatteras Abyssal Plain. The black arrows indicate the direction of movement of turbidity currents on the abyssal plain (modified from Cleary and others, 1977). The areal extent of the Black Shell Turbidite correlated by Elmore (1976) is outlined.

lower continental rise (Figure 2). The rise here acts as an unusual fan system. It appears that the sediments flow through the low regions (troughs) between the hills across to the plain. In this situation a typical deep-sea fan has not developed. The Hatteras Canyon System is the southernmost major source for turbidity currents. Here, the Hatteras Fan is a typical deep-sea fan with a suprafan, channels, and leeves (Cleary and Conolly, 1974a).

OCEAN CIRCULATION

Four major ocean currents greatly influence sedimentation in the western North Atlantic (Hollister, 1967). Two of them, the Gulf Stream and the Slope Water, are warm (5-25°C, 35 °/oo salinity) shallow currents (< 700m). The other two, the Antarctic and Arctic Bottom Waters, are cold (< 5°C, 34-35 °/oo salinity) deep currents. Because of the depth of the Hatteras Abyssal Plain, the cold, deep-water currents have the most direct influence on sedimentation in the study area.

The Arctic Bottom Water flows southward along the continental slope and rise off the eastern United States (Figure 3). The Arctic Bottom Water is driven by the sinking of cold dense waters at the northern polar region. Coriolis forces, created by the rotation of the earth, push the current toward the western edges of the ocean basins.

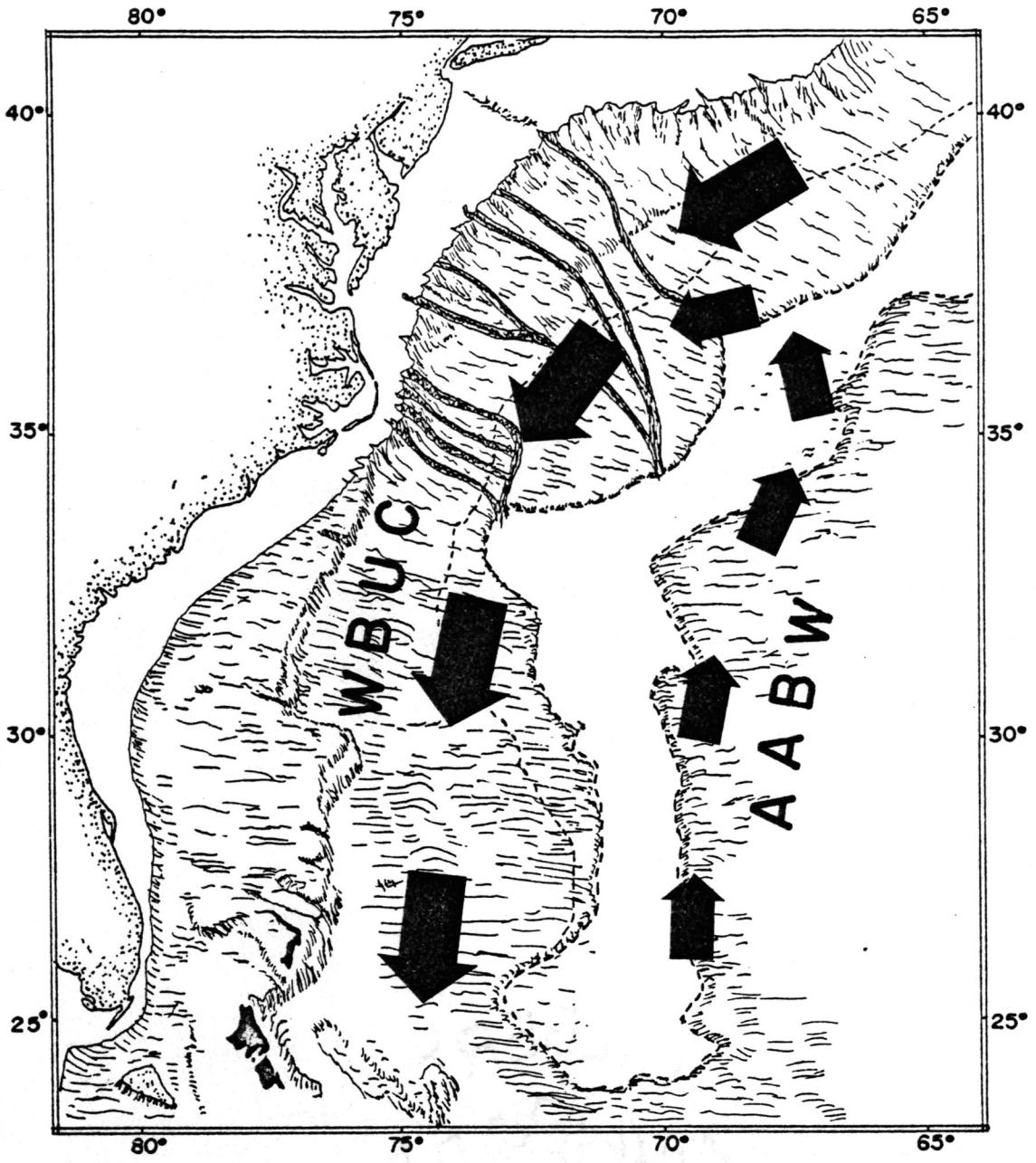

Figure 3. Circulation of the Western Boundary Undercurrent (WBUC), a part of the Arctic Bottom Water and the Antarctic Bottom Water (AABW) (modified from Heezen and Tharp, 1968).

Because such currents flow along the ocean basin margins, parallel to the regional contours, they are called contour or boundary currents. The part of the Arctic Bottom Water which acts as a contour current is known as the Western Boundary Undercurrent. It reworks bottom sediments and greatly influences sedimentation on the continental margin between the 200m and 4000m isobaths. The current reaches velocities of 18 cm/sec on the lower rise (Heezen and others, 1966).

The Antarctic Bottom Water is initiated in the southern polar region and flows north. In the western North Atlantic, this current flows along the Bermuda Rise where it attains velocities as high as 17 cm/sec. It diminishes in strength as it flows northward, and eventually turns to the west where it is incorporated into the south flowing Arctic Bottom Water (Figure 3) (Hollister, 1967).

The Gulf Stream is a northeasterly flowing current that is situated between the warmer Sargasso Sea to the east, and the colder Slope Water to the west (Figure 4). The stream flows as a narrow, high velocity current whose effects are principally confined to shallow waters (1000m) (Hollister, 1967).

The Slope Water lies between the less saline coastal waters on the shelf and waters of the Gulf Stream. The width of this current varies from 120 km off the Chesapeake Bay to over 340 km off Nova Scotia. The Slope Water flows

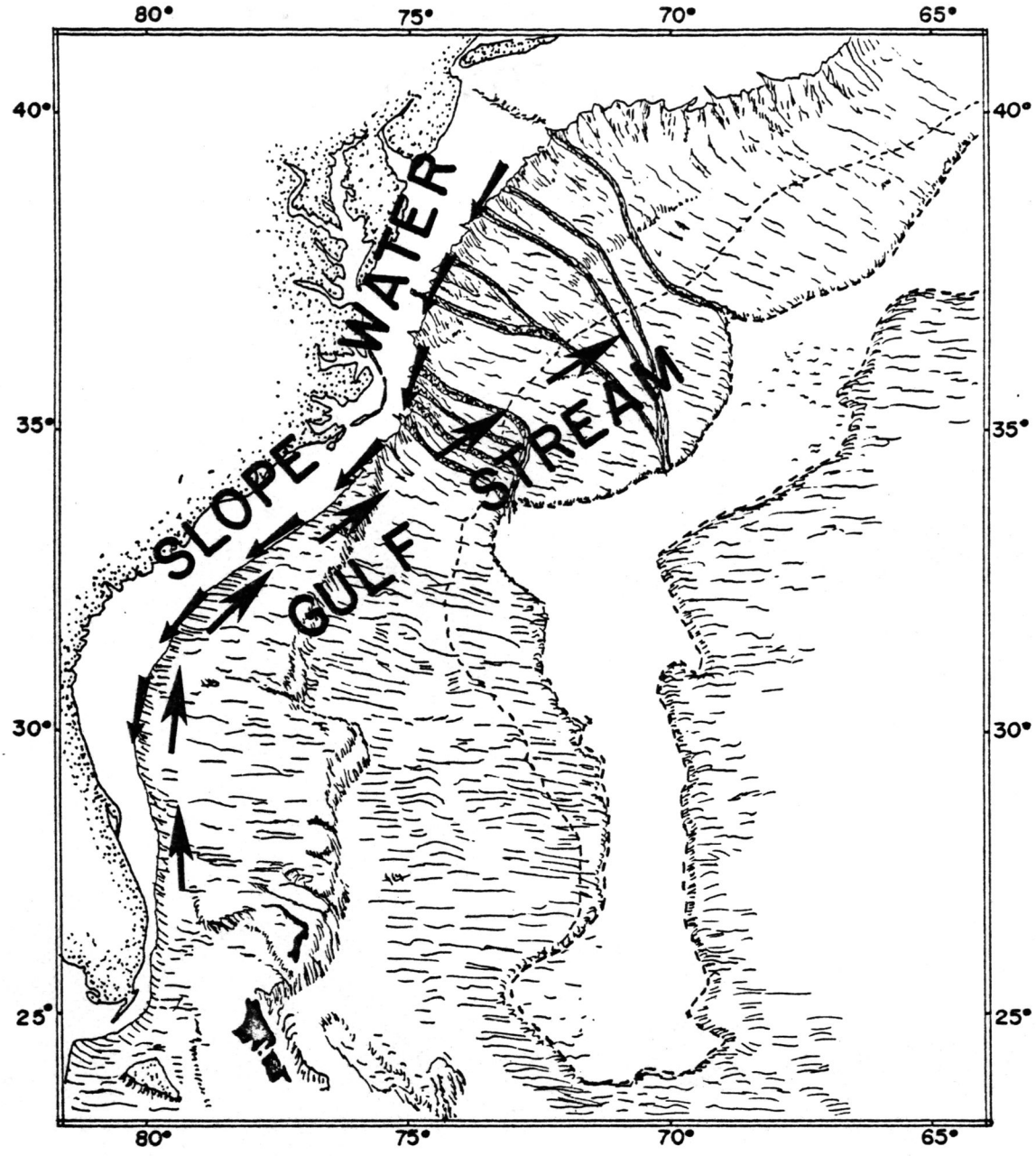

Figure 4. Circulation of the Slope Water and the Gulf Stream off the eastern United States (modified from Heezen and Tharp, 1968).

toward the southwest at depths from 1500 m to 3000 m, with near-bottom velocities of approximately 20 cm/sec (Hollister, 1967).

The geologic effects of these currents are significant. Hollister (1967) and Damuth (1977) show that the continental rise off the eastern United States is formed primarily by contour current deposits known as contourites. Rona (1969) and Heezen and others (1966) hypothesized that the lower rise hills off the eastern United States are, in reality, huge abyssal antidunes, created in response to the Western Boundary Current. Numerous features on the continental margin are directly related to the effects of the currents. The Western Boundary Undercurrent has shaped the Hatteras and Blake Outer Ridges, and the Blake Plateau has undergone extensive erosion by the Gulf Stream (Emery and Uchupi, 1972). In addition, local effects of the currents are revealed on oriented bottom photographs. These show such features as current lineations, ripple marks, the bending of sessile benthonic organisms, and scour marks.

Recently, a thick layer of water, laden with suspended sediment, has been reported off the coast of the eastern United States (Eittreim and others, 1969). Such sediment laden deep-water masses are known as nephloid layers. They have now been recognized in every major ocean. The nephloid layers contain sediment that is incorporated either by bottom erosion or by the injection of sediment from turbi-

dity currents.

Biscaye (1974) reports that the nephloid layer above the eastern Hatteras Abyssal Plain is relatively thin when compared to the one generated by the Western Boundary Undercurrent over the Blake-Bahama Outer Ridge. The nephloid layer above the Hatteras Abyssal Plain extends only 900 m above the bottom, as compared to 1500 m above the bottom over the Blake-Bahama Outer Ridge. The most concentrated part of the nephloid layer over the Hatteras Abyssal Plain is only 80 to 100 m above the bottom, compared to 150 to 300 m above the bottom over the Blake-Bahama Outer Ridge. The nephloid layer above the Hatteras Abyssal Plain is apparently the result of bottom erosion by the Antarctic Bottom Water (Biscaye, 1974). Photographs of the Hatteras Abyssal Plain indicate that here the current has little or no effect on the floor of the plain (Biscaye, 1974). The sediment in the nephloid layer was probably introduced farther to the south.

SEDIMENTATION AND STRATIGRAPHY

Sedimentation on the Hatteras Abyssal Plain occurs from either slow, uniform, day to day processes or from rapid catastrophic events. Pelagic deposition occurs continually and is considered the typical deep-sea depositional process. On the other hand, turbidity currents are

initiated by catastrophic events such as deep-sea slumps and earthquakes, and therefore occur irregularly.

Turbidity currents first attracted the attention of geologists when Daly (1936) suggested that they might have been responsible for the erosion of submarine canyons. Since that time, research into the origin and characteristics of turbidity currents has progressed until they are now accepted as a common mechanism for the emplacement of deep-sea sands.

Turbidity currents are thought to be commonly initiated at canyon heads near the shelf break. They then travel downslope, contained by either canyons or channels. Deposition occurs when 1) the currents experience an abrupt reduction of speed caused by a change in the bottom gradient, or 2) the currents are no longer channelized. When the currents enter the basin they spread laterally and immediately begin depositing their loads, forming broad horizontal layers of sediment. The turbidites are deposited evenly over the basin, smoothing the surface and burying relief.

Turbidity currents deposit their coarse sediments first, carrying the finest material until the current can no longer keep the sediment in suspension. Proximal turbidites are those deposited at or closest to the place where deposition is initiated. Proximal deposits can be recognized by their coarser mean grain size and thicker bedding.

Often, proximal turbidites are ungraded. Distal turbidites are finer, more thinly bedded, and often contain particles of coarse material whose settling velocities are greatly slowed by shape (i.e. mica grains).

As a turbidity current moves from its point of initiation it developes three distinct parts (Figure 5A): the head, the body, and the tail. Erosion of bottom sediments, most of which occurs at the head, can proceed even when the trailing parts are depositing their load. A dense water-sediment mixture must be continually supplied to the head in order for the current to continue flowing. At the tail, the turbidity current thins rapidly and becomes dilute. Mixing occurs between the tail and the surrounding water and produces an entrained layer. The entrained layer continues to flow even after the current has passed and may deposit fine sediment. Consequently, turbidity currents assume different hydrodynamic regimes as they deposit their load across a single point. This means that a single turbidity current can deposit one unit containing a series of different sedimentary structures. The Bouma sequence (Figure 5B) illustrates the normal succession of these sedimentary structures.

Deposits on the abyssal plain that have accumulated at very slow rates (5cm/1000 years) are commonly referred to as hemipelagic. The mechanics of this type of sedimentation are poorly understood. These deposits can be visual-

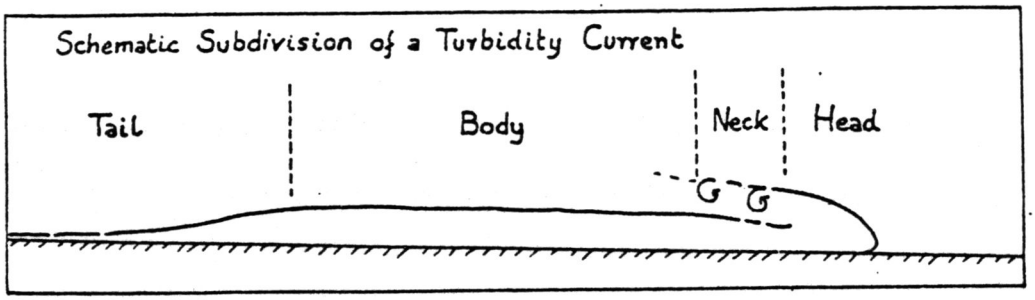

Figure 5A. Morphology of a turbidity current (after Middleton and Hampton, 1973).

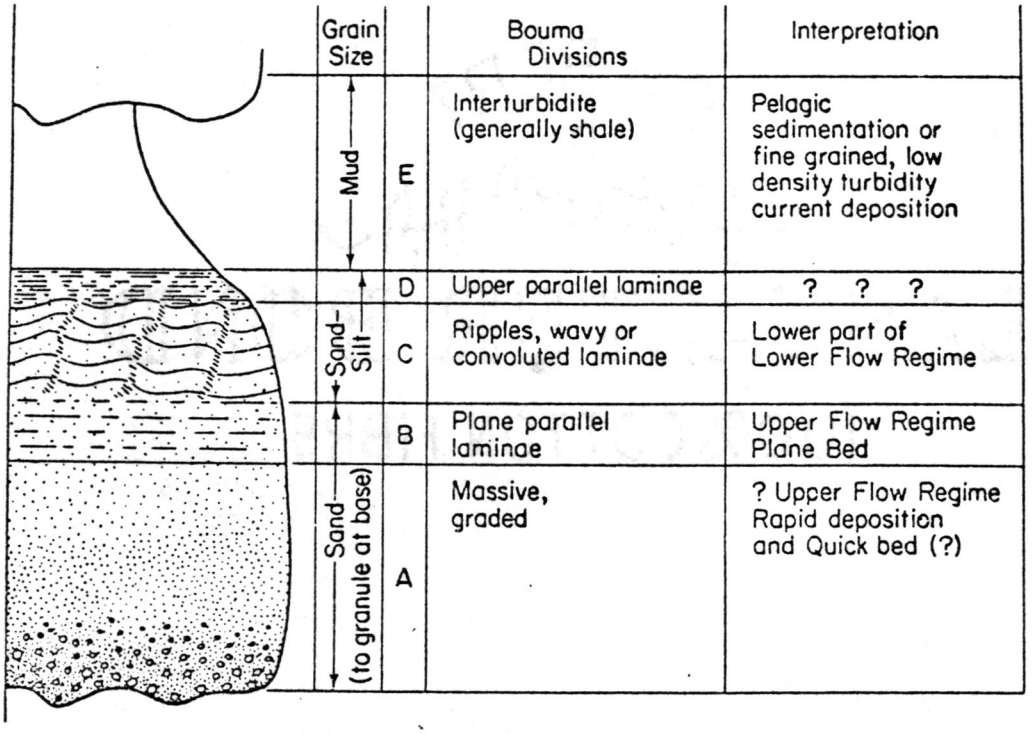

Figure 5B. Bouma's sequence for turbidite deposition (after Middleton and Hampton, 1973)

ized as analogs of the pelagic accumulations of biogenic material, the slow sinking of fine particles onto the ocean floor (Heezen and others, 1966).

Contour currents are also capable of depositing sediment. Such deposits are known as contourites. Contourites have not been recognized on the Hatteras Abyssal Plain. Yet, their is evidence suggesting that contour currents do flow northward across the plain (Biscaye, 1974).

It is essential in this study that the mode of deposition be established for all sampled intervals. Techniques for differentiating types of deep-sea deposits are discussed by Fritz and Pilkey (1975), Bouma and Hollister (1973), and Middleton and Hampton (1973). The most reliable method of differentiation is the study of sedimentary structures uning X-radiography.

Contourites are thinly bedded (<10 cm). X-radiographs often reveal fine laminations with heavy mineral placers. Turbidites are thicker and typically graded. Often, structures of the Bouma sequence can be seen in X-radiographs. Hemipelagic sequences can be recognized since they are composed of lutite and are unlaminated and homogeneous. Differentiation of distal turbidites and hemipelagic sequences is very difficult since both are visually identical and fine grained. However, most turbidites are unmottled because of their rapid rate of deposition. Hemipelagic sequences that have been slowly deposited are commonly mottled. Identifi-

cation of the mode of deposition is at times tenuous even when X-radiography is employed.

Cores recovered from the Hatteras Abyssal Plain consist of intercalated light brownish gray (5YR6/1), olive-gray (5Y3/2), pale yellowish brown (10YR6/2), and dusky brown (5YR2/2) lutites interbedded with light olive-gray (5Y5/2) silts and sands (Appendix 1). The hemipelagic lutite beds generally range in thickness from 1 to 20 cm, whereas the turbidites are frequently as thick as 1 m. Surface sediments over the entire abyssal plain and adjacent continental rise consist of brown lutite, 20 to 50 cm thick. This brown lutite layer is the result of Holocene sedimentation according to Ericson and others (1961) and Damuth (1975).

Seismic records taken across the plain indicate that the strata are smooth and horizonal. These strata are indicative of turbidite deposition. The largest single turbidite (the Black Shell Turbidite) ever correlated was described on the Hatteras Abyssal Plain by Elmore (1976) (Figure 2). The turbidite covers 44,000 km^2, and could be used to establish a time equivalent plane through two of the cores in this study.

MINERALOGY OF THE WESTERN NORTH ATLANTIC

The studies of Zemmels and others (1969) and Rex (1972) deal with the X-ray mineralogy of whole sediment

samples collected in the western North Atlantic. Samples for the studies were collected from Deep Sea Drilling Project sites on the continental rise areas adjacent to the Hatteras Abyssal Plain. Since their results were reported as weight percentages, their data cannot be compared directly to my data. The following non-clay minerals (in order of decreasing abundance) were reported: quartz, dolomite, mica, plagioclase, calcite, orthoclase, and pyrite. Beall and others (1969) using the results of Rex (1969), found no evidence for the authigenic origin of any of these minerals except dolomite. High dolomite content shows a significant correlation with high quartz content in the deposits. This correlation is especially good in paraglacial muds, which indicated that most dolomite is detrital. However, dolomite was also found in significant amounts in the hemipelagic sequences. This dolomite was probably contributed to the hemipelagic sediments by 1) authigenic formation, or 2) biological intermixing of turbiditic and hemipelagic sequences.

The studies of Pevear (1968) and Hathaway (1972) indicate that the shelf can be characterized by two clay mineral facies: 1) a northern facies rich in illite, chlorite, with traces of feldspar and hornblende, and 2) a southern facies rich in smectite (montmorillonite) and kaolinite. Hathaway shows that the two facies formed during the Pleistocene (Figure 6). Hathaway's study deals

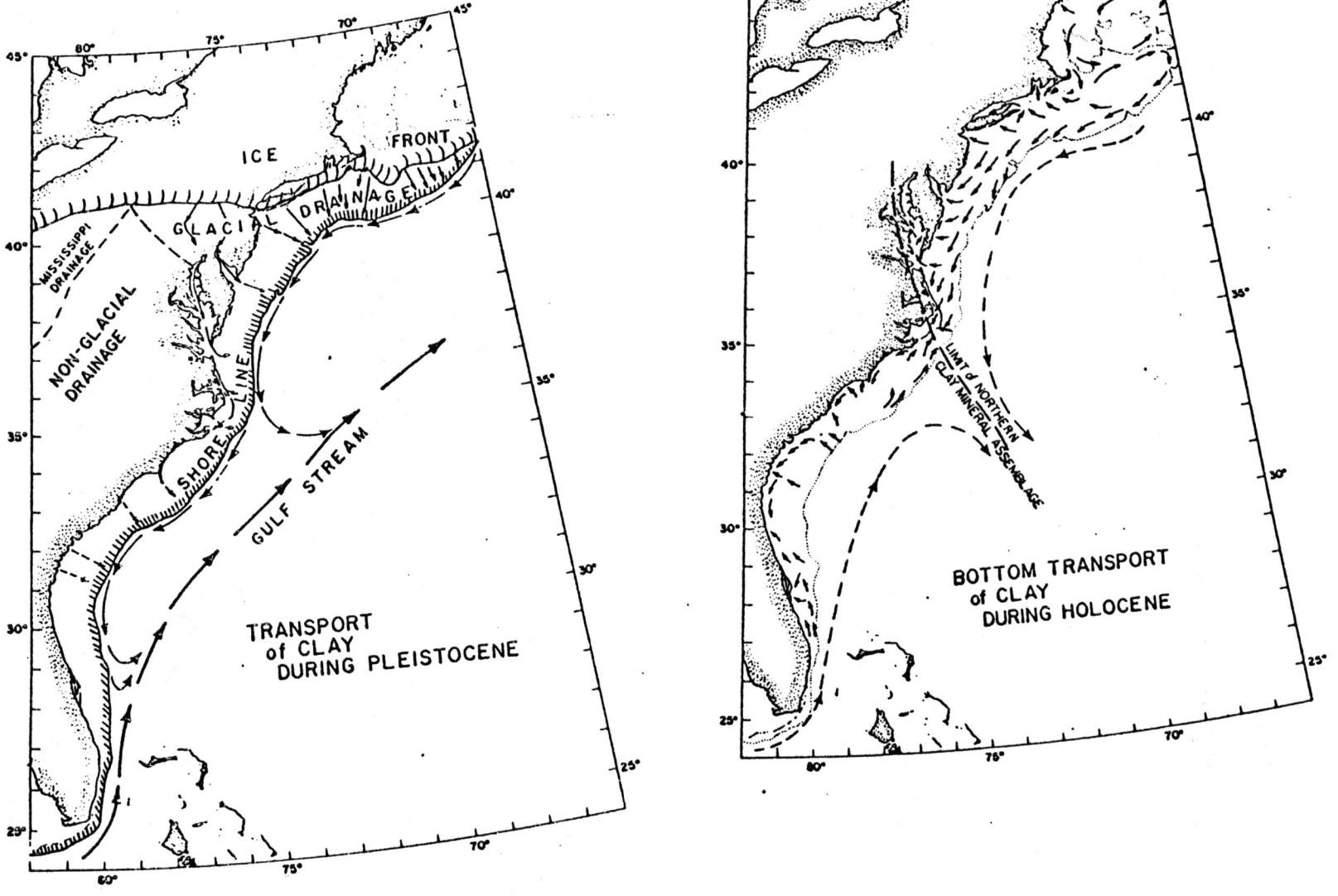

Figure 6. Transportation of clay minerals on the shelf during the Pleistocene and Holocene (from Hathaway, 1972).

principally with north-south variations. Terlecky (1966) and Pevear (1968) deal with the seaward variations in clay mineral content in the surface sediments. Both report a general seaward decrease of smectite (montmorillonite) and kaolinite. Pevear reports that the weight percentage of smectite is as high as 60 nearshore, and as low as 17 at the base of the continental rise. Illite generally increases seaward with values ranging from 11 percent nearshore to 60 percent at the base of the rise. The percentage of chlorite varies inversely to the percentage of kaolinite, with nearshore values for chlorite of 7 percent and seaward values up to 13 percent. Pevear reports a seaward decrease in the amount of gibbsite, with 5 percent on the shelf to as little as 1 percent at the base of the rise.

Zimmerman (1972) found that the upper Holocene sections of cores from the New England Continental Rise contain more smectite with respect to illite than do the Pleistocene sections of the same cores. Klasik and others (1975) studied cores from the continental rise adjacent to the northern section of the Hatteras Abyssal Plain. They found that kaolinite content increases slightly downward with respect to chlorite, and smectite decreases downward with respect to chlorite. Pierce (1971) used the $< 20\,\mu$ fraction and found a downward decrease in the amount of illite with respect to kaolinite. Such vertical variations in the clay

assemblages on the continental margin are the result of a changing sea level (Pierce, 1971).

Biscaye (1965) has published a comprehensive study on clay mineralogy in surficial sediments from the Atlantic ocean and adjacent seas. Results of this study indicate a latitudinal control of the clay mineral species chlorite, gibbsite, and kaolinite. Chlorite is concentrated at the high latitudes and was apparently derived by glacial erosion of chlorite-bearing rocks. Kaolinite and gibbsite are present in their greatest concentrations off tropical land masses where lateritic weathering occurs. Illite is the dominant clay mineral in the Atlantic. Its percentages apparently vary because of the addition of chlorite and kaolinite which are associated with individual climatic belts. The percentage of smectite (montmorillonite) appears to have no relation to latitude. Smectite is found in its highest concentration close to its source areas. In the Western North Atlantic, both the Mississippi Delta and the Laurentian Channel are thought to be major sources of smectite (Pevear, 1968; and Zimmerman, 1972). There is no evidence, in any of the above studies, that the authigenic formation of clays has occurred in the Atlantic (Hathaway, 1972).

ANALYTICAL TECHNIQUES

Samples used in this study were taken from piston cores recovered during three ten-day cruises of the R/V Eastward. The cores were extruded, described, and subsampled on shipboard immediately after recovery. Preparation of the subsamples for analyses followed the procedures outlined in Appendix 2. The samples were initially split into two parts. One split was used for clay mineral and coarse fraction analyses. The other was used to determine: 1) mineral constituents, 2) percentage of carbonate, and 3) percentage of organic carbon. When possible, portions of the second split were saved so that they could later be examined under light and scanning electron microscopes.

Surficial sediment samples that were analyzed were selected in order to assure complete coverage of the Hatteras Abyssal Plain. One core each was selected from the northern, middle, and southern portions of the plain. These cores (27834, 27825, and 29204) were than sampled for subsurface sediments (Figure 2). The core samples were selected on the basis of their mode of deposition (i.e. turbidity current and hemipelagic sedimentation) as determined by Sparks (personal communications, 1977) using X-radiography.

Clay mineralogy was studied using X-ray diffraction techniques (Carroll, 1970). Initially, the samples were dispersed in a 10% calgon solution. The clay fractions

($< 2\mu$) were later separated by allowing the coarser materials to settle from suspension according to Stoke's Law. The $< 2\mu$ fraction was then decanted and concentrated.

For X-ray analysis, the clays were mounted as oriented smear slides using a technique devised by Tien (1974). Smear slides were chosen over other types because they are not influenced by the effects of settling and are consequently more accurate (Gibbs, 1965). Five slides were produced for each sample. One slide was saved as a spare, another was allowed to air dry, and the remaining three slides were treated as follows: one slide was glycerated by spraying it with a light mist of a solution of 1 part glycerin to 3 parts water, one slide was heated to 450°C, and one slide was heated at 575°C for one-half hour.

Using a scan speed of 4 degrees per minute, the slides were X-rayed from 2° to 46° two theta with a General Electric XRD-6 diffractometer. The diffractometer was equipped with a Cu tube and a LiF minochrometer. The clay minerals smectite, illite, chlorite, and kaolinite were identified in every sample. Calcite, quartz, and feldspar were also present in the $< 2\mu$ fraction in most of the samples.

Identification of the clays was based on work by Carroll (1970). Briefly, chlorite was identified by the presence of a 4.7 Å peak. Upon heating at 575°C for one-half hour the peak at the 14 Å position intensifies, verifying the presence of chlorite. Illite was identified by a

sharp peak at the 10 Å position which intensified when heated to 450°C. Kaolinite was identified by a 7.15 Å peak that disappeared when the slide was heated at 575°C for one-half hour. Finally, smectite was identified by a 14 Å peak that expanded to 17 Å after glyceration.

Weight percentages of the clay minerals calculated from their diffraction patterns should be considered semi-quantitative (± 5%) at best (Carroll, 1970). Nevertheless, in order to compare results from this study with those of others, it is important that the weight percentages of the clay mineral constituents be calculated. This was accomplished using a method described by Pevear (1968). Peak intensities (Figure 7) from the glycerated samples were measured. Then, individual peaks were multiplied by one of the following factors: the montmorillonite (17 Å) peak by 1, the illite (10 Å) peak by 4, and the combined 7.15 Å kaolinite-chlorite peak by 1. These products were then normalized to 100%, which gives the weight percentage of the four clay minerals. Pevear (1963) demonstrates that this technique is a reliable means of quantifying clay mineral species in a marine assemblage.

The percentage of kaolinite and chlorite were then determined, using the method of Biscaye (1964). The glycerated slides were scanned at 1/4°/minute from 24° to 25° using nickel filtered Cu radiation. This allows the 3.54 Å peaks of kaolinite and chlorite to be resolved. The peak inten-

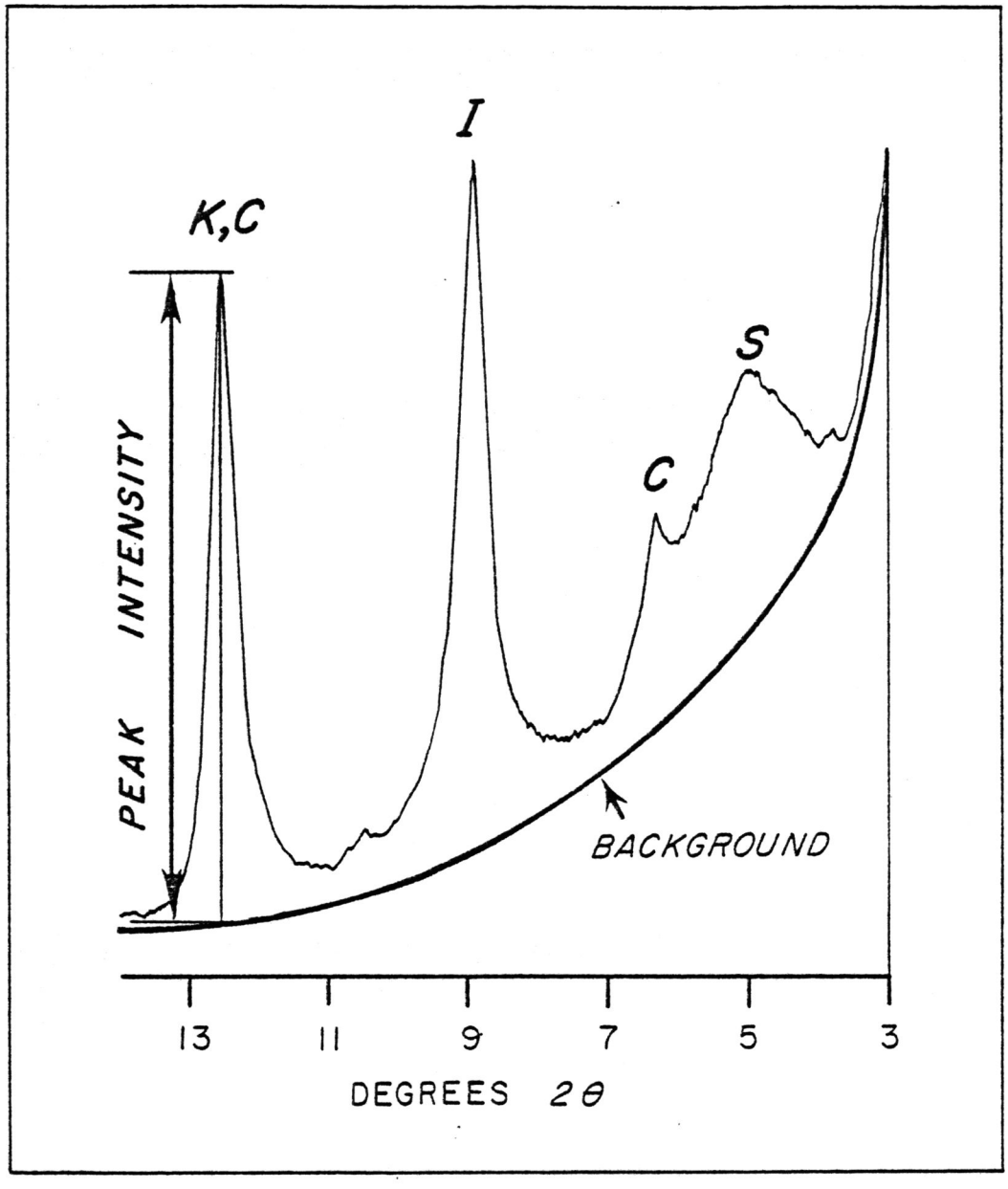

Figure 7. Interpretation of the X-ray Diffraction Patterns. X-ray diffraction pattern of the glycerated $< 2\mu$ slide of surface sample 30013 (scanned at 4°/minute). The peaks labeled K,C (kaolinite, chlorite), I (illite), and S (smectite) were used to calculate the peak intensities. The background was drawn using a flexible curve, as by Pevear (1968).

sities were measured and the contribution of each to the 3.54 Å peak was calculated. To do this, the peak intensities of kaolinite and chlorite were divided by the sum of their peak intensities. This value was then multiplied by the weight percentage of kaolinite plus chlorite calculated from the fast scan patterns. The products obtained are the weight percentages of kaolinite and chlorite contained in the clay fraction.

Another measure of quantity, percent peak intensity, was computed. This value is calculated by dividing the individual peak intensities by the sum of all four clay mineral peak intensities and multiplying the results by 100. These values indicate only relative quantities. However, they are preferred over weight percentages because they better reflect variations in the peak intensities of chlorite and kaolinite.

The entire sample was also analyzed by X-ray diffraction. Dried splits were crushed with a mortar and pestle until they passed through a 63 μ sieve. The powders were scanned (2°/min) from 3° to 67° two theta. The 1.64 Å peak of a silicon standard was scanned in order to normalize any changes in peak intensity that may have resulted from machine variations.

Identifications of the minerals were based on data presented in the A.S.T.M. (American Standard Testing and Material) X-ray Powder Data Files. One peak from each

mineral was selected (Table 1) to be used for quantitative purposes. This peak was selected for its high intensity, its lack of variation (resulting from slight compositional changes), and its relative freedom from the peaks of other minerals in the sample. The peaks for quartz and orthoclase required correction for the effects of the minerals muscovite and aragonite, respectively. Correction values were based on data taken from the A.S.T.M. X-ray Data Files. The quartz peak intensity was corrected by subtracting 28% of the 8.9° (9.94 Å) peak intensity of muscovite. The orthoclase peak intensity was corrected by subtracting 1.12 times the intensity of the 33.2° (2.66 Å) aragonite peak. Quantities obtained from this analysis are only relative values and are expressed as the peak intensity of the mineral divided by the peak intensity (1.64 Å) of the silicon standard.

The percentage of carbonate (calcite, aragonite, and dolomite; Appendix 3) was determined by weighing the samples and then treating them with a 10% solution of HCL. Percent carbonate was determined by weight loss. The carbonate free material was then used for the determination of organic carbon with a Leco induction furnace and a Dietert Carbon Analyzer (Appendix 3) The furnace burns the sample at 1500°C. This is accomplished by an induced magnetic field which excites and heats iron and copper accelerator chips that are placed in the combustion chamber along with the sample.

TABLE 1. Peaks used for whole-sample X-ray diffraction analysis (from A.S.T.M. Data Files).

Mineral	2θ angle *	d-value
Aragonite	33.2°	2.66
Calcite	29.4°	3.01
Chlorite	12.5°	7.07
Dolomite	31.0°	2.85
Muscovite	8.9°	9.94
Plagioclase	27.9°	3.17
K-Feldspar	27.4°	3.22
Quartz	26.5°	3.33

* $CuK\alpha$ radiation

Complete combustion is accomplished by introducing pure oxygen into the combustion chamber. Gases from the combustion flow through a dust trap, a sulfur oxide trap, and a catalytic converter which converts CO to CO_2. The CO_2 is then fed into the carbon analyzer which determines weight percent carbon in the sample.

The coarse fraction (> 63μ) from each sample was described using a binocular microscope. Figure 8 shows a summary of the coarse fractions. Approximation of the volume and composition of the coarse fraction in each sample was made visually. Each sample was placed into one of three catagories: 1) those containing < 1% sand, 2) those containing 1-10% sand, and 3) those containing > 10% sand. Composition of the coarse fraction was determined, and each sample was given a descriptive name. The name designates mean grain size (very fine, fine, medium) and any constituents that comprise more than 10% of the sample (eg. foraminifers, quartz, and mica, listed in order of increasing abundance).

ANALYTICAL PRECISION

Abyssal plain sample 22347 (surface) was processed using the procedures for clay mineral analyses discussed above. Three sets of smear slides were produced from the sample and the best slide from each of the three sets was selected. These three slides were then used to evaluate

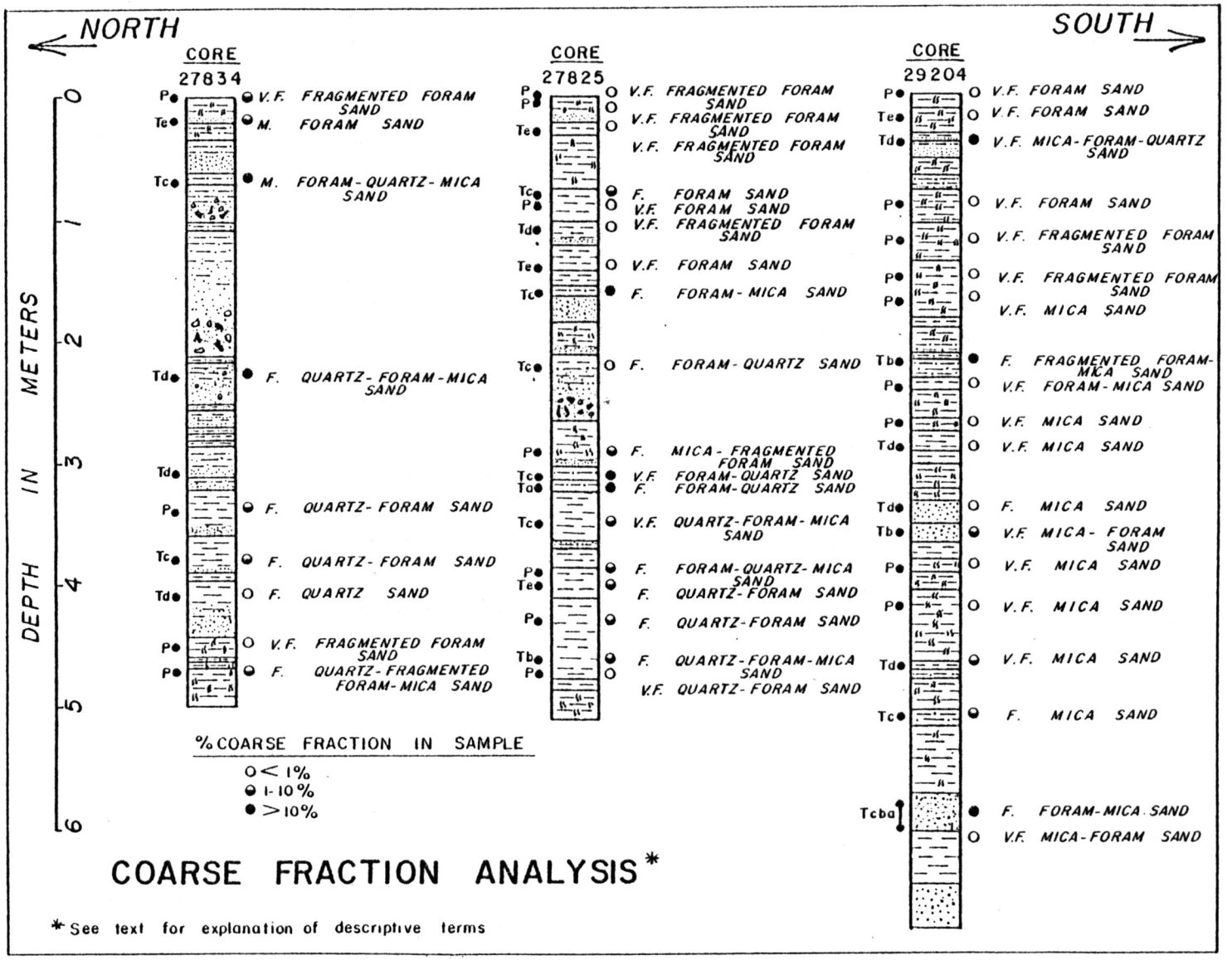

Figure 8. Coarse fraction analysis of the samples taken from cores 27834, 27825, and 29204. (P = hemipelagic sample; Ta-e = turbiditic sample, subscript indicating the division of Bouma's sequence; V.F. = very fine sand, 3-4 ∅; F. = fine sand, 2-3 ∅; M. = medium sand, 1-2 ∅).

the precision of the analytical procedure. Each slide was scanned (4^{o}/min) three times. Between scans, the slides were left undisturbed in the goniometer. Results of the replicate scans are shown in Table 2. The powdered sample 27834 (core interval 340-342 cm) was also analyzed using the techniques described above for whole sample X-ray diffraction. The powdered sample was split into three parts and an X-ray mount was prepared from each split. The mounts were each scanned (2^{o}/min) three times. Between scans, the mounts were left undisturbed in the goniometer. The results of the replicate X-ray diffraction analyses of the powders are tabulated on Table 3.

Variation in the peak intensities resulting when the same smear slide is rescanned can be attributed to counting error of the diffractometer. Peak intensity variations which occurred in the scanning of the three smear slides (A,B,C) should be attributed to the technique used to prepare the slides. In the same manner, variation in the results of the replicate analyses of the powder mounts should be attributed to counter errors and problems with the mounting technique.

No attempt was made to calculate mineral weight percentages from the X-ray diffractograms of the whole sample powders. The weight percentage of carbonate was, however, plotted against the sum of the carbonate peak intensities for each of the 73 samples analyzed (Figure 9). Using

TABLE 2. Precision of the clay mineral X-ray analyses. Results of replicate analyses of sample 22347 (surface) are shown.

Slide	Scan	%Smectite	%Illite	%Kaolinite	%Chlorite
A	1	8	77	7	8
	2	7	78	7	8
	3	7	77	8	8
B	1	6	78	8	8
	2	7	78	7	8
	3	7	77	7	9
C	1	6	78	7	9
	2	8	77	7	8
	3	7	77	8	8

TABLE 3. Precision of the whole-sample X-ray analyses. Results of the replicate analyses of powdered sample 27834 (340 cm) are shown. The results are reported as the peak intensity of the mineral divided by the intensity of the 1.64 Å peak of the silicon standard. (M = muscovite, C = chlorite, Q = quartz, K = potassium feldspar, P = plagioclase, CAL = calcite, D = dolomite, ARA = aragonite)

Slide	Scan	M	C	Q	K	P	CAL	D	ARA
A	1	0.21	0.18	0.82	0.02	0.18	0.11	0.04	0.02
	2	0.21	0.19	0.86	0.00	0.18	0.11	0.06	0.02
	3	0.22	0.18	0.87	0.00	0.18	0.10	0.04	0.02
B	1	0.21	0.19	0.86	0.02	0.18	0.11	0.06	0.02
	2	0.22	0.18	0.84	0.00	0.21	0.11	0.07	0.02
	3	0.25	0.18	0.88	0.01	0.21	0.14	0.07	0.02
C	1	0.18	0.18	0.72	0.00	0.16	0.11	0.06	0.01
	2	0.19	0.16	0.73	0.01	0.18	0.12	0.07	0.02
	3	0.18	0.20	0.82	0.01	0.18	0.13	0.08	0.01

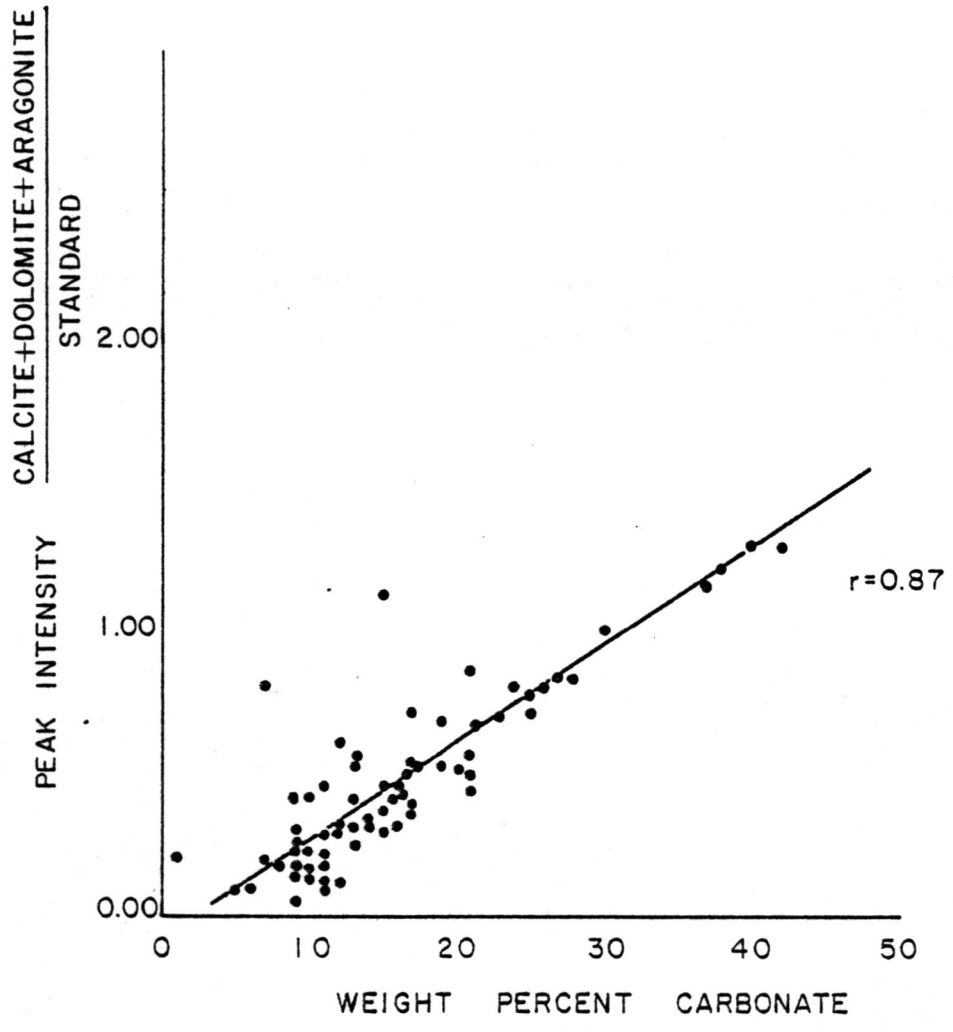

Figure 9. Linear correlation of peak intensity and weight percentage of the carbonate minerals. The sum of the carbonate peak intensities is divided by the peak intensity of the silicon standard and plotted against the weight percent carbonate for each sample. The line was fitted with a linear regression. There is a good correlation (correlation coefficent r = 0.87) between the two sets of data.

linear regression, a line ($y = 0.32x - 0.72$) of best fit was calculated for the set of data. The correlation coefficient r equals 0.87 indicating that a significant correlation exists between the weight percent carbonate and the sum of the carbonate peak intensities.

Replicate carbon analyses were performed on known samples provided by the manufacturer of the carbon analyzer (Table 4). The known samples contained 0.403% ($\pm$0.009%) carbon. Results of four replicate analyses of the known sample averaged 0.38% (sd. = 0.02). Maximum variation in the four analyses was 0.04%.

RESULTS

A total of twenty-sex surface samples, from the Hatteras Abyssal Plain and the adjacent continental rise, and seventy-one subsurface samples, from the Hatteras Abyssal Plain, were analyzed to determine the following: 1) mineral composition of the $< 2\mu$ fraction, 2) mineral composition of the whole sample, 3) composition of the coarse fraction ($> 63\mu$), and 4) weight percentage of organic carbon and carbonate. Nine surface samples from the rise were included in order to compare the characteristics of surface sediments from the rise and the abyssal plain.

Illite, smectite, chlorite, and kaolinite are the clay minerals found in the surface sediments. Illite is

TABLE 4. Precision of the organic carbon analyses. Results of the replicate analyses of a known standard that contains 0.403% carbon (± 0.009%) are shown. The mean of the replicate analyses equals 0.38% (s.d. = 0.02).

Run	Weight percent carbon
1	0.37
2	0.37
3	0.38
4	0.41

always most abundant, with an average weight percentage of 78.4 (Table 5). Smectite is always the second most abundant, having an average weight percentage of 9.7. Chlorite is slightly less abundant, with an average weight percentage of 8.2, and kaolinite is the least abundant, with an average weight percentage of 7.4.

Very little difference in the clay mineral content was noted between rise and abyssal plain surface sediments. Those of the rise were only slightly richer in smectite, kaolinite, and chlorite (Table 5). However, given the small group of rise samples studied, the differences between the clay mineral content of the rise and the abyssal plain samples are not significant. It is interesting that the weight percentages of the individual clay minerals from the rise deviate more from sample to sample than do the abyssal plain surface samples. Rise samples have standard deviations for the weight percentages of the clay minerals that are at least two times greater than those for the abyssal plain samples. No areal trends in the clay mineral content could be recognized in either the rise or abyssal plain sediments (Appendix 4A-D). As previously mentioned, significant variations in the peak intensities of both kaolinite and chlorite are suppressed by the calculation of weight percentages. Because of this, the percent peak intensities of clay minerals in the surface samples were calculated and plotted (Appendix 4E-I). This technique revealed no trends either.

TABLE 5. Weight percentages of clay minerals in hemipelagic and turbiditic sediments.

Surface Samples		Smectite	Illite	Kaolinite	Chlorite
Rise	$\bar{x}$	9.9	74.1	7.8	8.2
9 samples	sd.	3.9	3.9	1.4	1.3
Plain	$\bar{x}$	9.6	75.1	7.1	8.1
17 samples	sd.	1.8	1.7	0.7	0.8
Total	$\bar{x}$	9.7	74.8	7.4	8.1
26 samples	sd.	2.6	1.6	1.1	1.0
Core 29204					
Turbidites	$\bar{x}$	10.5	75.5	6.4	7.6
10 samples	sd.	2.5	2.0	1.0	1.3
Hemipelagic	$\bar{x}$	9.8	76.3	6.5	7.5
12 samples	sd.	2.8	3.3	0.8	0.7
Total	$\bar{x}$	10.1	75.8	6.4	7.5
22 samples	sd.	2.7	2.7	0.8	1.0
Core 27825					
Turbidites	$\bar{x}$	9.4	75.2	7.1	8.2
18 samples	sd.	2.0	2.2	0.7	0.7
Hemipelagic	$\bar{x}$	9.6	74.3	7.5	8.5
19 samples	sd.	2.7	2.6	0.6	0.7
Total	$\bar{x}$	9.5	74.7	7.3	8.4
37 samples	sd.	2.3	2.4	0.7	0.7

TABLE 5. (Continued)

		Smectite	Illite	Kaolinite	Chlorite
Core 27834					
Turbidites	$\bar{x}$	11.0	73.9	7.1	8.0
7 samples	sd.	1.6	1.9	0.7	0.6
Hemipelagic	$\bar{x}$	10.0	74.6	7.2	8.2
5 samples	sd.	1.0	1.6	0.4	0.8
Total	$\bar{x}$	10.5	74.2	7.1	8.1
12 samples	sd.	1.3	1.8	0.5	0.7
Total Cores					
Turbidites	$\bar{x}$	10.3	74.8	6.8	7.9
35 samples	sd.	2.0	2.0	0.8	0.8
Hemipelagic	$\bar{x}$	9.8	75.0	7.0	8.1
36 samples	sd.	2.1	2.5	0.6	0.7
Total	$\bar{x}$	10.0	74.9	7.0	8.0
71 samples	sd.	2.1	2.3	0.8	0.8

The ratios of kaolinite to chlorite were also calculated and plotted (Appendix 4I) for all the surficial samples. This ratio normally decreases toward the polar regions in the western North Atlantic (Biscaye, 1965). On the Hatteras Abyssal Plain, there is not a clear trend in kaolinite/chlorite in the surficial sediment, but there is a slight increase in the ratio to the north. This trend, although small, is significant since it is the reverse of the trend demonstrated by Biscaye (1965).

Quartz, feldspar, and calcite are found in the $< 2\,\mu$ fraction of most of the surface samples (Appendix 4K). The quantities of $< 2\,\mu$ feldspar and quartz have no apparent relationship with the location of the sample. Less than $2\,\mu$ calcite, however, is more abundant in the rise samples, indicating that a relationship exists where calcite decreases in abundance with increasing water depth of the sample (Appendix 4J).

In the whole-sample mineral analyses of the surface sediments, the following eight minerals were identified: muscovite, chlorite, quartz, potassium feldspar, plagioclase, calcite, dolomite, and aragonite. These minerals were quantified to show only the relative abundance of one mineral species from sample to sample. They do not reflect the relative abundance of the eight minerals in a single sample.

The mineral species quartz, potassium feldspar, plagio-

clase, calcite, and dolomite were all significantly more abundant on the surface of the rise than on the surface of the abyssal plain (Table 6). The micaceous minerals, muscovite and chlorite, were slightly more abundant on the abyssal plain. Areal trends of these minerals in the surface samples were not apparent (Appendix 5A-G).

The weight percentages of carbonate and organic carbon were determined for twenty-two of the surface samples (Table 7). The weight percentages of carbonate are apparently related to the water depth of the sample (Appendix 5H). The average value of carbonate in surface sediments of the rise is 27.4 percent, compared with an average of 20.8 percent for surface samples from the abyssal plain (Table 7). Organic carbon in the samples from the surface of the rise averages 0.41 percent (Appendix 5I). This is higher than the average 0.38 percent contained in samples from the surface of the abyssal plain (Table 7). But this variation cannot be considered significant given the precision of the carbon analyses.

In order to observe vertical variations in the composition of the sediments, a total of 71 samples were selected from three abyssal plain cores. They were then analyzed in the same manner that was previously outlined for the study of surface sediment. Based on the work of Sparks (personal communications, 1977) the samples were selected from both turbidite and hemipelagic units throughout the

TABLE 6. Statistics: quantity of minerals contained in the whole-sample powders of hemipelagic and turbiditic sediments (expressed as peak intensity mineral/standard). See table 3 for an explanation of the mineral abbreviations.

Surface Samples		M	C	Q	K	P	CAL	D	A
Rise	$\bar{x}$	0.16	0.12	1.13	0.07	0.38	0.75	0.13	0.02
5 samples	s d.	0.05	0.03	0.40	0.11	0.24	0.38	0.08	0.02
Plain	$\bar{x}$	0.17	0.14	0.92	0.02	0.18	0.46	0.10	0.01
17 samples	s d.	0.05	0.04	0.27	0.04	0.04	0.24	0.04	0
Total	$\bar{x}$	0.17	0.13	1.03	0.05	0.28	0.61	0.12	0.02
22 samples	s d.	0.05	0.04	0.34	0.08	0.14	0.31	0.06	0.01
Core 29204									
Turbidites	$\bar{x}$	0.28	0.17	1.13	0.28	0.35	0.21	0.26	0.01
10 samples	sd.	0.11	0.05	0.31	0.62	0.16	0.14	0.19	0.01
Hemipelagic	$\bar{x}$	0.15	0.12	0.77	0.01	0.17	0.08	0.09	0.01
12 samples	sd.	0.04	0.02	0.15	0.01	0.03	0.14	0.03	0.01
Total	$\bar{x}$	0.22	0.15	0.95	0.15	0.26	0.15	0.18	0.01
22 samples	sd.	0.08	0.03	0.23	0.61	0.10	0.14	0.11	0.01
Core 27825									
Turbidites	$\bar{x}$	0.22	0.18	1.13	0.03	0.26	0.27	0.16	0.02
11 samples	sd.	0.06	0.04	0.42	0.07	0.21	0.15	0.11	0.01
Hemipelagic	$\bar{x}$	0.17	0.15	0.88	0	0.14	0.19	0.07	0.01
7 samples	sd.	0.03	0.02	0.33	0	0.03	0.14	0.02	0.01
Total	$\bar{x}$	0.20	0.17	1.01	0.15	0.20	0.23	0.12	0.02
18 samples	sd.	0.05	0.03	0.38	0.35	0.12	0.15	0.07	0.01

TABLE 6. - (Continued)

		M	C	Q	K	P	CAL	D	A
Core 27834									
Turbidites	$\bar{x}$	0.24	0.20	1.20	0.05	0.25	0.28	0.11	0.01
7 samples	sd.	0.07	0.07	0.25	0.07	0.11	0.28	0.06	0.01
Hemipelagic	$\bar{x}$	0.19	0.17	0.96	0.04	0.19	0.19	0.09	0.01
5 samples	sd.	0.02	0.03	0.11	0.05	0.02	0.20	0.02	0.01
Total	$\bar{x}$	0.22	0.19	1.08	0.05	0.22	0.24	0.10	0.01
12 samples	sd.	0.05	0.05	0.18	0.06	0.07	0.24	0.04	0.01
Total Cores									
Turbidites	$\bar{x}$	0.25	0.18	1.15	0.12	0.29	0.25	0.18	0.01
28 samples	sd.	0.08	0.05	0.33	0.25	0.16	0.19	0.12	0.01
Hemipelagic	$\bar{x}$	0.17	0.15	0.87	0.02	0.17	0.15	0.08	0.01
24 samples	sd.	0.03	0.02	0.20	0.03	0.03	0.16	0.02	0.01
Total	$\bar{x}$	0.21	0.17	1.01	0.12	0.23	0.21	0.09	0.01
52 samples	sd.	0.06	0.04	0.26	0.34	0.10	0.18	0.07	0.01

TABLE 7. Statistics: weight percentage carbonate and organic carbon in hemipelagic and turbiditic sediments.

Surface Sample		Carbonate	Organic Carbon
Rise	$\bar{x}$	27.4	0.41
5 samples	sd.	12.2	0.25
Plain	$\bar{x}$	20.8	0.38
17 samples	sd.	6.1	0.10
Total	$\bar{x}$	24.1	0.40
22 samples	sd.	9.2	0.18
Core 29204			
Turbidites	$\bar{x}$	12.9	0.28
10 samples	sd.	3.9	0.28
Hemipelagic	$\bar{x}$	11.4	0.21
12 samples	sd.	3.8	0.07
Total	$\bar{x}$	12.2	0.25
22 samples	sd.	3.8	0.18
Core 27825			
Turbidites	$\bar{x}$	14.6	0.45
10 samples	sd.	5.8	0.14
Hemipelagic	$\bar{x}$	13.0	0.40
7 samples	sd.	5.1	0.11
Total	$\bar{x}$	13.8	0.43
17 samples	sd.	5.5	0.13

TABLE 7. (Continued)

		Carbonate	Organic Carbon
Core 27834			
Turbidite	$\bar{x}$	14.4	0.38
7 samples	sd.	8.2	0.09
Hemipelagic	$\bar{x}$	10.6	0.39
5 samples	sd.	7.1	0.10
Total	$\bar{x}$	12.5	0.39
12 samples	sd.	7.7	0.10
Total Cores			
Turbidite	$\bar{x}$	14.0	0.37
	sd.	6.0	0.09
Hemipelagic	$\bar{x}$	11.7	0.33
	sd.	5.3	0.11
Total	$\bar{x}$	12.8	0.35
	sd.	5.7	0.10

cores. Thirty-five turbidites and 36 hemipelagic sequences were sampled. For the distribution of the samples within the cores see Appendix 6.

Suprisingly, little difference exists between the average clay mineral content of the turbidites and the hemipelagic sequences. Samples from turbidites were slightly richer in smectite (Table 5) and samples from hemipelagic sequences contained slightly more illite, kaolinite, and chlorite. But these variations were so small ($< 1\%$), that given the precision of the analyses, the clay mineral suites of the hemipelagic and turbiditic sediments should be considered identical.

For the subsurface samples, the ratios of kaolinite to chlorite, illite to chlorite, smectite to illite, and of smectite to chlorite were plotted (Appendix 6A-C). These ratios were chosen because previous researchers (Zimmerman, 1972; Pierce, 1971; Terleckey, 1966) have demonstrated that vertical trends in these ratios exist in cores taken on the adjacent continental slope and rise. All of these trends are thought to be related to climatic and circulatory changes which took place during the Pleistocene. There were no trends evident in the abyssal plain cores. Apparent relationships between the clay mineral peak intensities and their mode of deposition are also lacking (Appendix 6D-G).

The mineral assemblages in the whole-samples of the subsurface sediment were qualitatively similar to those in

the whole-samples from the surface sediment. The minerals muscovite, chlorite, quartz, potassium feldspar, plagioclase, dolomite, calcite, and aragonite were present (Appendix 7A-H). When compared to hemipelagic sediments, the turbidites on the average contain a greater amount of all the minerals except aragonite (Table 6).

Downcore trends in the abundance of the clay and non-clay minerals in hemipelagic units only occur in calcite. The abundance of calcite decreases with depth in the cores (Appendix 7H). The content of the other non-clay minerals remains constant with depth.

The overall weight percentage of organic carbon is relatively higher in the turbidites, averaging 0.37%. This compares with 0.33% in the hemipelagic sequences. Although these differences are small, they are significant. Organic carbon, which is commonly concentrated in the fine fractions of sediment ($<63\ \mu$), would normally comprise a greater percentage of the hemipelagic sequences, because of their finer grain sizes. The southernmost core (29204) contains less organic carbon (average is 0.25%) than the northern cores which contain an average of 0.43% (core 27834) and 0.40% (core 27825) (Table 7). Significant variations of organic carbon content do not occur with depth in the hemipelagic sequences (Appendix 7H). The percentage of carbonate decreases with depth in the hemipelagic sequences of all three cores (Appendix 7I). This decrease apparently re-

flects the downward decrease in calcite.

The coarse fractions (>63 μ) were separated from 20 surface and 50 subsurface samples and were described using a binocular microscope. The coarse fractions consist only of sand-size sediment. Descriptions of the coarse fractions were made to 1) determine the mineral composition in the coarse fraction (>63 μ), and 2) see what differences in the composition of the coarse fractions occur between the hemipelagic and the turbidite sediments. The descriptive terminology used here is explained in the section on analytical techniques.

The majority of the twenty-six surface samples contain from one to ten percent typically very fine, fragmented foraminiferal sands (Figure 8). Coarse fractions from the surface of the abyssal plain rarely contain quartz. But, in several surface samples from the rise, the coarse fractions contain enough quartz to be described as medium foraminiferal-quartz sands. Accessory constituents (those which occur in quantities of less than 10%) in both the rise and abyssal plain surface samples consist of mica grains, sponge spicules, echinoderm spines, phosphorite grains, and manganese oxide granules.

Subsurface samples contain a greater variety of constituents in their coarse fractions. Only the samples from turbidites contain more than 10 percent sand (Figure 8). In contrast, some of the turbidites contain less than

one percent sand. The turbidites with low sand content occur most frequently in the southern part of the plain. Hemipelagic deposits usually contain less than one percent sand, and never contain more than 10 percent sand. The coarse fraction never exceeds 70 percent in any sample.

Turbidites typically contain a very fine quartz-foraminiferal-mica sand. A fine mica sand occurs in only a few turbidites, but was common in hemipelagic deposits. The coarse fractions of the near surface and the surface hemipelagic sequences contain enough foraminifers to be classified as very fine, fragmented foraminiferal-mica sand, or as very fine, fragmented foraminiferal sand. Accessory grains in the coarse fractions of the turbidites were plentiful and diverse. Benthonic and planktonic foraminifera, mica grains, sponge spicules, phosphate and glauconite grains, echinoid fragments, pyrite grains, manganese oxide micronodules and granules, hematite granules, pteropod fragments, gastropod fragments, and pelecypod fragments all occur. Hemipelagic sediments had a smaller content and a less diverse assemblage of accessory grains. Hemipelagic units contained mica grains, planktonic foraminifera, pyrite granules, hematite granules, sponge spicules, and occassional quartz grains. One tektite was found in a hemipelagic sequence.

It is important to emphasize that no dolomite was identified in any of the coarse fractions. In petrographic

studies of turbidite sands from the lower continental rise (Ayers and Cleary, in preparation) and from the Hatteras Abyssal Plain (Cleary and Conolly, 1974b) little or no dolomite was observed.

DISCUSSION AND SUMMARY

On the basis of previous clay mineral studies on the continental margin (Terlecky, 1966; Pierce, 1971; and Pevear, 1968), the distribution of clay minerals on the surface of the continental rise and abyssal plain could have been predicted. The values of smectite, illite, kaolinite, and chlorite obtained from this study have been plotted with comparable data taken from Pevear (1968) (Figures 10-13). Seaward trends in clay mineral content on the margin are the same as those discussed by Pevear (1968) and Terlecky (1966). Illite and chlorite increase seaward as kaolinite and smectite decrease.

Seaward decreases in the quantities of smectite and kaolinite apparently reflect the diminishing influence of the clay mineral assemblage from the southeastern United States. Kaolinite is supplied to the shelf primarily by the rivers of the southeastern United States. Previous studies (Hathaway, 1972; Pevear, 1968) indicate that little, if any, fine sediment has been able to escape from the estuaries of the southeastern United States during the

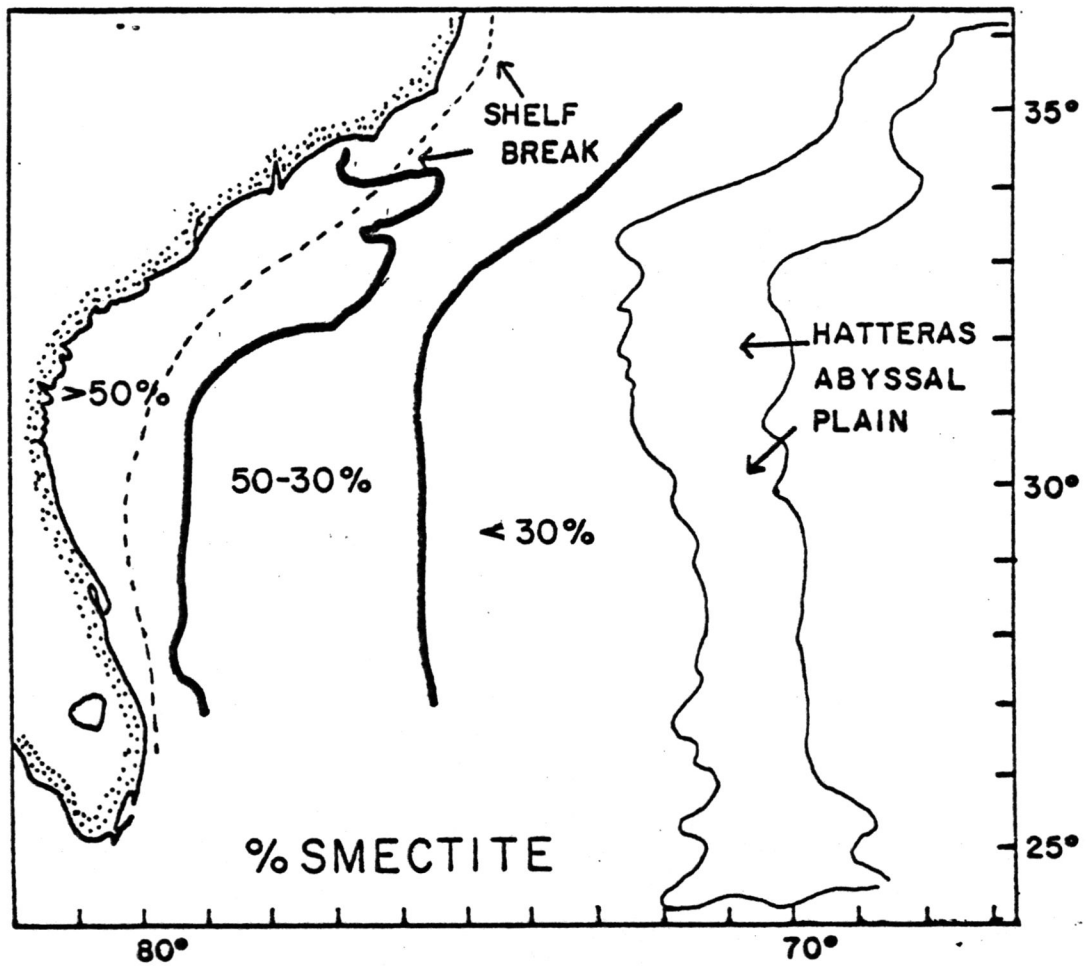

Figure 10. Smectite distribution off the southeastern United States. The data for the shelf is from Pevear (1968).

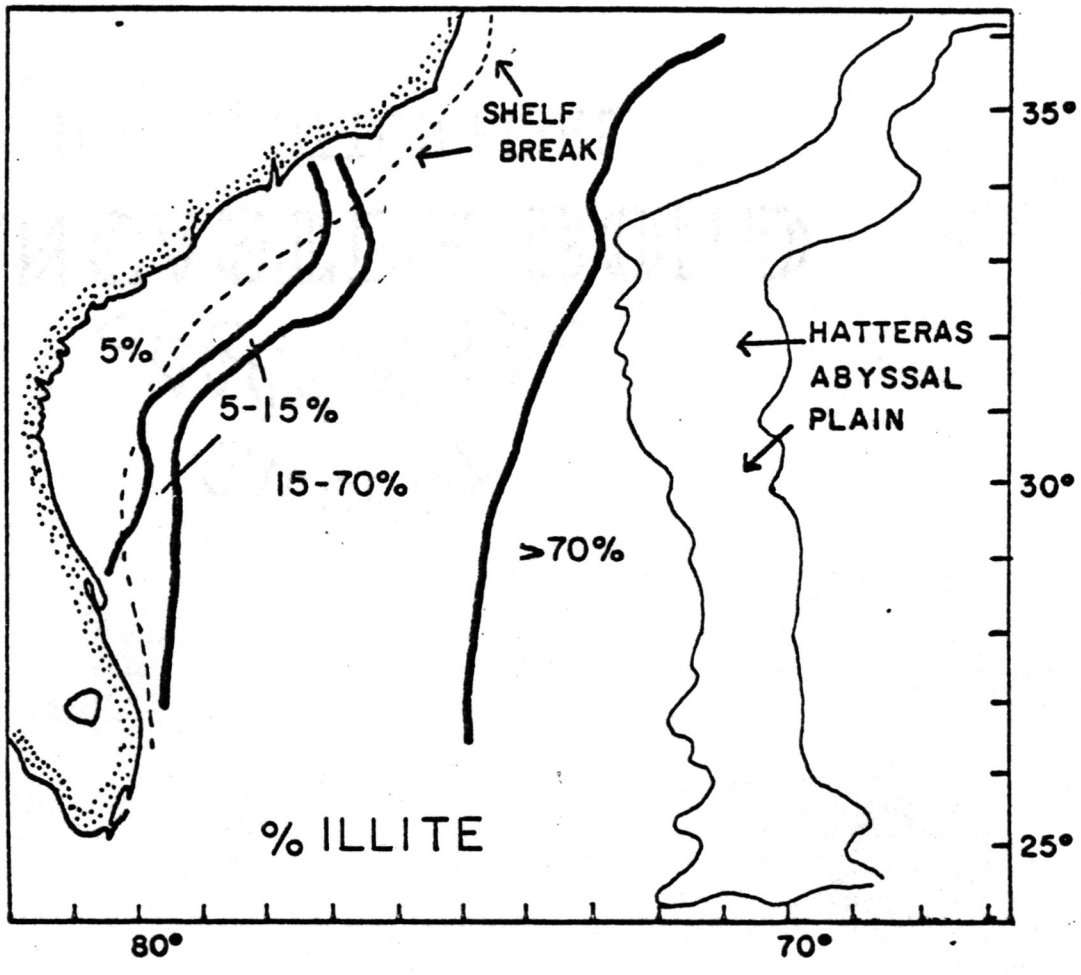

Figure 11. Illite distribution off the southeastern United States. The data for the shelf is from Pevear (1968).

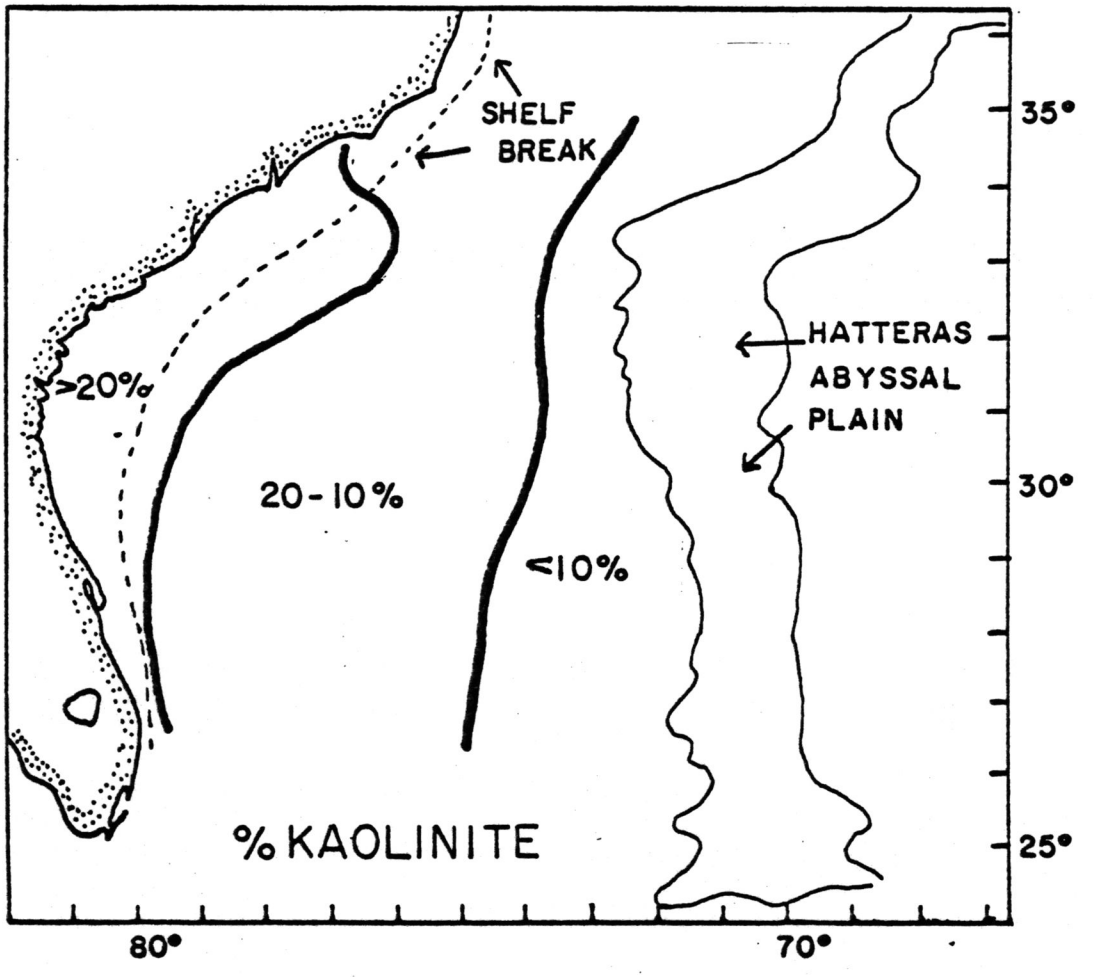

Figure 12. Kaolinite distribution off the southeastern United States. The data for the shelf is from Pevear (1968).

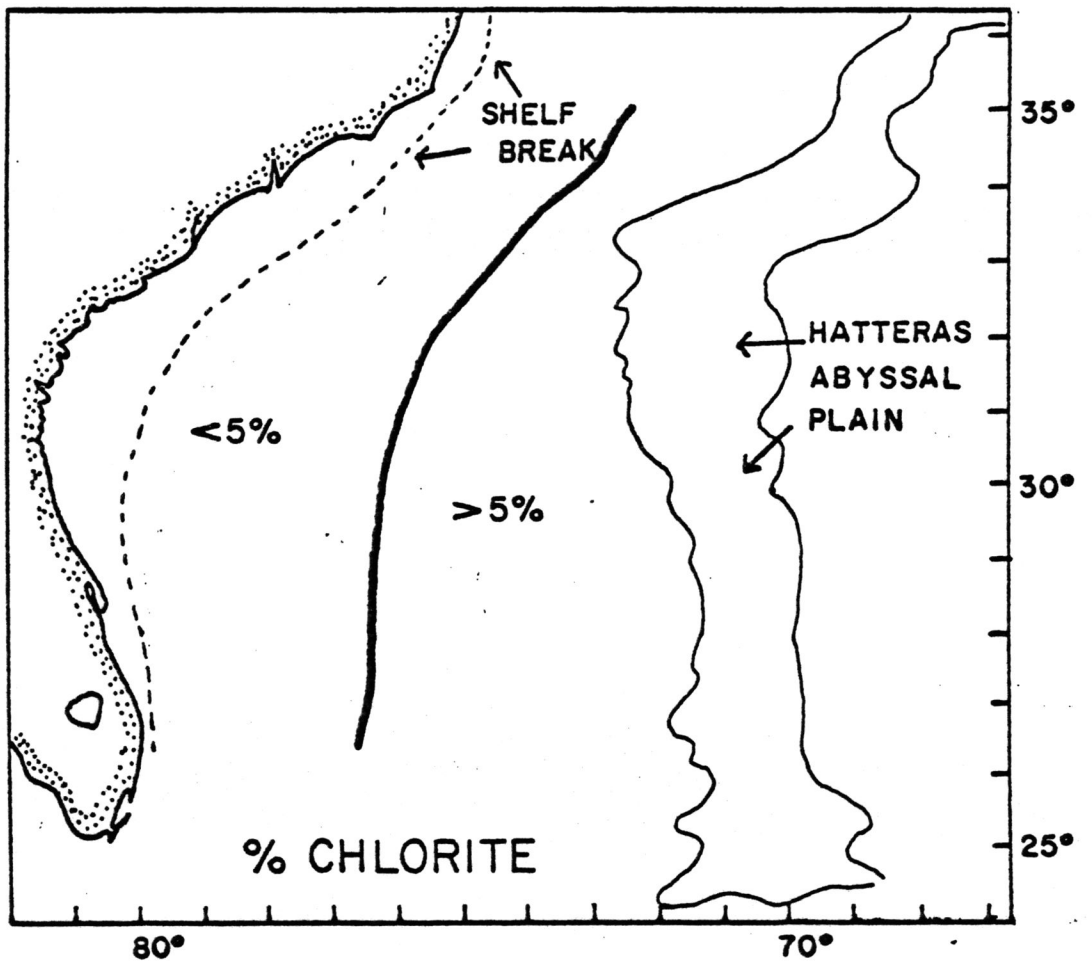

Figure 13. Chlorite distribution off the southeastern United States. The data for the shelf is from Pevear (1968).

Post-Pleistocene rise in sea level. Therefore, it seems likely that any kaolinite presently on the shelf was supplied during the Pleistocene. The source of smectite on the shelf is more difficult to assess. Pevear (1968) reports the presence of low quantities of smectite (montmorillonite) in the southeastern United States rivers. He concluded that the major source of smectite on the continental shelf must be either the erosion of Pleistocene sediments outcropping on the shelf, or the northward transport of smectite-rich Gulf Coast and Caribbean sediments by the Gulf Stream. More recently, two other sources of smectite on the lower rise have been recognized. Smectite is supplied to the lower rise via the southward transport of smectite-rich Laurentian Channel lutites by the Western Boundary Undercurrent (Zimmerman, 1972). This northern source of smectite is probably important only on the rise. The Western Boundary Undercurrent does not flow over the surface of the Hatteras Abyssal Plain. Therefore, this is an unlikely source of smectite on the abyssal plain. Gulf Stream erosion of smectite-rich Miocene sediments outcropping on the Florida-Hatteras Slope could also contribute smectite to the study area.

Chlorite and illite are not abundant on the shelf of the southeastern United States. In order to explain their abundance in the study area there must be an additional source area. There are three logical source areas for

chlorite: 1) the chlorite-rich sediments of the northeastern United States shelf, 2) the chlorite-rich lutites of the Arctic, and 3) the chlorite-rich lutites of the Antarctic (Biscaye, 1965; and Hathaway, 1972). Chlorite could be supplied to the rise from the north via the Arctic Bottom Water. Because of the reasons given previously it is unlikely that chlorite transported by the Arctic Bottom Water is deposited on the Hatteras Abyssal Plain.

Biscaye (1965) reports a distinct relationship between the K/C ratio and the latitude of bottom sediments in the Atlantic. In both the northern and southern Atlantic, K/C ratio increases toward the equator. The K/C ratios for the Hatteras Abyssal Plain surface sediments trend opposite of the normal Atlantic trends, with the ratios on the Hatteras Abyssal Plain decreasing to the south (Appendix 4I). A likely explanation for this deviation might be the added input of chlorite in the southern Hatteras Abyssal Plain. The source of such an input of chlorite might be the deposition of chlorite-rich sediment by the Antarctic Bottom Water.

Because mica is present in many rock types, and is relatively resistant to chemical weathering, the exact sources of illite ($< 2\,\mu$ mica) are difficult to determine. Illite is present in varying quantities in all source areas that supply sediment to the Atlantic. Biscaye (1965) suggests that illite is ubiquitous in the $< 2\,\mu$ fraction of

all recent Atlantic bottom sediments. Northeastern North America is an immediate source of illite to the continental margin of the Western North Atlantic. During the Pleistocene, rivers carried illite-rich sediments from glacially eroded areas of northeastern North America to the northern continental slope (Hathaway, 1972). The Western Boundary Undercurrent then carried the illite-rich sediment to the southeastern continental slope and rise of the United States.

The areal distribution of the whole-sample mineralogy on the surface of the rise and the abyssal plain is directly related to sample depth and to the prevailing energy regimes at the point of deposition. Rise samples contain greater than average amounts of all minerals except muscovite and chlorite. Aragonite was not abundant enough to be quantitatively evaluated (Table 6). The greater abundances of quartz, orthoclase, plagioclase, and dolomite on the rise can be best explained by the lateral spreading of turbiditic sand across the rise by the Western Boundary Undercurrent. This line of reasoning would also explain the higher quantities of mica on the abyssal plain. Strong currents, such as the Western Boundary Undercurrent, would tend to winnow the micas on the continental rise. On the abyssal plain, sediments are subjected to currents of lower velocity.

Presumably, the higher abundances of calcite (whole sample) on the continental rise are a function of the depth

of deposition. The greater depth of the abyssal plain causes greater dissolution of calcite and aragonite. More abundant calcite in the $< 2\mu$ fraction (Appendix 4J), and the higher percentage of carbonate in the rise samples, also indicate the greater dissolution of carbonates with increasing water depth.

Clay mineral content in the samples from the three Hatteras Abyssal Plain cores is similar to those of the surface samples. Illite, the most abundant mineral, averaged 75 percent (by weight), smectite averaged 10 percent, chlorite averaged 8 percent, and kaolinite averaged 7 percent. The down core trends in clay mineral ratios that were demonstrated by previous work (Pierce, 1971; Pevear, 1968; and Zimmerman, 1972) on the continental margin are lacking on the abyssal plain. Perhaps the greater distance from the continent, coupled with the slower rates of hemipelagic deposition, best explain the lack of vertical trends of clay minerals in my cores.

During the Pleistocene, most turbidity currents that deposited sediment on the Hatteras Abyssal Plain were initiated at the shelf edge (Cleary and others, 1977; Elmore, 1976). These turbidites would have contained a $< 2\mu$ mineral assemblage that was characteristic of the shelf where the currents were initiated. The $< 2\mu$ mineral assemblage on the northern shelf was a mixture of chlorite, illite, hornblende, and feldspar (Hathaway, 1972). On the

southern shelf, the < 2 μ mineral assemblage consisted of smectite and kaolinite, and smaller amounts of illite (Hathaway, 1972; Pevear, 1968).

Turbidity currents initiated at the heads of the Hudson and Wilmington Canyons would have contained a northern < 2 μ mineral assemblage (Figure 14). In contrast, turbidity currents initiated at the head of the Hatteras Canyon System would have contained a southern < 2 μ mineral assemblage. During the Pleistocene, the three canyon systems were all important sources of turbidity currents on the Hatteras Abyssal Plain (Cleary and others, 1977; Elmore, 1976). Therefore, the suite of turbiditic sequences analyzed would not be expected to contain the consistent and homogeneous assemblages of < 2 μ minerals found in this study (Table 5). The standard deviations of relative abundance among the four clay minerals present in the turbidites are smaller than or equal to those for the hemipelagic sequences. Additionally, the < 2 μ mineral assemblage of the turbiditic sediment is identical to that of the hemipelagic sediment (Table 5).

The < 2 μ mineral assemblages in the turbidites on the abyssal plain can be best explained by the behavior of fines in turbidity currents. All turbidity currents require a continual supply of fluid in order to maintain their flows over long distances (Allen, 1971; Middleton, 1966). This fluid is incorporated into the current from the surrounding water by intermixing that occurs immediately behind the head

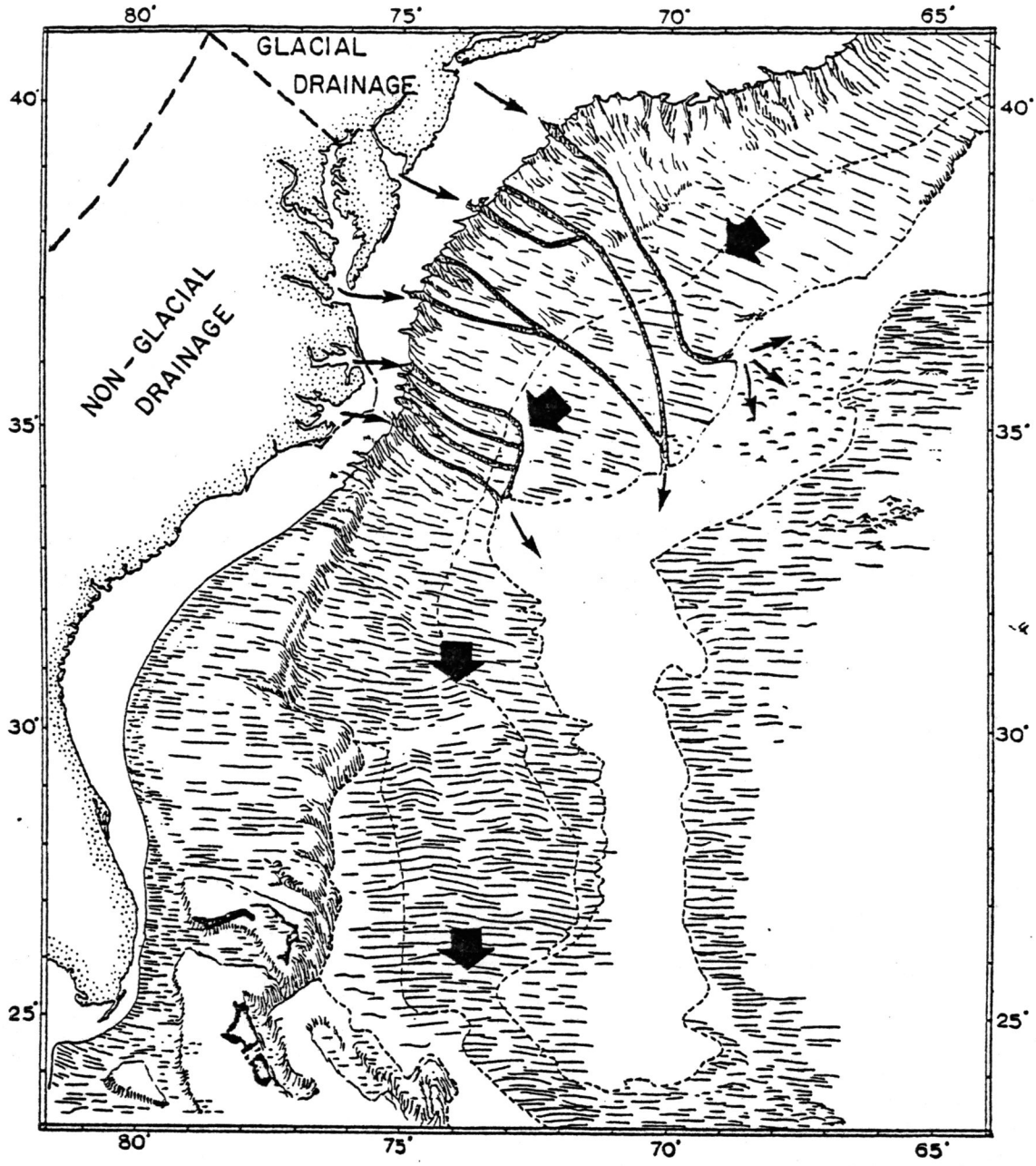

Figure 14. Source areas of turbidites on the Hatteras Abyssal Plain. The drainage provinces are from Hathaway (1972). Immediately west of the area labeled non-glacial drainage is the Mississippi drainage province. The large arrows indicate the flow direction of the Western Boundary Undercurrent. The small arrows indicate the flow of rivers across the shelf and the dispersal paths of turbidity currents on the basin floor during the Pleistocene (modified from Cleary and others, 1977).

of the current (Middleton, 1966; Figure 15A), and in tunnels at the toe of the current (Allen, 1971; Figure 15B). Fluid incorporated into a turbidity current contains a large amount of suspended sediment for the following reasons: 1) the disturbance created by the current erodes and suspends sediment, and 2) the bottom waters off most continental margins normally contain a large amount of suspended fine sediment in nephloid layers.

It is well known that sediment is lost from turbidity currents through eddy currents along the water-current interface (Middleton, 1966). Coarse sediment, lost in this way, falls back into the current. Finer sediment is either deposited after the current passes or is injected into nephloid layers, depending on the prevailing energy regime. Because of this flux of fines within a turbidity current, it is probable that fine sediment is constantly being exchanged (Figure 16). Turbidity currents expand in volume when the intake of fluid, usually laden with suspended sediment, is greater than the fluid and sediment lost through eddy currents and deposition (Allen, 1971). This dilution and exchange of fine sediments explains the homogeneity of clay minerals of the Hatteras Abyssal Plain.

Rupke and Stanley (1974), however, have successfully used the clay mineralogy of Baleric Abyssal Plain (Mediterranean Sea) cores to distinguish hemipelagic and turbiditic sequences. The dimensions of the depositional

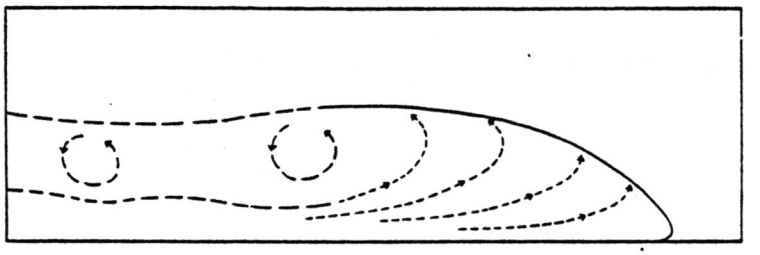

Figure 15A. Flow in the turbidity current head. Ambient fluids (clay-water mixtures) are incorporated into the current at the top, right behind the head (Middleton, 1966).

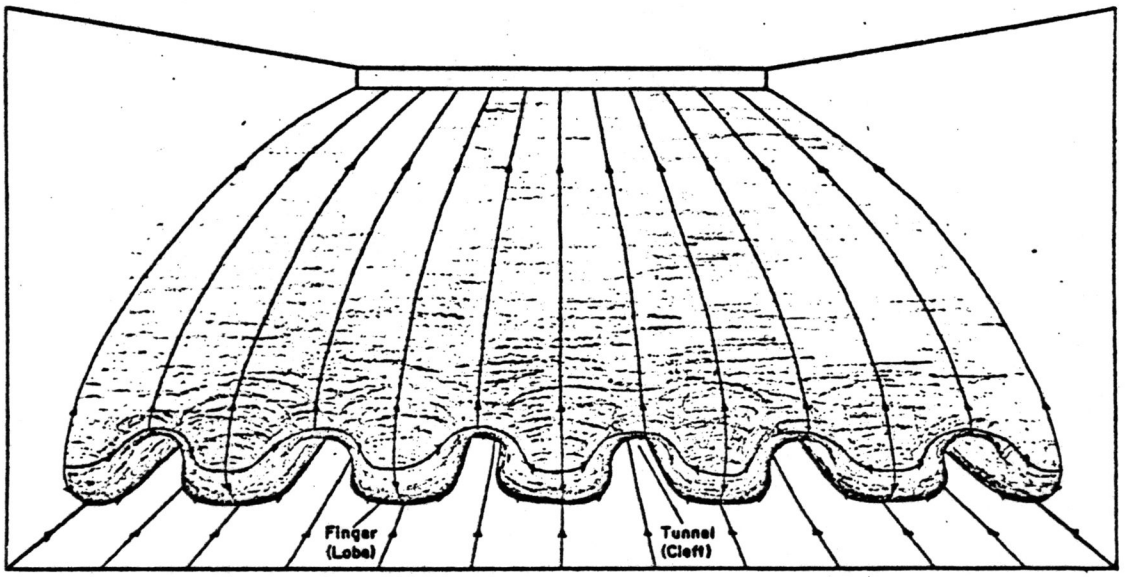

Figure 15B. Hypothetical reconstruction of a turbidity current head (Allen, 1971). Ambient fluid (clay-water mixture) is incorporated through the tunnels at the base of the current.

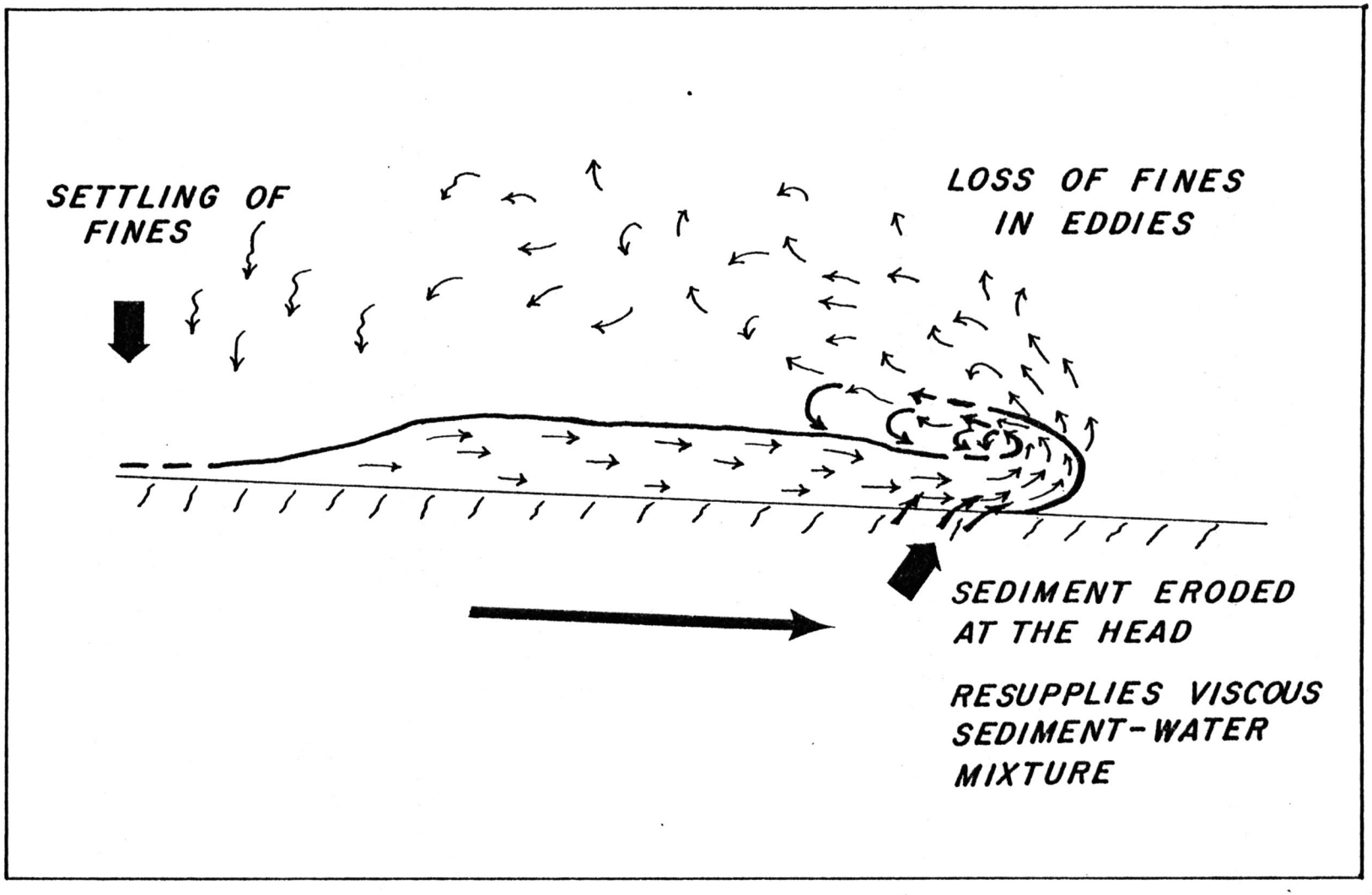

Figure 16. Schematic representation of fine sediment exchange. Ambient fluids (clay-water mixtures) are incorporated at the base of the current and at the water-current interface, just behind the head. Ambient fluids are lost at the tail and through eddy currents at the water-current interface.

basin and the geometry of the slope must affect the quantity of fine sediment exchange that occurs in a turbidity current. Therefore, the "clay mineral character" of a turbidity current is not always lost, even though it is probably always modified.

In this study the "clay mineral character" of the turbidites was not useful in distinguishing turbidites from hemipelagic sequences of in determining provenance. However, the greater abundance of dolomite in some turbidites serves as a tool for distinguishing both the mode of deposition and the provenance. The relative abundance of dolomite has been plotted against the relative abundance of quartz (Figure 17). Results here duplicate those of Beall (1969). The highest contents of dolomite and quartz occur in the turbidite sequences. The fact that not all turbidites contain abundant dolomite is apparently related to the source area. Most of the dolomite is thought to be a rock flour, created by glacial erosion (Beall, 1969). Consequently, dolomite should be most abundant in turbidites from the northern shelf. Elmore (1976) has proven that two of the turbidite sequences analyzed in this study are from the southern source area. Both of these turbidites contain small quantities of dolomite (Figure 17). While this is inconclusive, it adds strength to Beall's (1969) conclusion.

Dolomite also occurs in smaller quantities in hemi-

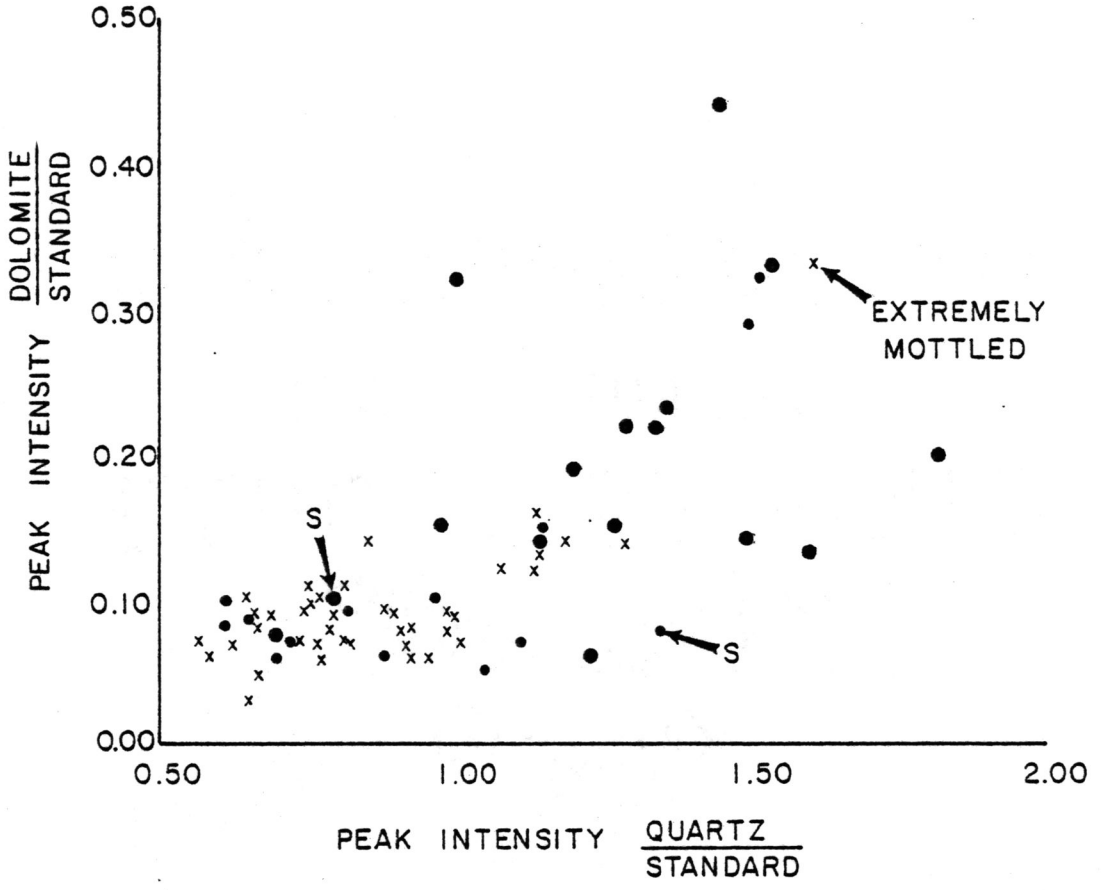

Figure 17. Abundance of dolomite and quartz in Hatteras Abyssal Plain Sediments. The peak intensity of dolomite is divided by the peak intensity (1.64 Å) of the silicon standard and plotted above against the peak intensity of quartz divided by the peak intensity of the silicon standard for each sample (x = hemipelagic samples; • = turbiditic sample of Bouma's sequence d and e; ● = turbiditic sample of Bouma's sequence a,b, and c). The turbiditic samples labeled "S" are from a southern source (non-glacial). The hemipelagic sequence labeled "extremely mottled" lies above a dolomite-rich turbidite and apparently has a large dolomite content because of the biogenic intermixing of the units.

pelagic sequences. Beall (1969) suggests this as evidence for the authigenic formation of dolomite in the deep sea. Evidence here suggests that none of the dolomite is authigenic. The dolomite content in the hemipelagic sediment does not increase up the cores even though the rate of hemipelagic deposition has slowed during the Holocene (Pilkey, personal communications, 1978). If dolomite was authigenic, its contribution to the sediment (and hence its quantity) would increase when the rate of hemipelagic deposition slowed. The only hemipelagic sequence which contains a large quantity of dolomite is extremely mottled and lies above a dolomite-rich turbidite (Appendix 7F). Bioturbation is capable of mixing turbiditic dolomite into the hemipelagic deposits. Dolomite in the hemipelagic sediment is more easily explained by bioturbation than by authigenic formation.

Because the dolomite occurs only in the silt fraction, and not in the clay fraction, it is reasonable to assume that the dolomite is coarse enough to fall back into the current, while finer sediment might be lost. This would explain why the original clay mineral assemblage in a turbite is lost while the dolomite is retained. It also suggests that in all turbidity currents there is a limit to the grain size of sediment that can be lost through eddy currents. Of turbidites in this study that contain dolomite, this size limit must occur somewhere in the silt sizes ($< 63\mu$ $> 2\mu$).

APPENDICES

APPENDIX 1

Sample Log

Munsell Color Codes Used in the Sample Log

color	code
Light Moderate Brown	5 YR 4/4
Moderate Brown	5 YR 3/4
Pale Yellowish Brown	10 YR 6/2
Moderate Yellowish Brown	10 YR 5/4
Dark Yellowish Brown	10 YR 4/2
Light Olive Brown	5 Y 4/4
Light Brown	5 YR 6/4
Pale Brown	5 YR 5/2
Dusky Brown	5 YR 2/2
Medium Gray	N 5
Light Greenish Gray	5 GY 8/1
Light Olive Gray	5 Y 6/1
Olive Gray	5 Y 4/1
Pale Olive	10 Y 6/2

Sample	Shipboard Description	Location	Depth
L1918-0cm	N. A.	32° 32. 5' N, 73° 01. 0' W	5200 m
L1921-0cm	N. A.	32° 02. 0' N, 72° 59. 0' W	5260 m
L2454-0cm	N. A.	34° 32. 5' N, 72° 54. 0' W	4560 m
L2455-0cm	N. A.	33° 24. 0' N, 72° 58. 5' W	4700 m
L2457-0cm	N. A.	34° 08. 0' N, 72° 03. 0' W	4770 m
22347-0cm	5 YR 4/4 lutite, highly mottled	34° 27. 7' N, 69° 16. 1' W	5256 m
24637-0cm	10 YR 6/2 lutite, mottled	33° 50. 0' N, 71° 05. 0' W	N. A.
24641-0cm	10 YR 6/2 lutite, mottled	33° 41. 5' N, 70° 34. 1' W	N. A.
24647-0cm	10 YR 6/2 lutite, mottled	32° 37. 6' N, 70° 11. 2' W	N. A.
24658-0cm	10 YR 6/2 lutite, mottled	31° 00. 0' N, 71° 13. 0' W	N. A.
24662-0cm	10 YR 6/12 lutite, mottled	30° 59. 5' N, 70° 08. 4' W	N. A.
27812-0cm	10 YR 5/4 lutite, mottled	30° 42. 1' N, 71° 35. 2' W	5354 m
27817-0cm	10 YR 5/4 lutite, mottled, w/hydrotroilite	29° 30. 0' N, 70° 15. 0' W	5377 m
27820-0cm	10 YR 5/4 lutite, mottled	28° 26' N, 69° 54. 5' W	5393 m
27825-0cm	10 YR 5/4 lutite, mottled	29° 48. 0' N, 70° 50. 0' W	5374 m
27826-0cm	10 YR 5/4 lutite, mottled	30° 22. 0' N, 70° 40. 0' W	5365 m
27831-0cm	10 YR 5/4 lutite, mottled	32° 17. 8' N, 70° 37. 5' W	5351 m
27834-0cm	10 YR 5/4 lutite, mottled	32° 25. 1' N, 71° 31. 1' W	5332 m
27840-0cm	10 YR 5/4 silty lutite, mottled	32° 36. 9' N, 71° 59. 0' W	5313 m
29195-0cm	5 YR 3/4 lutite	27° 25. 5' N, 70° 24. 9' W	5460 m
29204-0cm	5YR 3/4 lutite, mottled	25° 50. 0' N, 70° 05. 0' W	5446 m
29210-0cm	5 YR 6/4 lutite, mottled	24° 35. 0' N, 69° 56. 5' W	5510 m
30004-0cm	5 YR 3/4 lutite	34° 18. 0' N, 71° 46. 0' W	4670 m
30006-0cm	5 YR 3/4 lutite	34° 49. 1' N, 70° 54. 8' W	4665 m
30008-0cm	5 YR 3/4 lutite, mottled	35° 19. 3' N, 71° 00. 7' W	4350 m
30013-0cm	5 YR 3/4 lutite, w/foraminifera	35° 35. 6' N, 69° 54. 0' W	4680 m

Sample	Shipboard Description	Location	Depth
27825-0cm	10 YR 5/4 lutite, mottled	29° 48.0' N, 70° 50.0' W	5374 m
2-5cm	10 YR 5/4 lutite, mottled		
5-10cm	10 YR 5/4 lutite, mottled		
10-15cm	10 YR 5/4 lutite, mottled		
15-19cm	5 YR 3/4 lutite, mottled		
19-20cm	10 YR 4/2 silt		
20-25cm	5 YR 5/2 lutite		
25-30cm	5 YR 5/2 lutite		
30-35cm	N 5 lutite, mottled		
35-40cm	N 5 lutite, mottled		
40-45cm	N 5 lutite, mottled		
45-50cm	N 5 lutite, mottled		
50-55cm	N 5 lutite, mottled		
55-60cm	N 5 lutite, mottled		
60-65cm	N 5 lutite, mottled		
65-70cm	N 5 lutite, mottled		
70-75cm	N 5 lutite, mottled		
75-80cm	5 Y 6/1 lutite		
80-83cm	5 Y 6/1 lutite		
83-86cm	5 Y 6/1 lutite		
86-90cm	5 Y 6/1 lutite		
90-95cm	5 Y 6/1 lutite		
95-100cm	5 Y 6/1 lutite		
100-105 cm	5 Y 4/1 lutite		
105-110 cm	5 Y 4/1 lutite		
140 cm	5 Y 6/1 lutite		

Sample Log (cont.)

Sample	Shipboard Description	Location	Depth
27825-160cm	5 Y 4/1 silt	29° 48.0' N, 70° 50.0' W	5374 m
-220cm	N 5 silt		
-290cm	10 Y 6/2 lutite, extremely mottled		
-310cm	N 5 silt		
-320cm	N 5 silty lutite, w/foraminifera		
-350cm	5 Y 4/1 lutite		
-390cm	10 YR 5/4 lutite, w/hydrotroilite		
-400cm	10 YR 5/4 lutite, w/hydrotroilite		
-430cm	5 Y 6/1 lutite		
-460cm	5 Y 6/1 lutite, w/silt		
-470cm	5 Y 6/1 lutite		

Sample Log (cont.)

Sample	Shipboard Description	Location	Depth
27834-0cm	10 YR 5/4 lutite, mottled	32° 25.1' N, 71° 31.1' W	5332 m
-20cm	10 YR 6/2 silty lutite, mottled		
-70cm	5 Y 6/1 silty lutite, w/foraminifera		
-230cm	5 Y 4/1 silty fine sand, foraminifera		
-260cm	5 Y 6/1 lutite		
-310cm	5 Y 4/1 silt		
-340cm	5 Y 6/1 lutite, w/hydrotroilite bands		
-350cm	5 Y 6/1 lutite, w/hydrotroilite bands		
-380cm	5 Y 6/1 lutite, w/hydrotroilite bands		
-410cm	5 Y 6/1 lutite		
-450cm	5 Y 6/1 lutite, mottled		
-470cm	5 Y 6/1 lutite, w/ hydrotroilite bands		

Sample Log (cont.)

Sample	Shipboard Description	Location	Depth
29204-0cm	5 YR 3/4 lutite, mottled	25° 50.0' N, 70° 05.0' W	5446 m
-20cm	5 YR 6/4 lutite, mottled		
-40cm	5 Y 4/4 lutite, silty		
-90cm	5 YR 5/2 lutite, mottled		
-120cm	5 YR 5/2 lutite, mottled		
-150cm	5 YR 6/4 lutite, mottled		
-170cm	5 YR 3/4 lutite, mottled		
-220cm	5 Y 4/4 silty lutite, w/mica		
-240cm	5 YR 5/2 lutite, mottled, w/hydrotroilite		
-270cm	5 YR 6/4 lutite, mottled		
-290cm	5 YR 3/4 lutite, mottled		
-340cm	5 YR 2/2 silt		
-360cm	5 Y 4/4 silt		
-390cm	5 YR 6/4 lutite, mottled, w/hydrotroilite		
-420cm	5 YR 6/4 lutite, mottled		
-440cm	5 YR 6/4 lutite, mottled		
-470cm	5 GY 8/1 lutite, mottled, w/hydrotroilite		
-510cm	5 GY 8/1 lutite, silty, w/mica		
-530cm	5 YR 5/2 lutite, mottled, w/hydrotroilite		
-580-600cm	N 5 very coarse silt, w/mica		
-610cm	5 Y 4/4 lutite, silty, w/mica		
-650-680cm	5 Y 4/4 sandy coarse silt, w/mica		

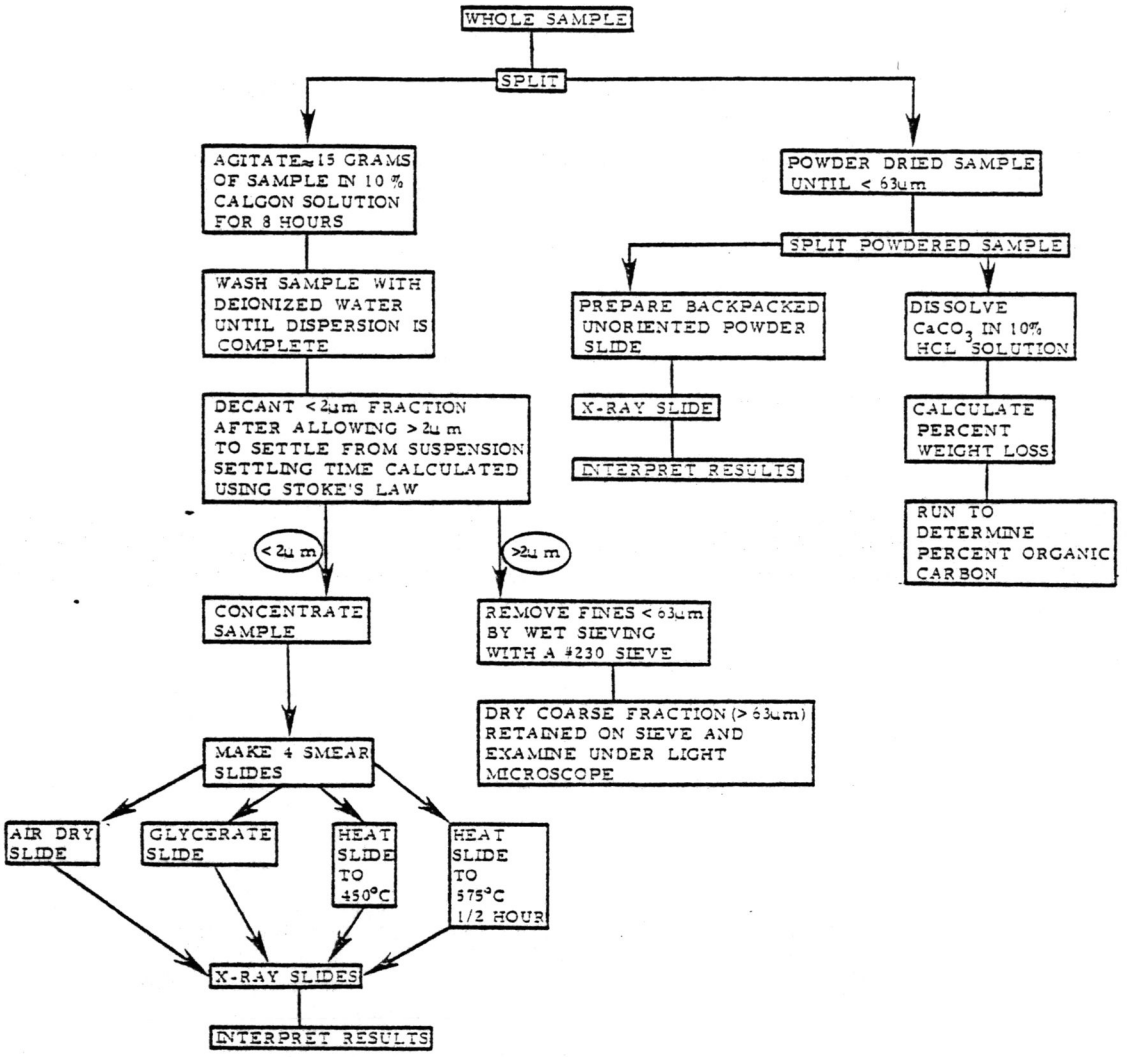

Appendix 2. Flow chart of the analytical procedure used in this study.

APPENDIX 3

Percent Carbonate and Organic Carbon

Sample	% Organic Carbon	% Carbonate
L1918-0cm	0.35	21
L1921-0cm	0.16	13
L2454-0cm	0.83	38
L2455-0cm	0.28	23
L2457-0cm	0.43	42
22347-0cm	0.50	37
24637-0cm	0.35	25
24641-0cm	0.23	16
24647-0cm	0.51	28
24658-0cm	0.31	16
24662-0cm	0.53	25
27812-0cm	0.23	15
27817-0cm	0.43	16
27820-0cm	0.39	17
27825-0cm	0.45	19
27826-0cm	0.49	21
27831-0cm	0.45	26
27834-0cm	0.38	21
27840-0cm	0.35	24
29195-0cm	0.23	15
29204-0cm	0.27	20
29210-0cm	0.35	13

Percent Carbonate and Organic Carbon

Sample	% Organic Carbon	% Carbonate
27825-0cm	0.45	19
2-5cm	0.39	21
25-30cm	0.42	15
86-90cm	0.27	17
90-95cm	0.38	14
105-110cm	0.69	17
160cm	0.41	19
220cm	0.46	12
290cm	0.19	9
310cm	0.35	7
320cm	0.38	27
350cm	0.34	10
390cm	0.39	9
400cm	0.69	13
430cm	0.53	10
460cm	0.45	9
470cm	0.49	9

Percent Carbonate and Organic Carbon

Sample	% Organic Carbon	% Carbonate
27834-0cm	0.38	21
20cm	0.34	30
70cm	0.23	11
230cm	0.39	11
260cm	0.38	11
310cm	0.35	7
340cm	0.26	1
350cm	0.38	21
380cm	0.51	9
410cm	0.46	12
450cm	0.41	9
470cm	0.53	11

Percent Carbonate and Organic Carbon

Sample	% Organic Carbon	% Carbonate
29204-0cm	0.27	20
20cm	0.23	11
40cm	0.80	12
90cm	0.23	9
120cm	0.30	10
150cm	0.26	14
170cm	0.08	11
220cm	0.46	17
240cm	0.15	12
270cm	0.19	11
290cm	0.15	5
340cm	0.00	13
360cm	0.15	13
390cm	0.12	10
420cm	0.23	10
440cm	0.15	6
470cm	0.11	9
510cm	0.68	17
530cm	0.30	8
580-560cm	0.04	17
610cm	0.19	16
650-680cm	0.15	15

APPENDIX 4

Mineral composition of the <2μ fraction of the surficial sediments.

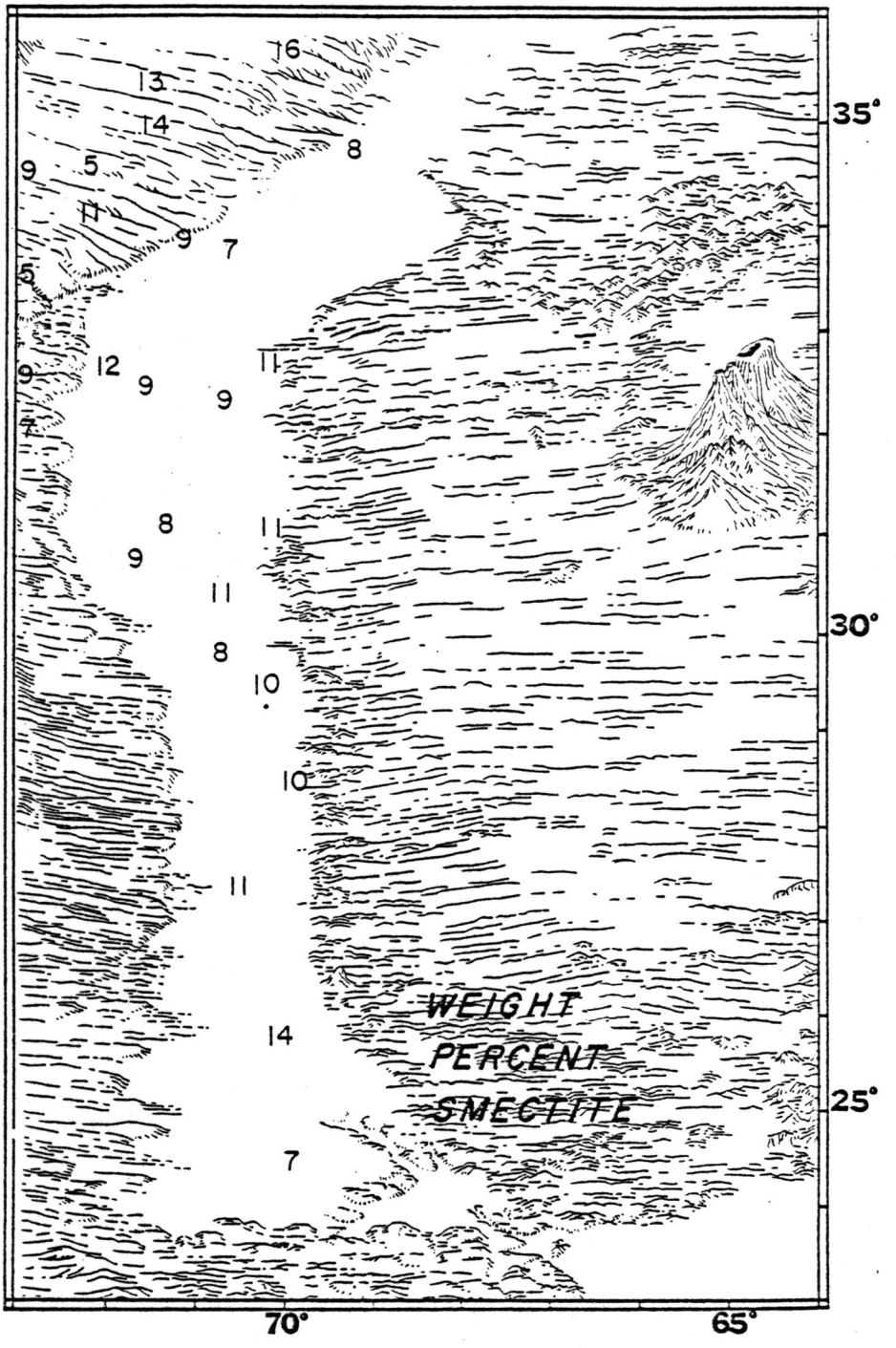

Appendix 4A. Weight percent smectite in the < 2μ fraction of surface samples from the continental rise and abyssal plain.

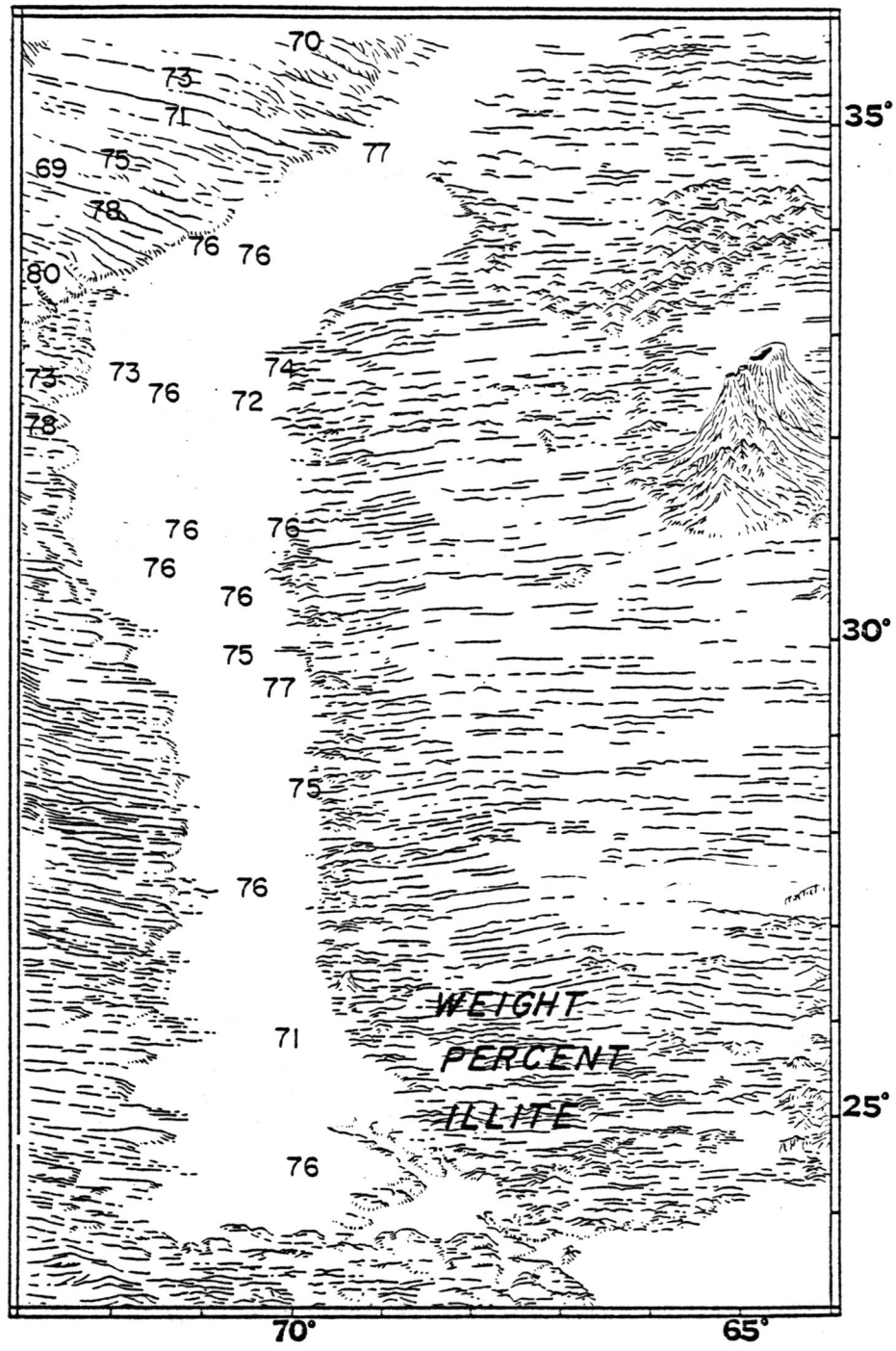

Appendix 4B. Weight percent illite in the <2μ fraction of surface samples from the continental rise and abyssal plain.

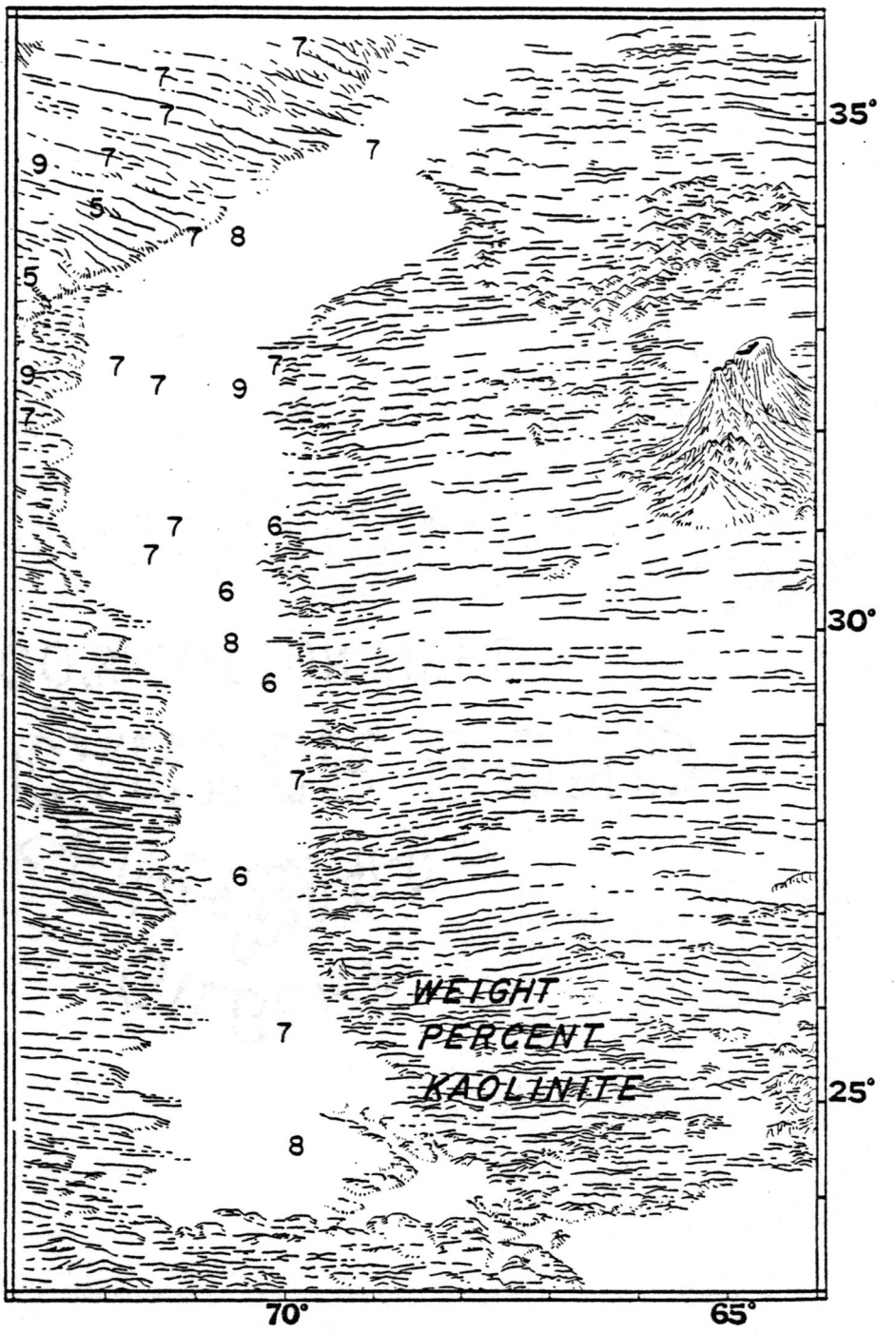

Appendix 4C. Weight percent kaolinite in the <2μ fraction of surface samples from the continental rise and abyssal plain.

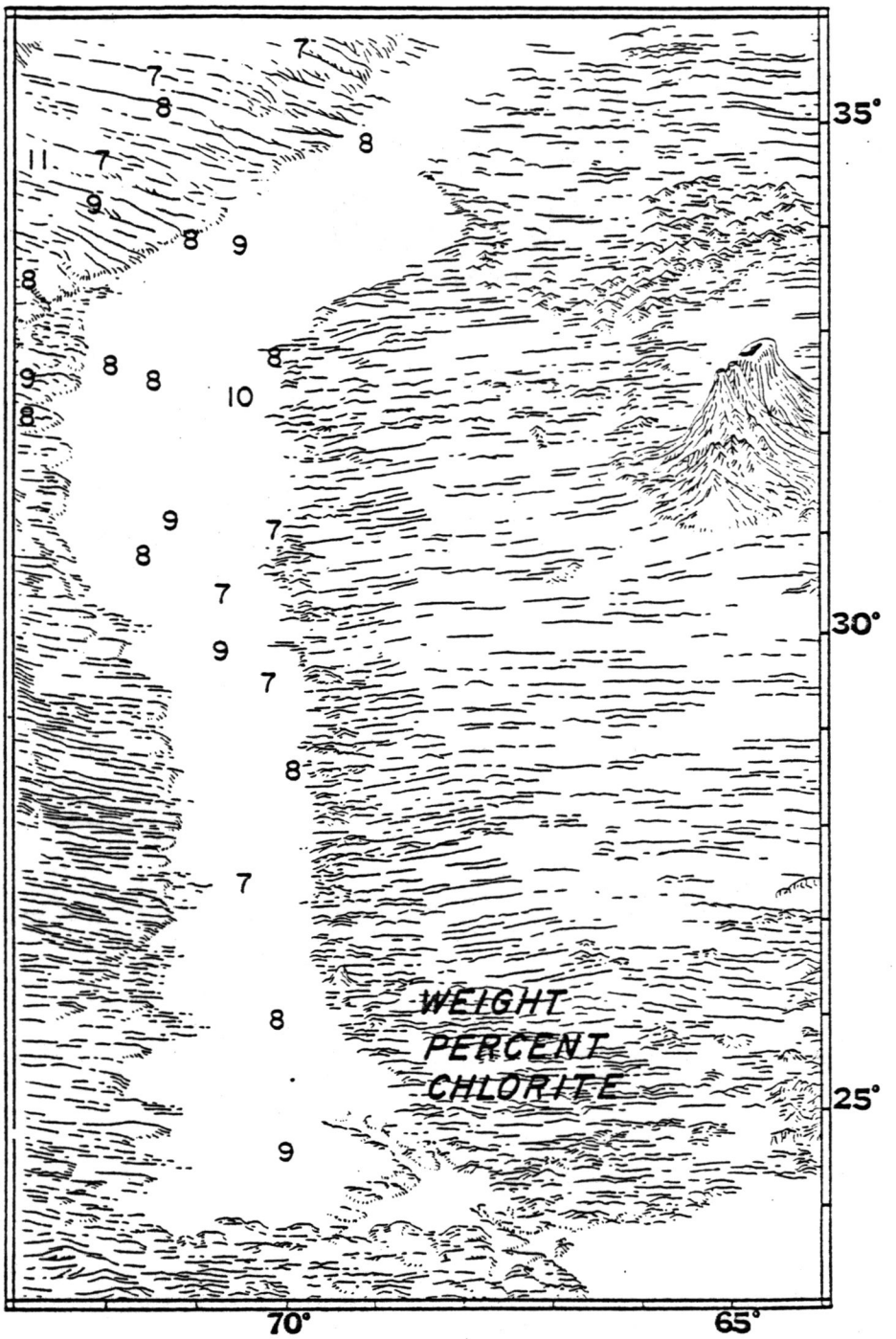

Appendix 4D. Weight percent chlorite in the <2 μ fraction of surface samples from the continental rise and abyssal plain.

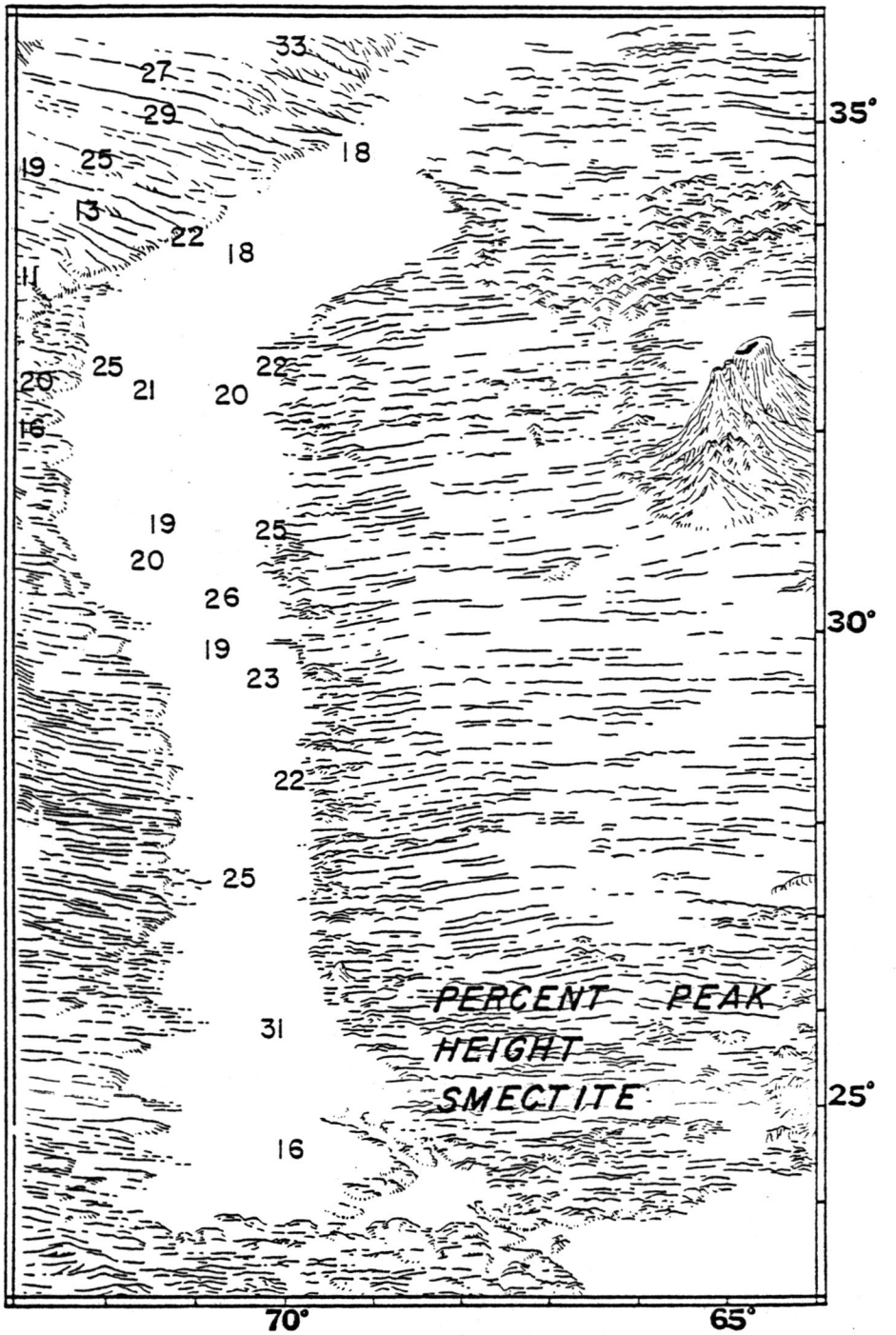

Appendix 4E. Percent peak height of smectite in the <2μ fraction of surface samples from the continental rise and abyssal plain.

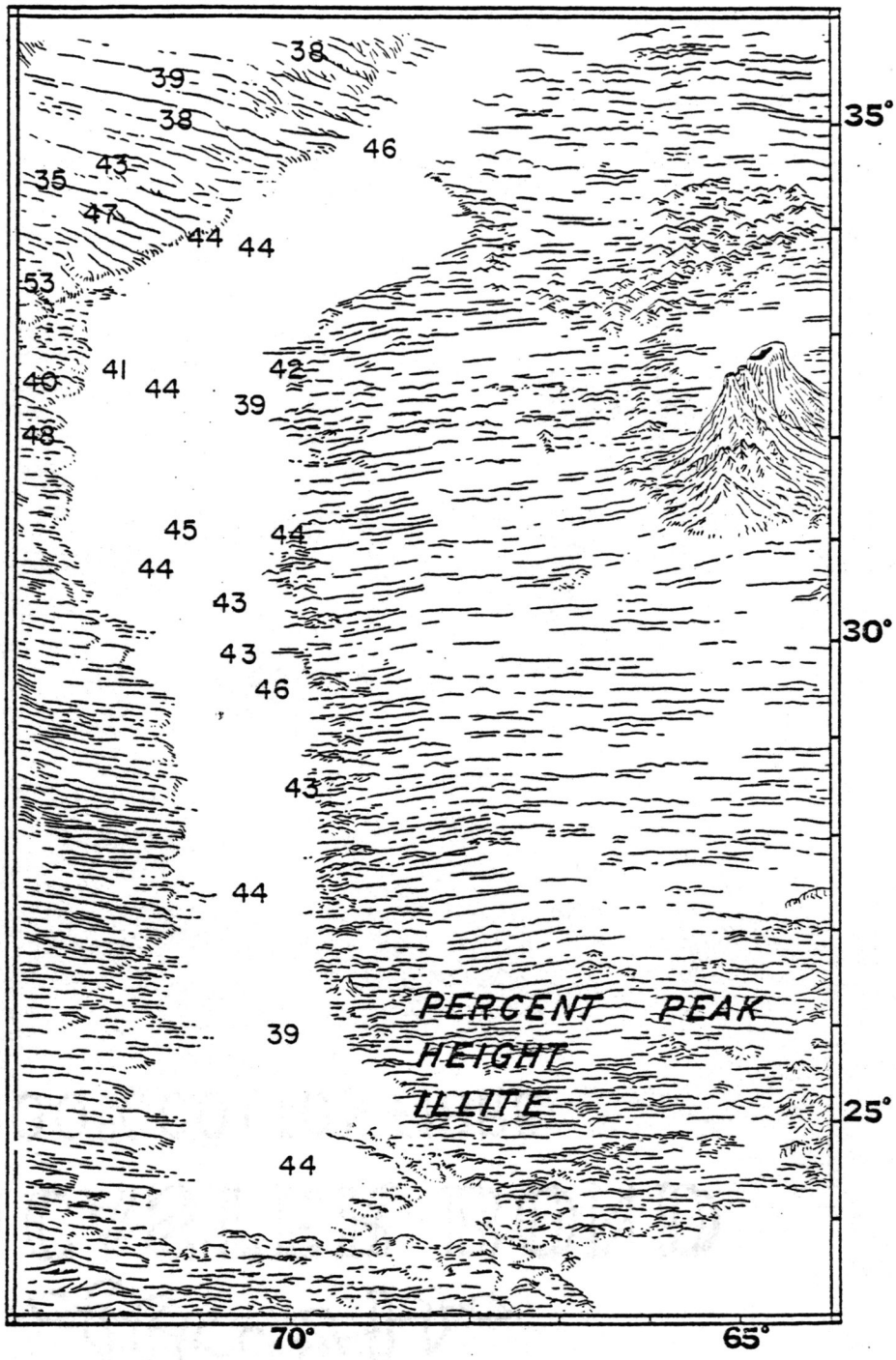

Appendix 4F. Percent peak height of illite in the $<2\mu$ fraction of surface samples from the continental rise and abyssal plain.

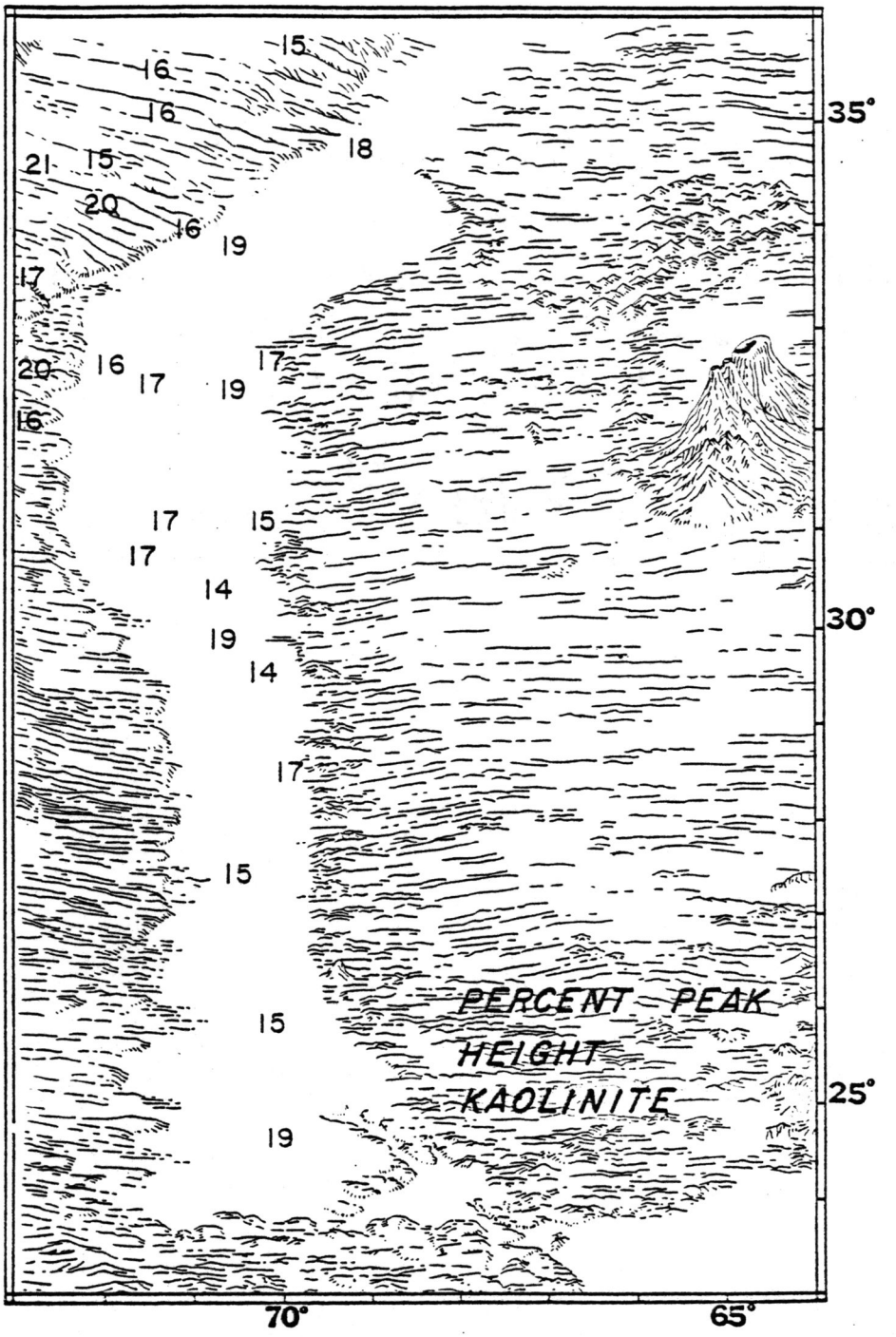

Appendix 4G. Percent peak height of kaolinite in the <2μ fraction of surface samples from the continental rise and abyssal plain.

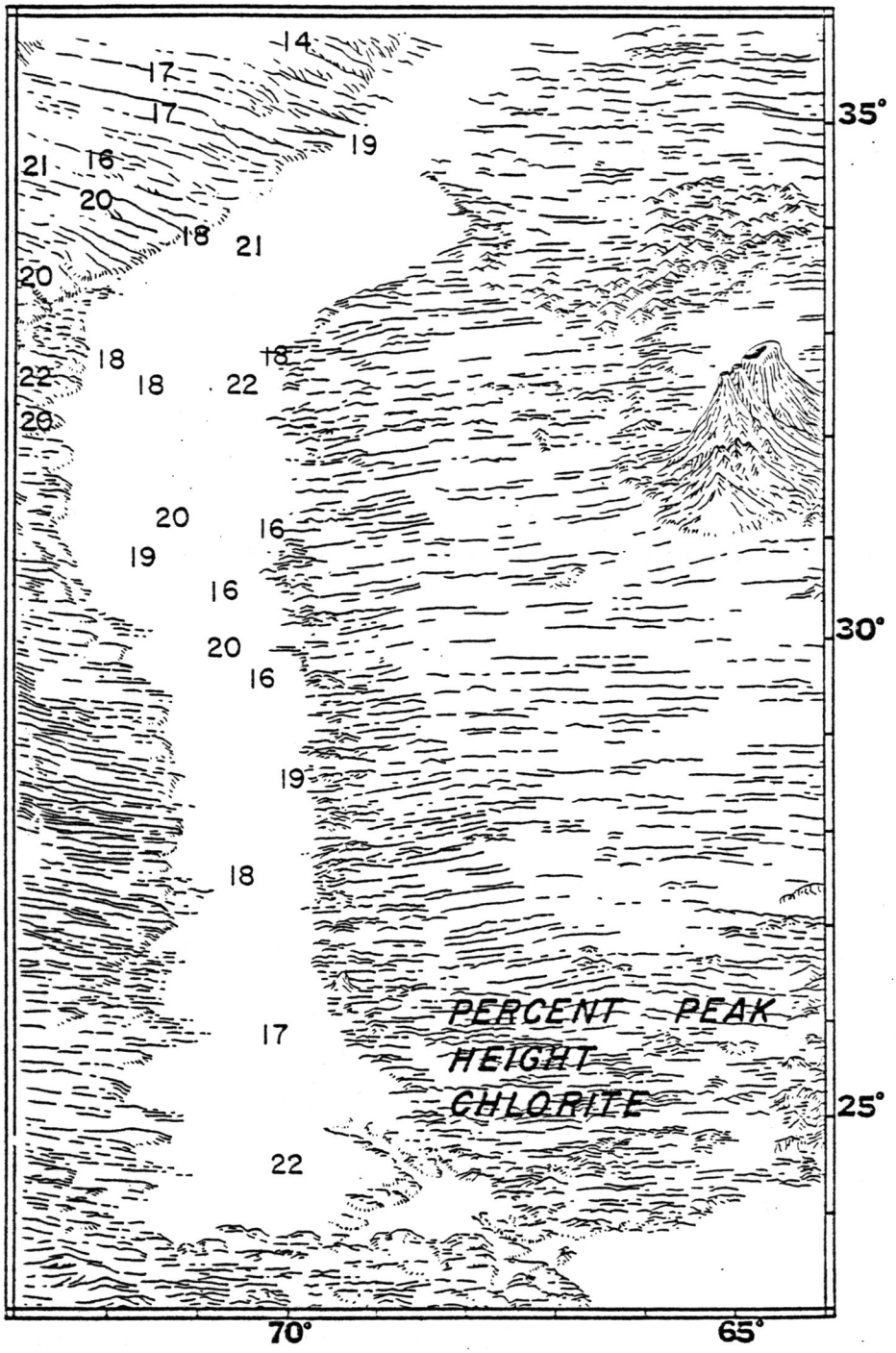

Appendix 4H. Percent peak height of chlorite in the $<2\mu$ fraction of surface samples from the continental rise and abyssal plain.

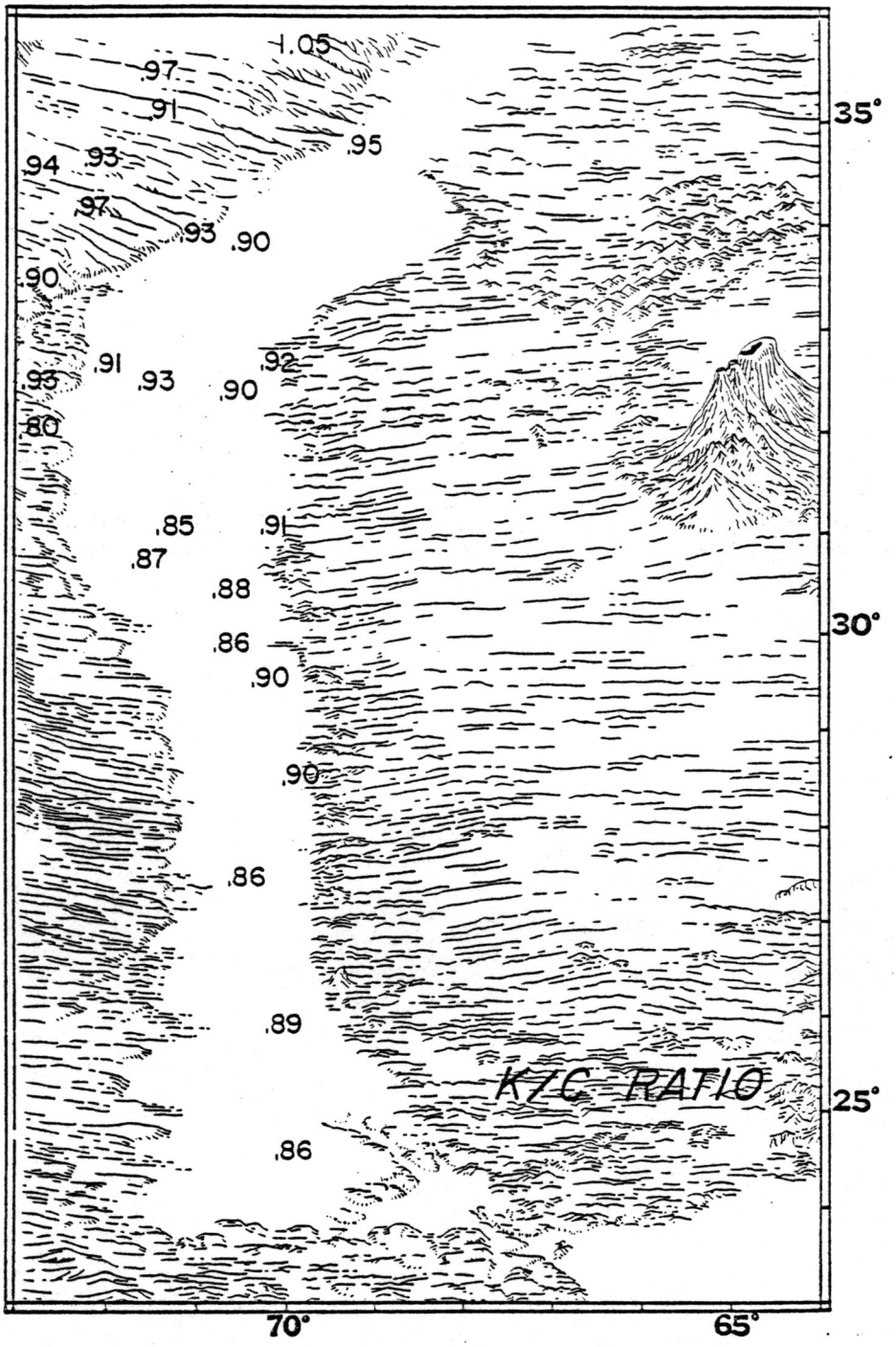

Appendix 4I. The ratio of the peak height of kaolinite, divided by the peak height of chlorite for the $<2\mu$ fraction of surface samples from the rise and abyssal plain.

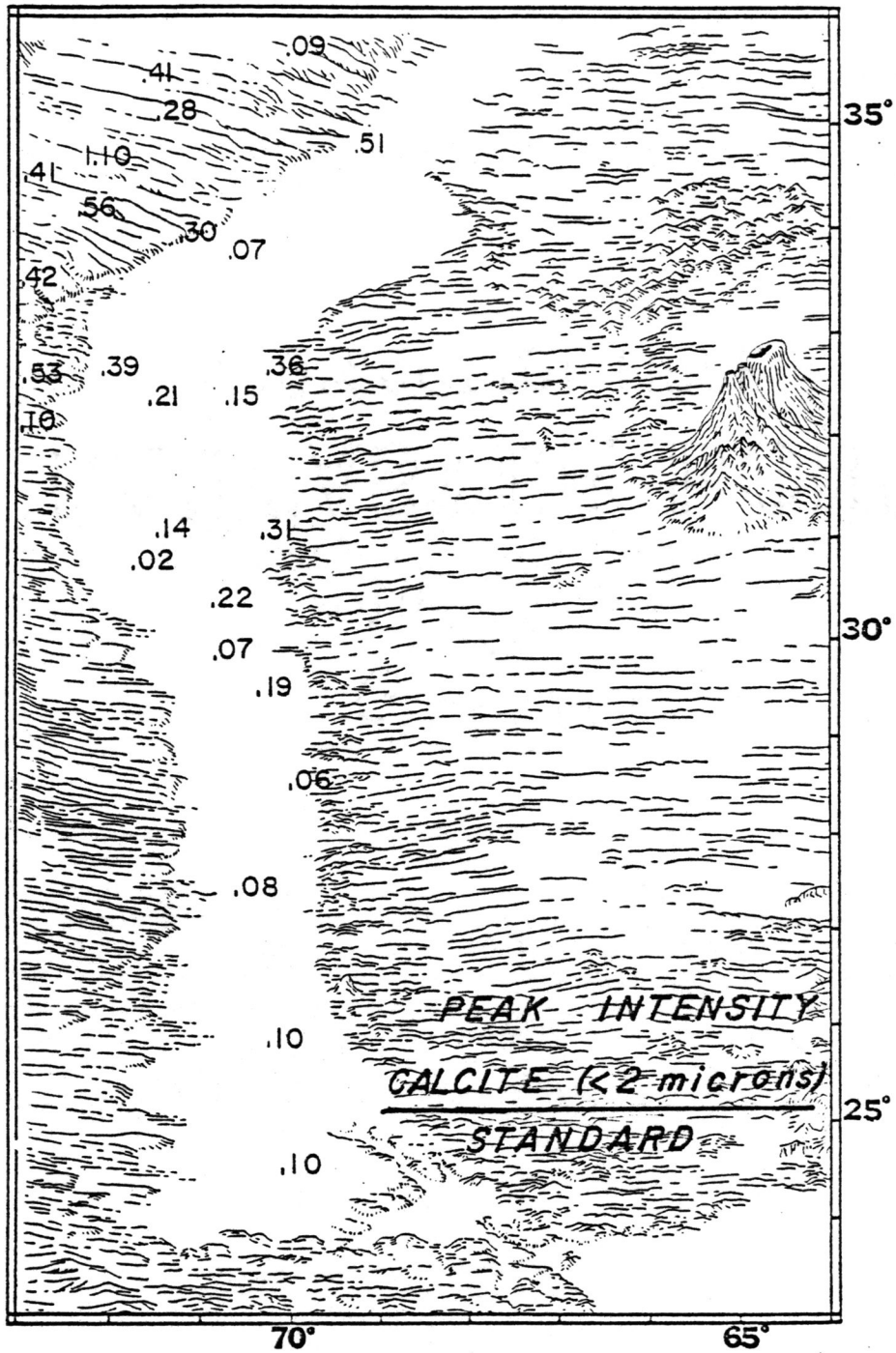

Appendix 4J. The peak intensity of calcite, for the $< 2\,\mu$ fraction of surface samples from the continental rise and abyssal plain, divided by the peak intensity of the quartz standard.

Appendix 4K. Non-clay minerals (< 2μ fraction), Peak Intensity (mineral)/Peak Intensity (standard)

Sample	Feldspar	Calcite	Quartz
L1918-0 cm	0.02	0.46	0.02
L1921-0 cm	0	0.06	0.06
L2454-0 cm	0.05	0.32	0.04
L2455-0 cm	0.01	0.41	0.05
L2457-0 cm	0.05	0.60	0
22347-0 cm	0	0.52	0.08
24637-0 cm	0.04	0.28	0
24641-0 cm	0.05	0	0
24647-0 cm	0.08	0.33	0
24658-0 cm	0	0.12	0.04
24662-0 cm	0	0.31	0.08
27812-0 cm	0	0	0.02
27817-0 cm	0.06	0.17	0
27820-0 cm	0	0	0.04
27825-0 cm	0.01	0.07	0.06
27826-0 cm	0.06	0.19	0.06
27831-0 cm	0.04	0.13	0
27834-0 cm	0.04	0.20	0
27840-0 cm	0.04	0.37	0.03
29195-0 cm	0	0.06	0.04
29204-0 cm	0.06	0.08	0.06
29210-0 cm	0.06	0.10	0
30004-0 cm	0.18	0.97	0.03
30006-0 cm	0.04	0.33	0.09
30008-0 cm	0.05	0.40	0.03
30013-0 cm	0.05	0.09	0

APPENDIX 5

Composition of the whole-surface samples.

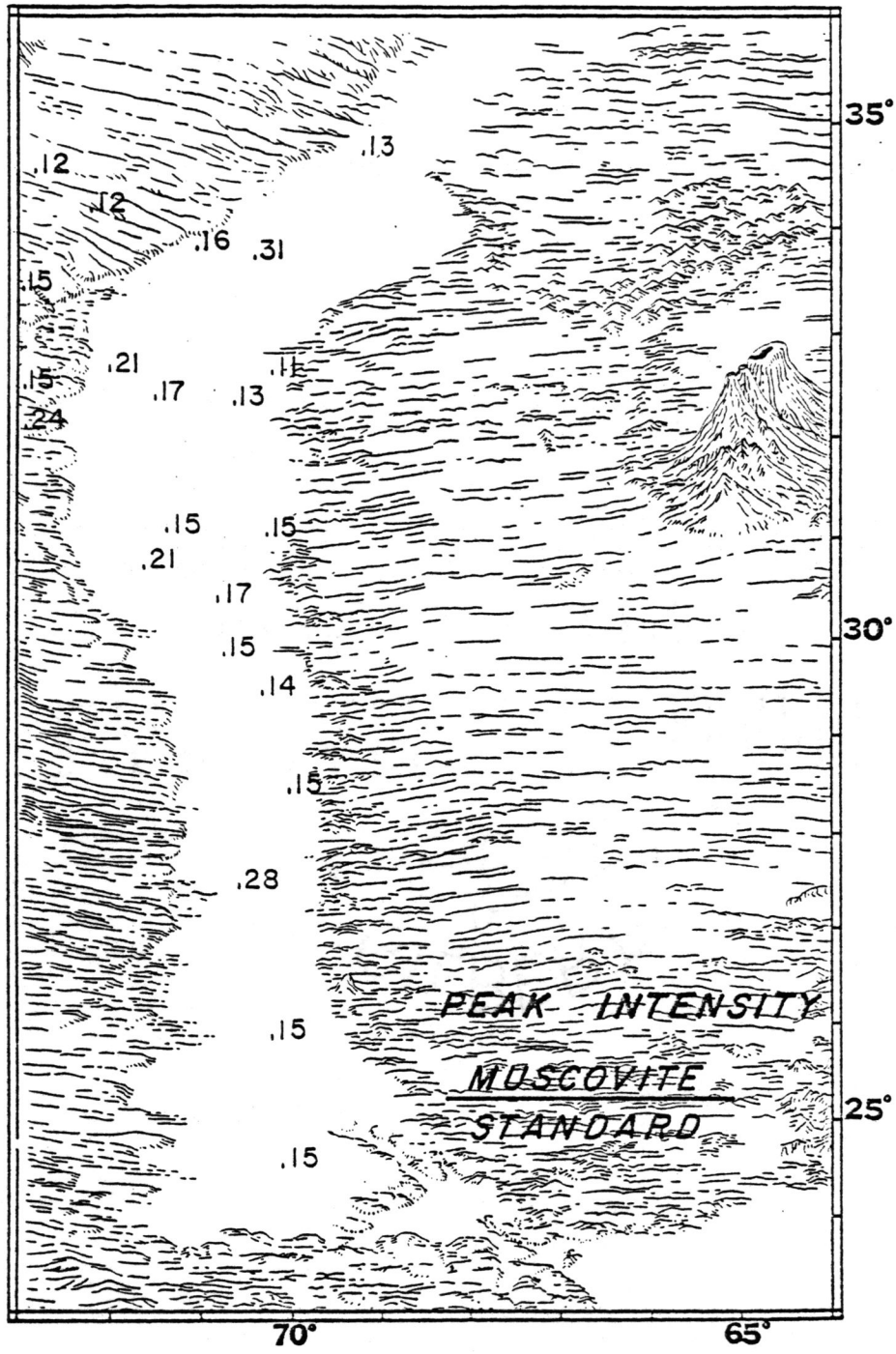

Appendix 5A. The peak intensity of muscovite divided by the peak intensity of the silicon standard (obtained by the whole-sample X-ray analyses of surface samples from the continental rise and abyssal plain).

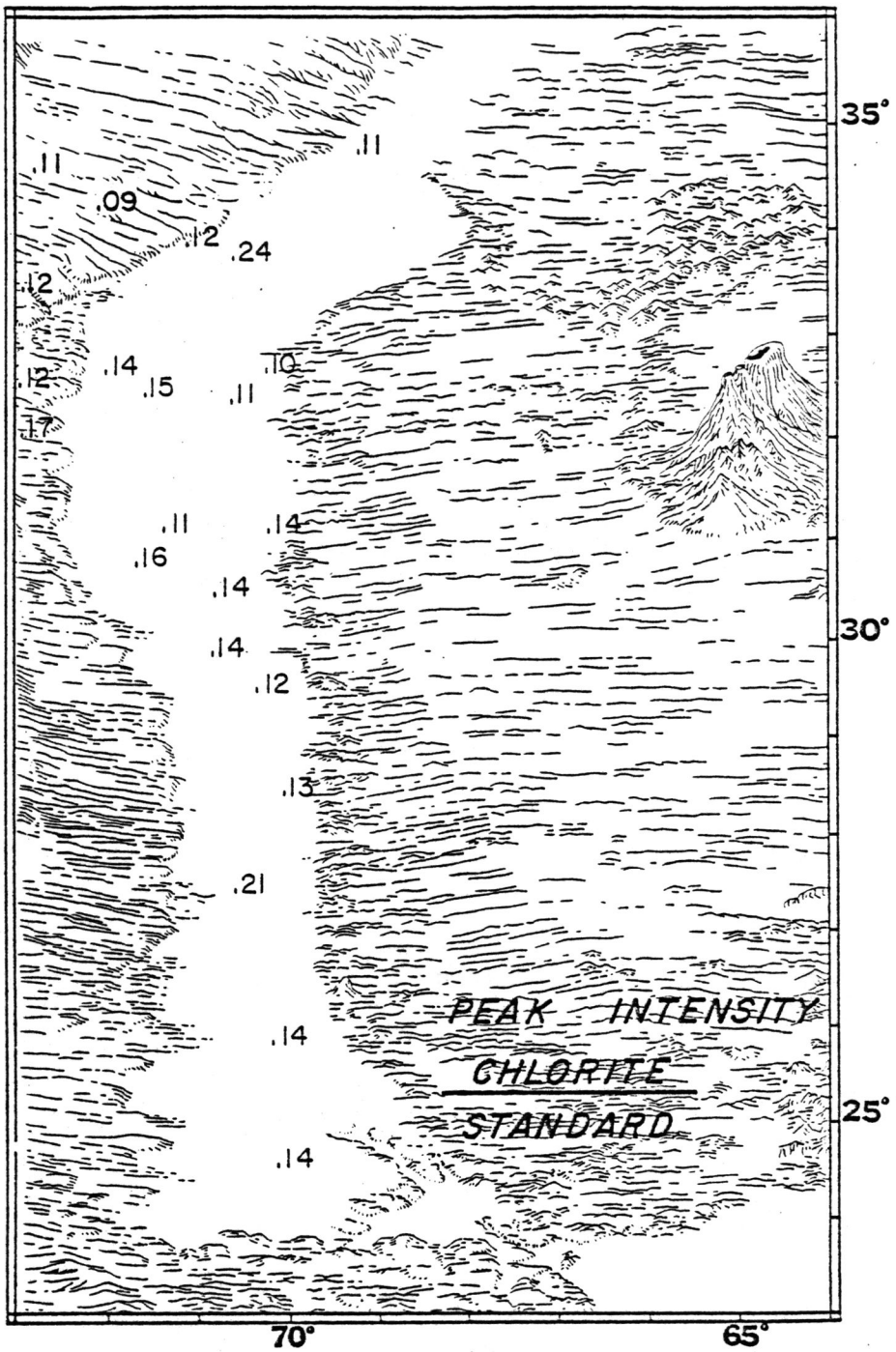

Appendix 5B. The peak intensity of chlorite divided by the peak intensity of the silicon standard (obtained by the whole-sample X-ray analyses of surface samples from the continental rise and abyssal plain).

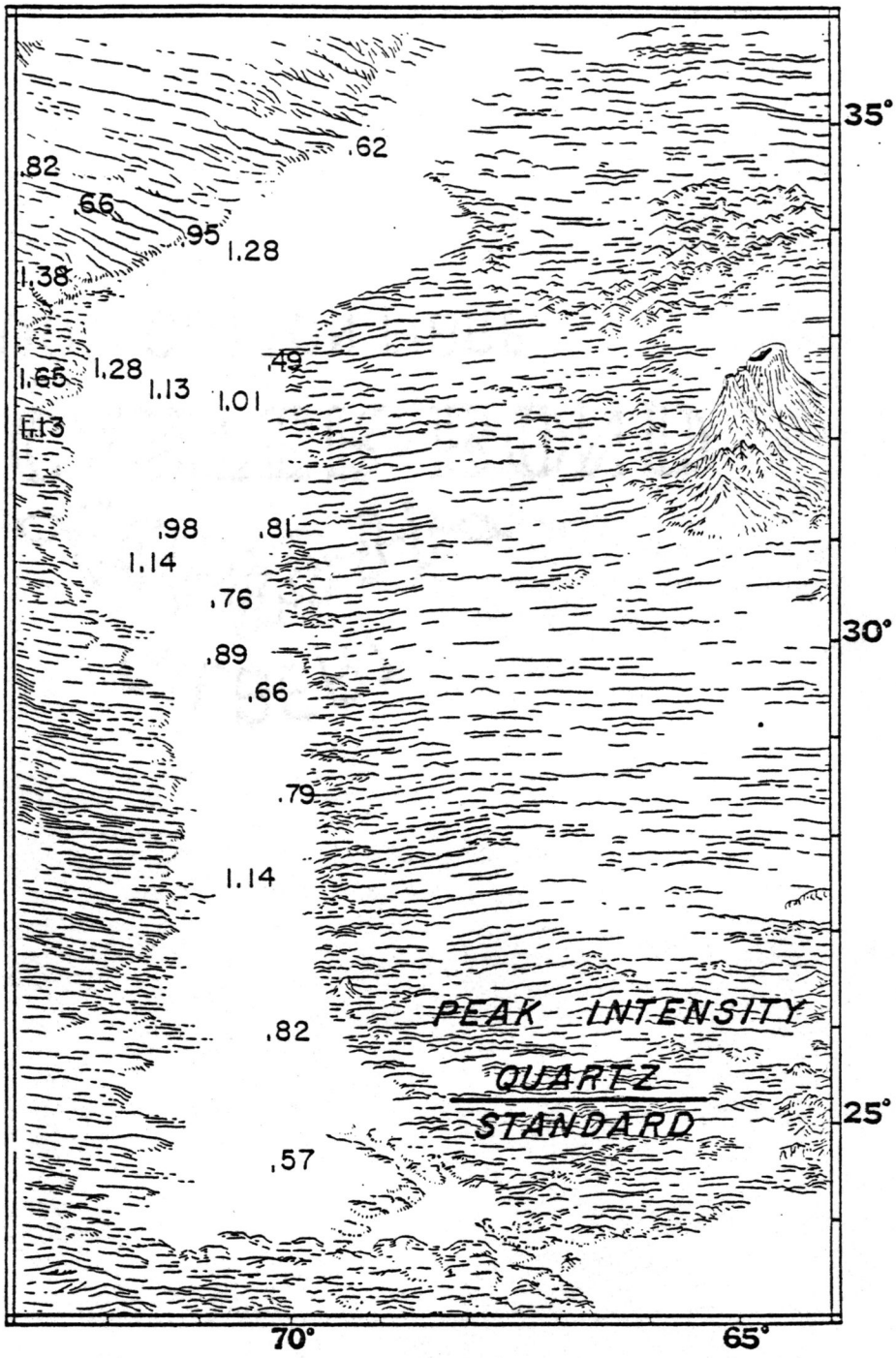

Appendix 5C. The peak intensity of quartz divided by the peak intensity of the silicon standard (obtained by the whole-sample X-ray analyses of surface samples from the continental rise and abyssal plain).

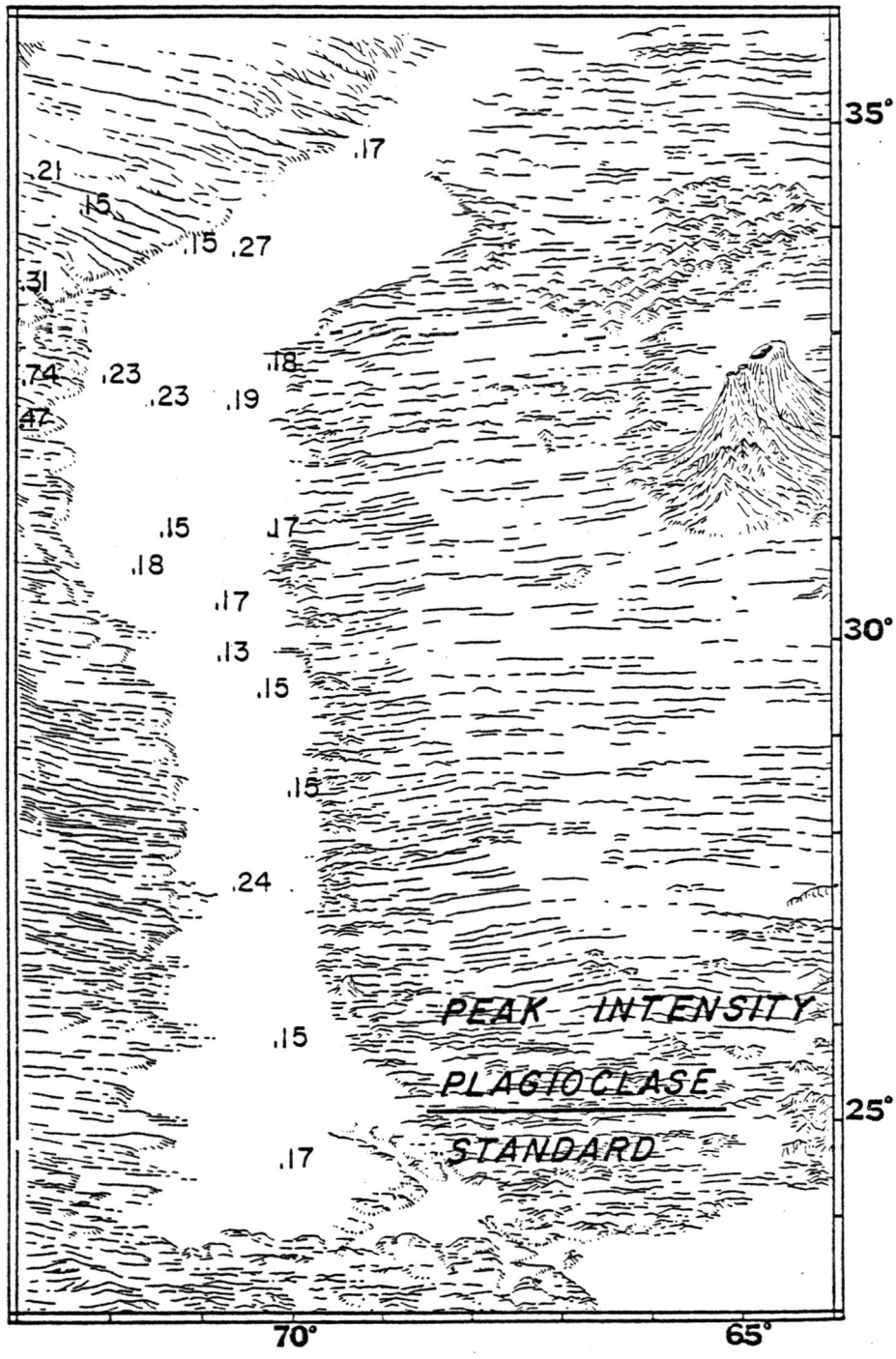

Appendix 5D. The peak intensity of plagioclase divided by the peak intensity of the silicon standard (obtained by the whole-sample X-ray analyses of surface samples from the continental rise and abyssal plain).

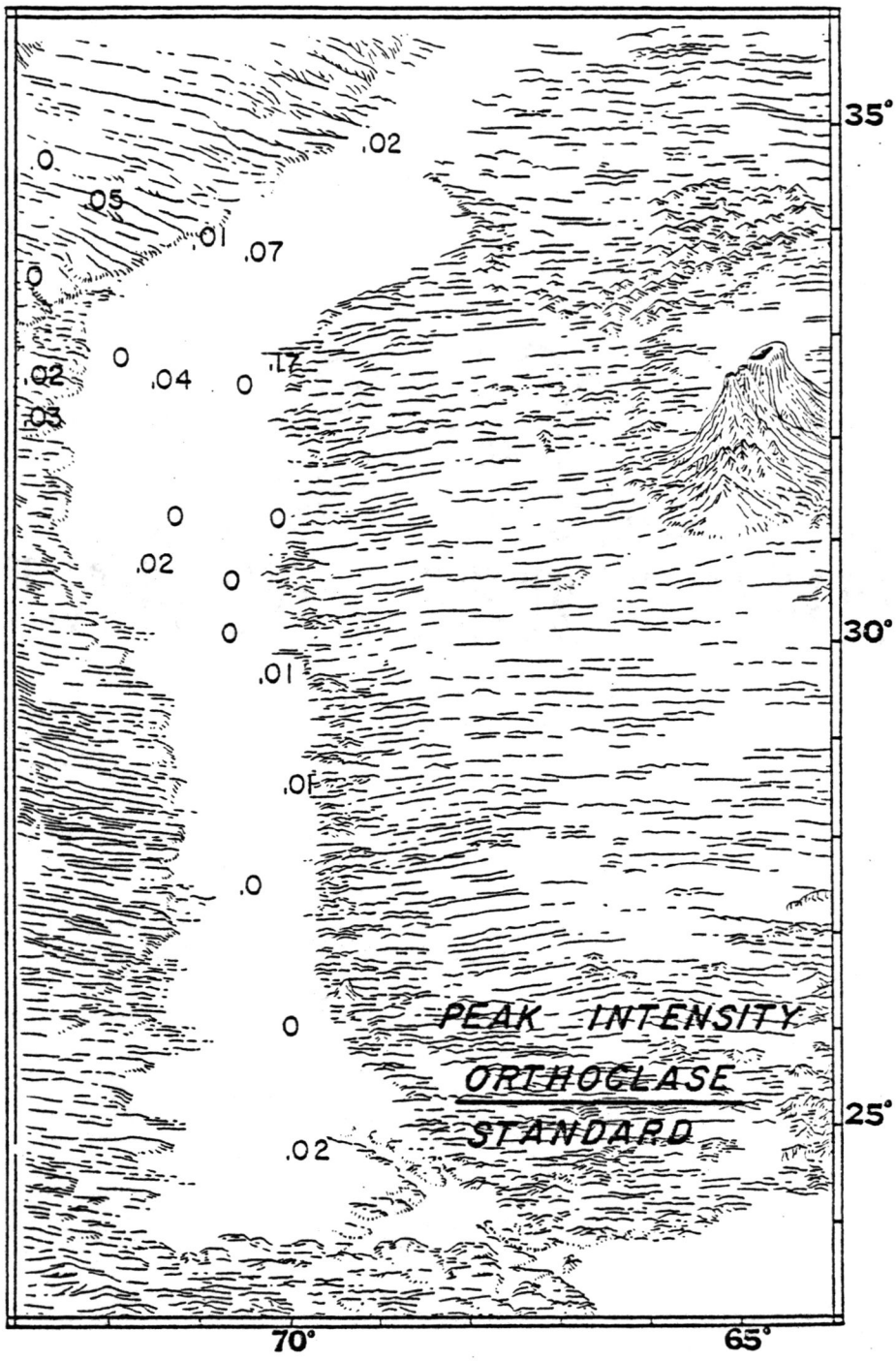

Appendix 5E. The peak intensity of orthoclase divided by the peak intensity of the silicon standard (obtained by the whole-sample X-ray analyses of surface samples from the continental rise and abyssal plain).

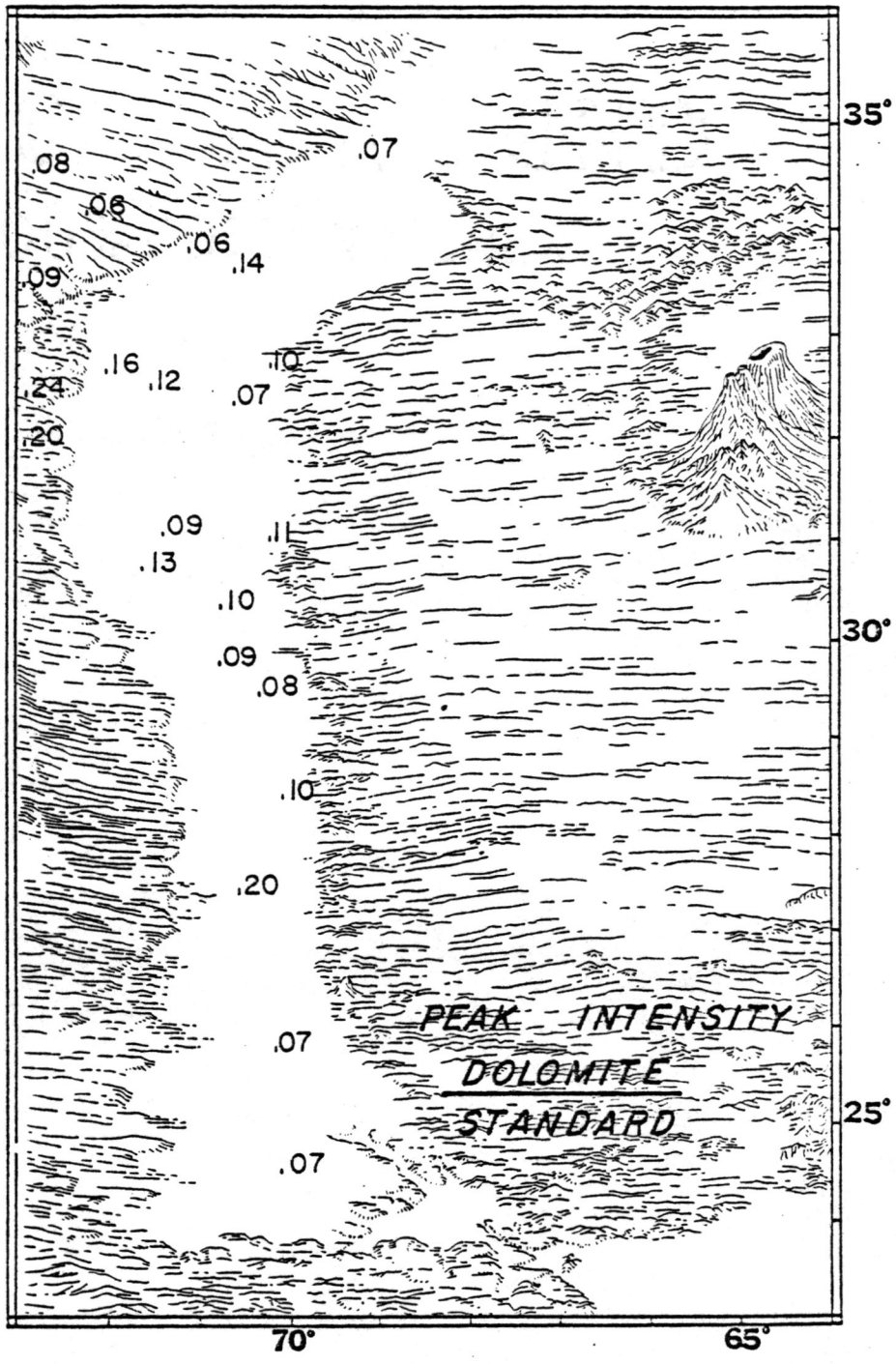

Appendix 5F. The peak intensity of dolomite divided by the peak intensity of the silicon standard (obtained by the whole-sample X-ray analyses of surface samples from the continental rise and abyssal plain).

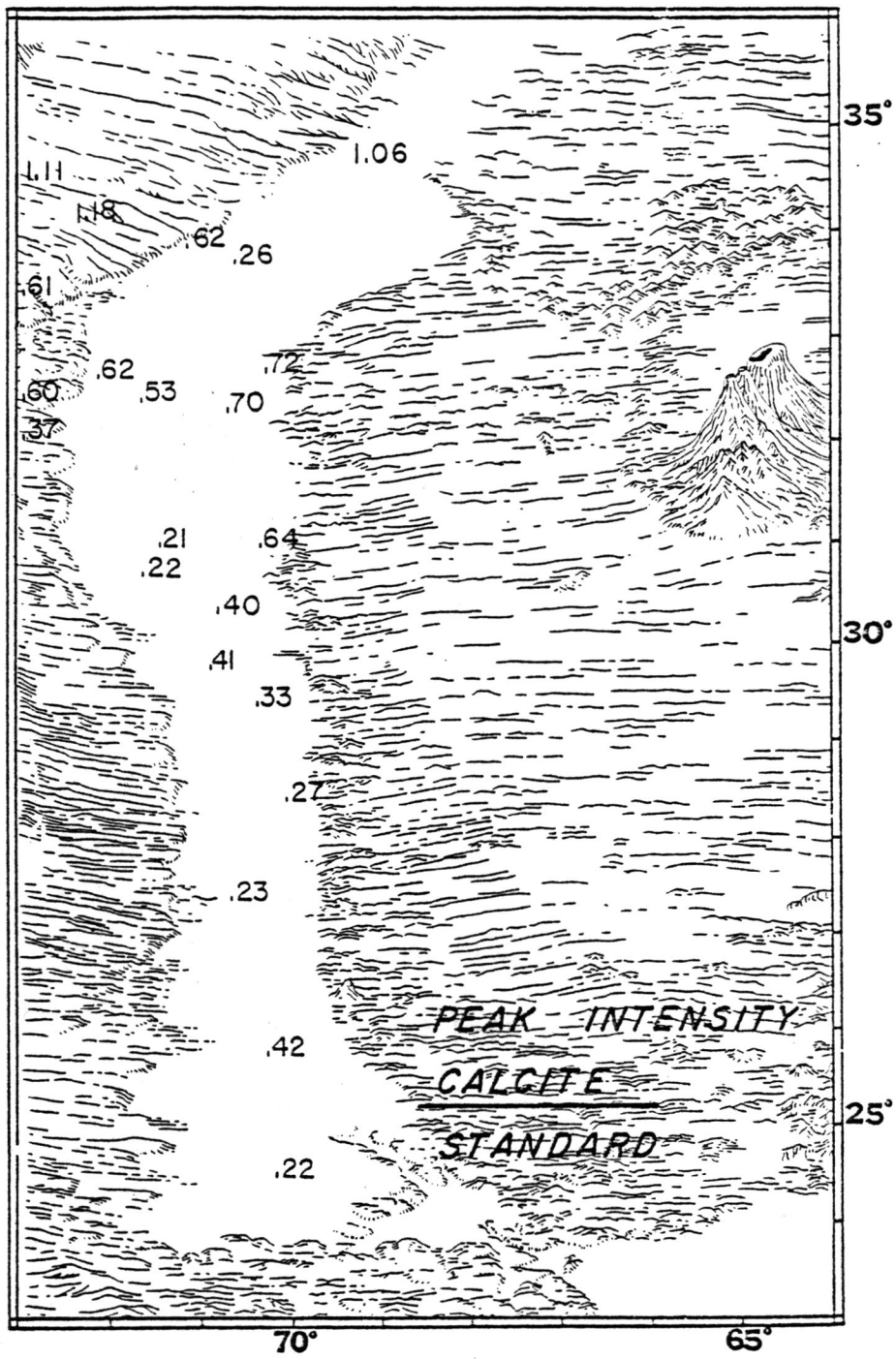

Appendix 5G. The peak intensity of calcite divided by the peak intensity of the silicon standard (obtained by the whole-sample X-ray analyses of surface samples from the continental rise and abyssal plain).

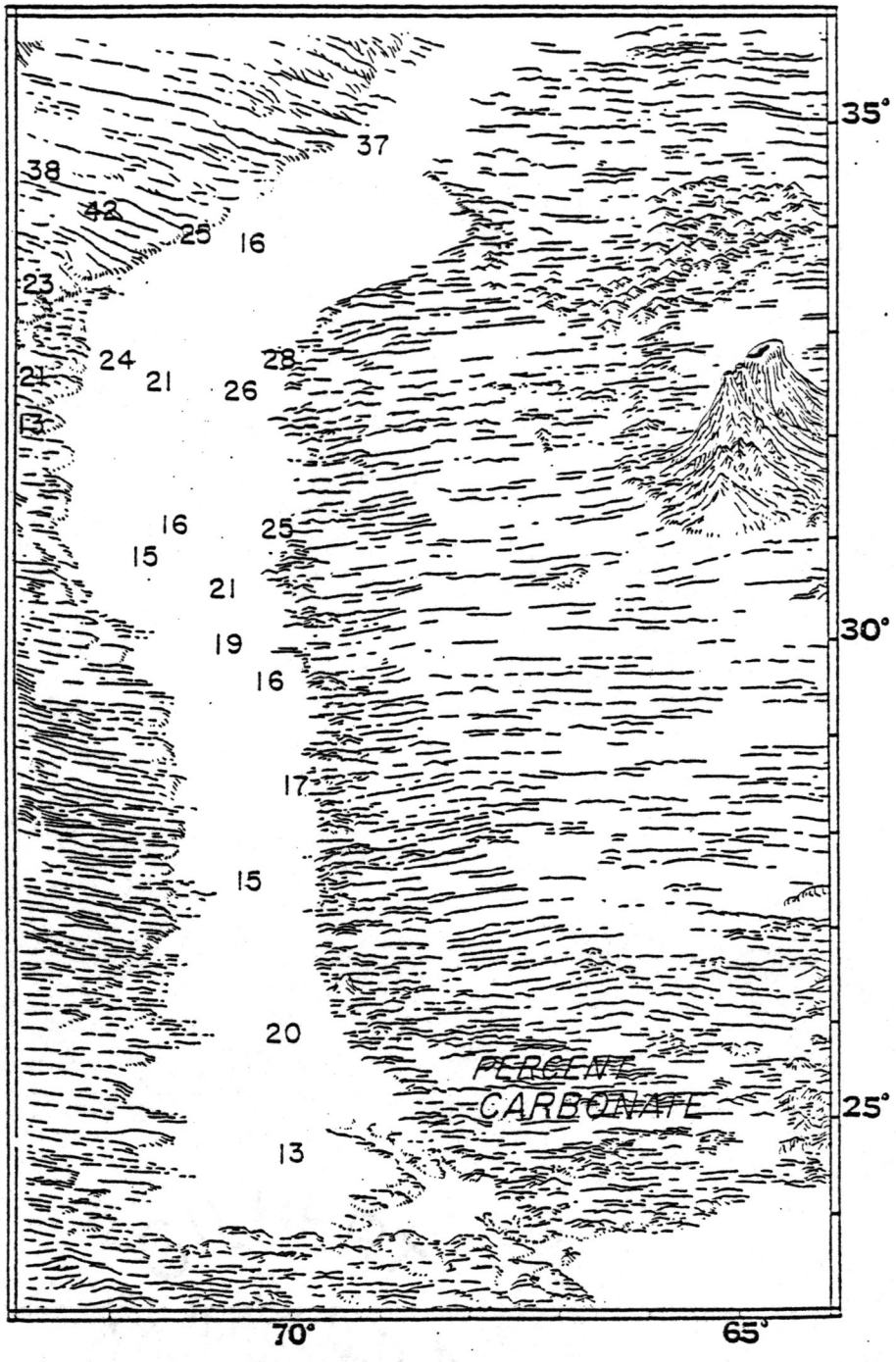

Appendix 5H. Weight percentage of carbonate in the surface samples from the continental rise and abyssal plain.

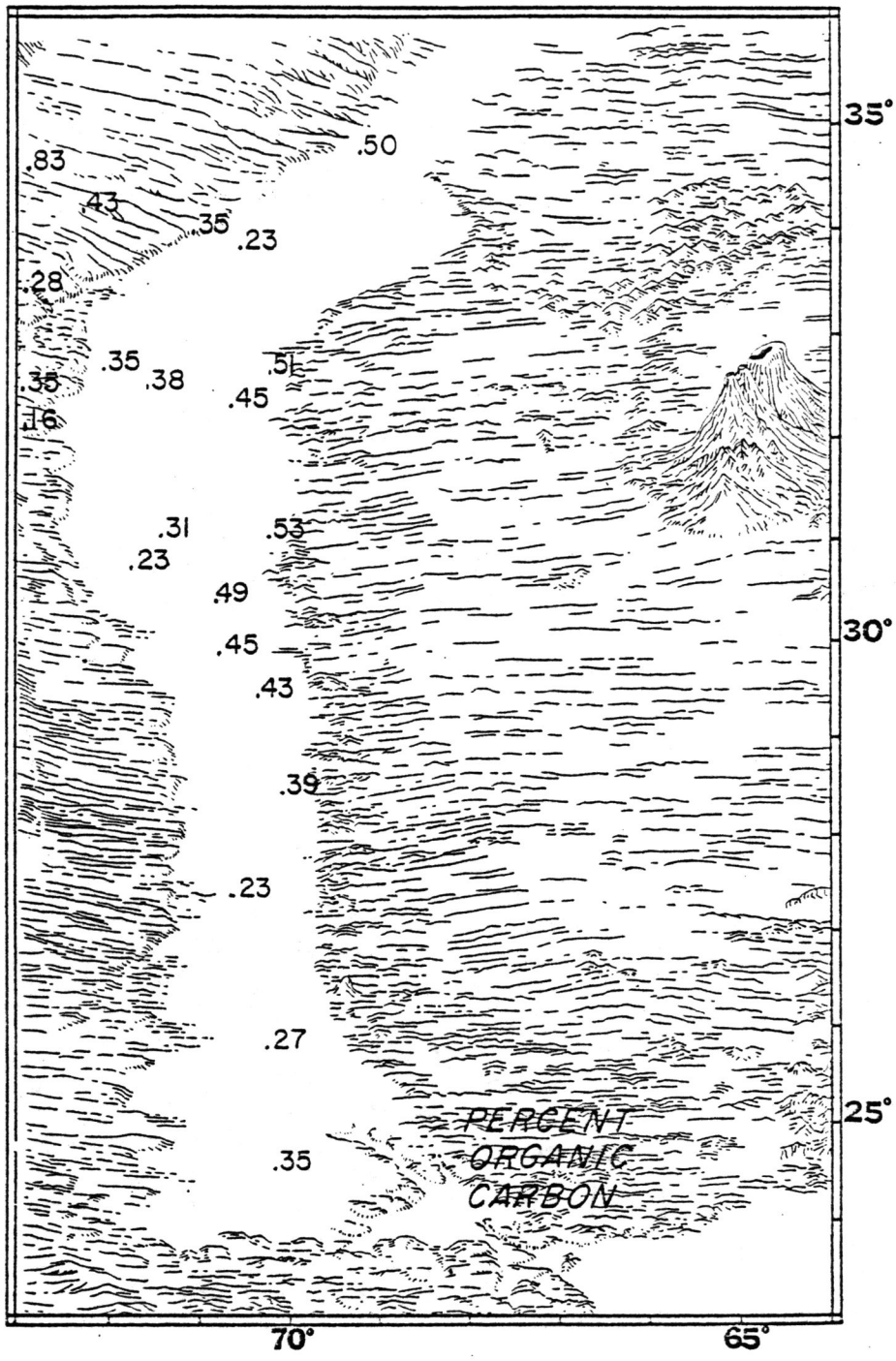

Appendix 5I. Weight percentage of organic carbon in the surface samples from the continental rise and abyssal plain.

APPENDIX 6

Mineral composition of the $< 2\mu$ fraction of subsurface samples.

Legend

- o Turbiditic deposit
- ■ Hemipelagic deposit
- T_{A-E} Turbidite (with indication of Bouma's Sequence)
- P Hemipelagic unit

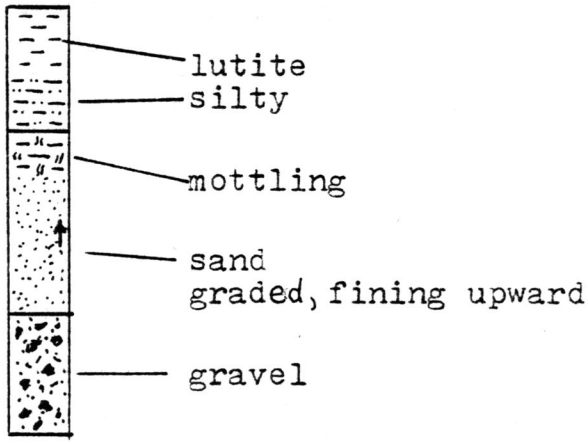

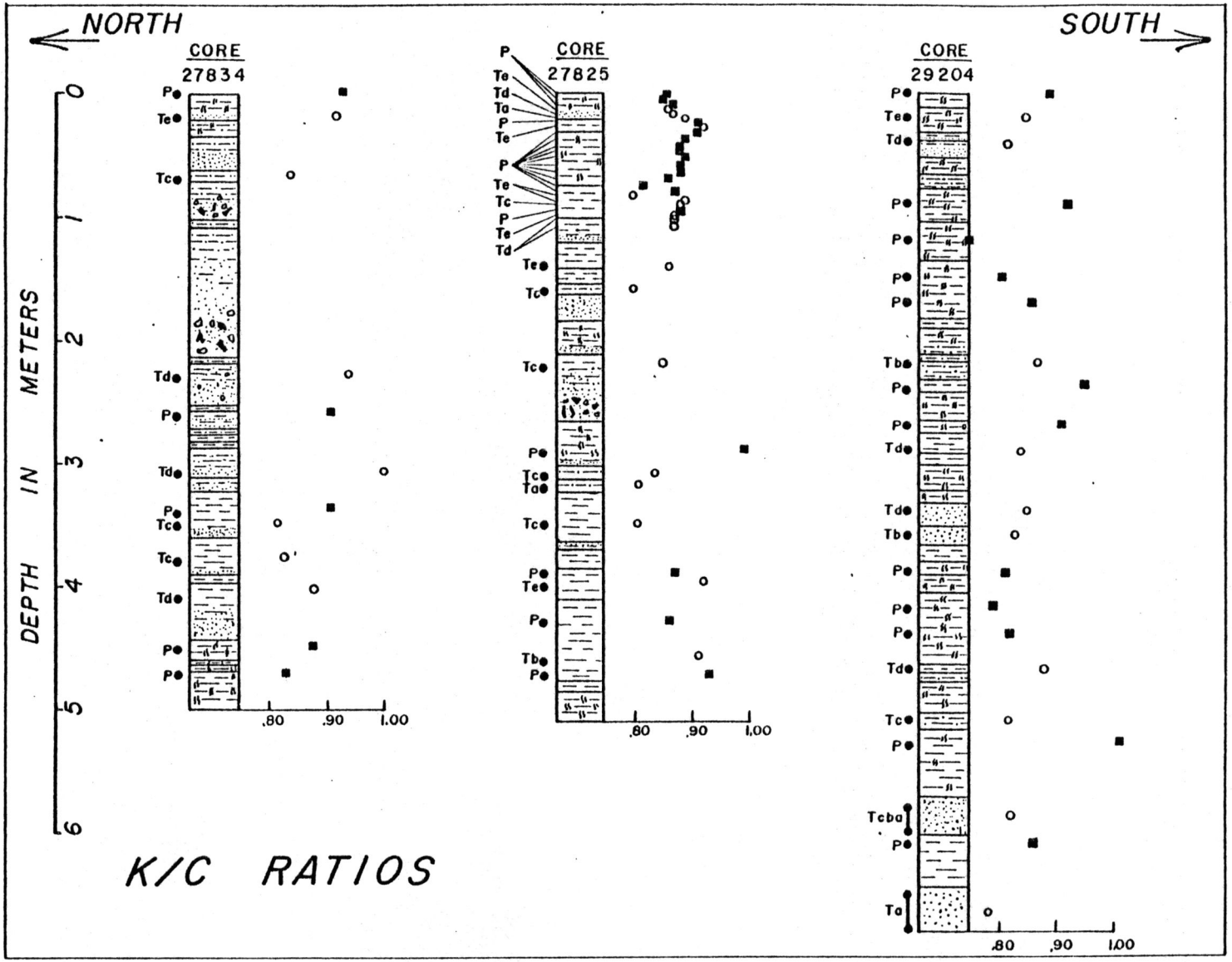

Appendix 6A. K/C ratios of the <2μ samples from the cores. For an explanation of the symbols see the first page of this appendix.

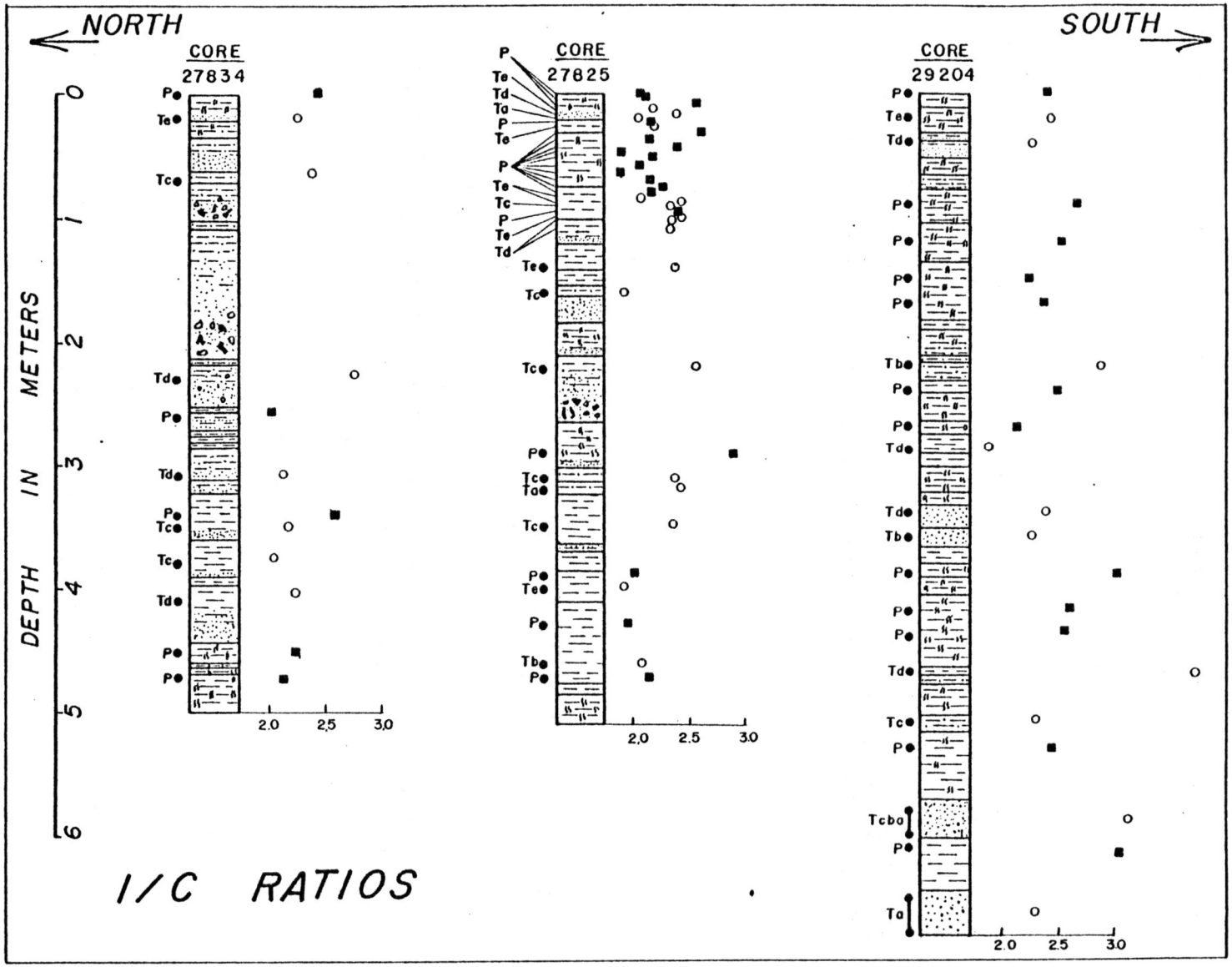

Appendix 6B. I/C ratios of the <2μ samples from the cores. For an explanation of the symbols see the first page of this appendix.

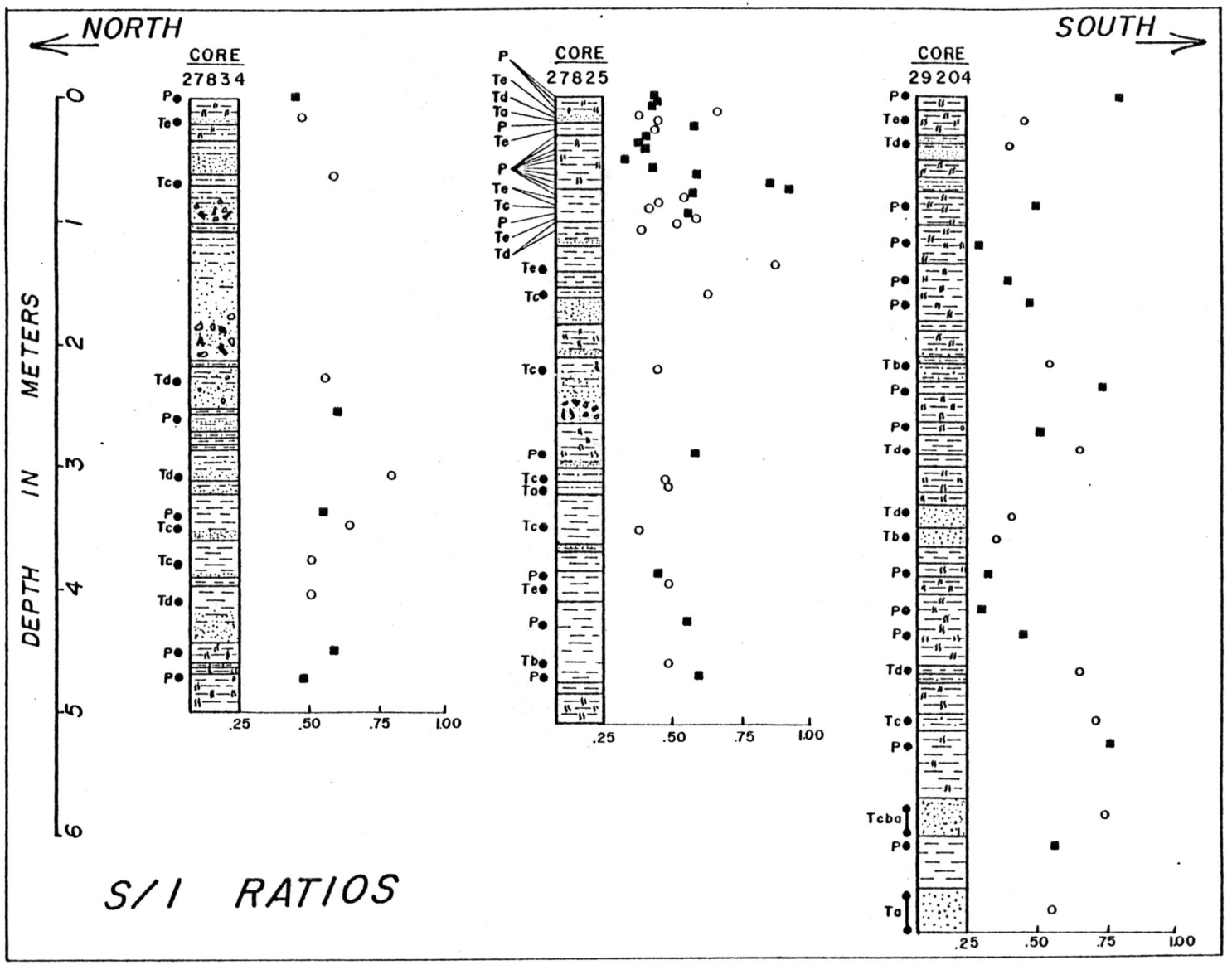

Appendix 6C. S/I ratios of the <2μ samples from the cores. For an explanation of the symbols see the first page of this appendix.

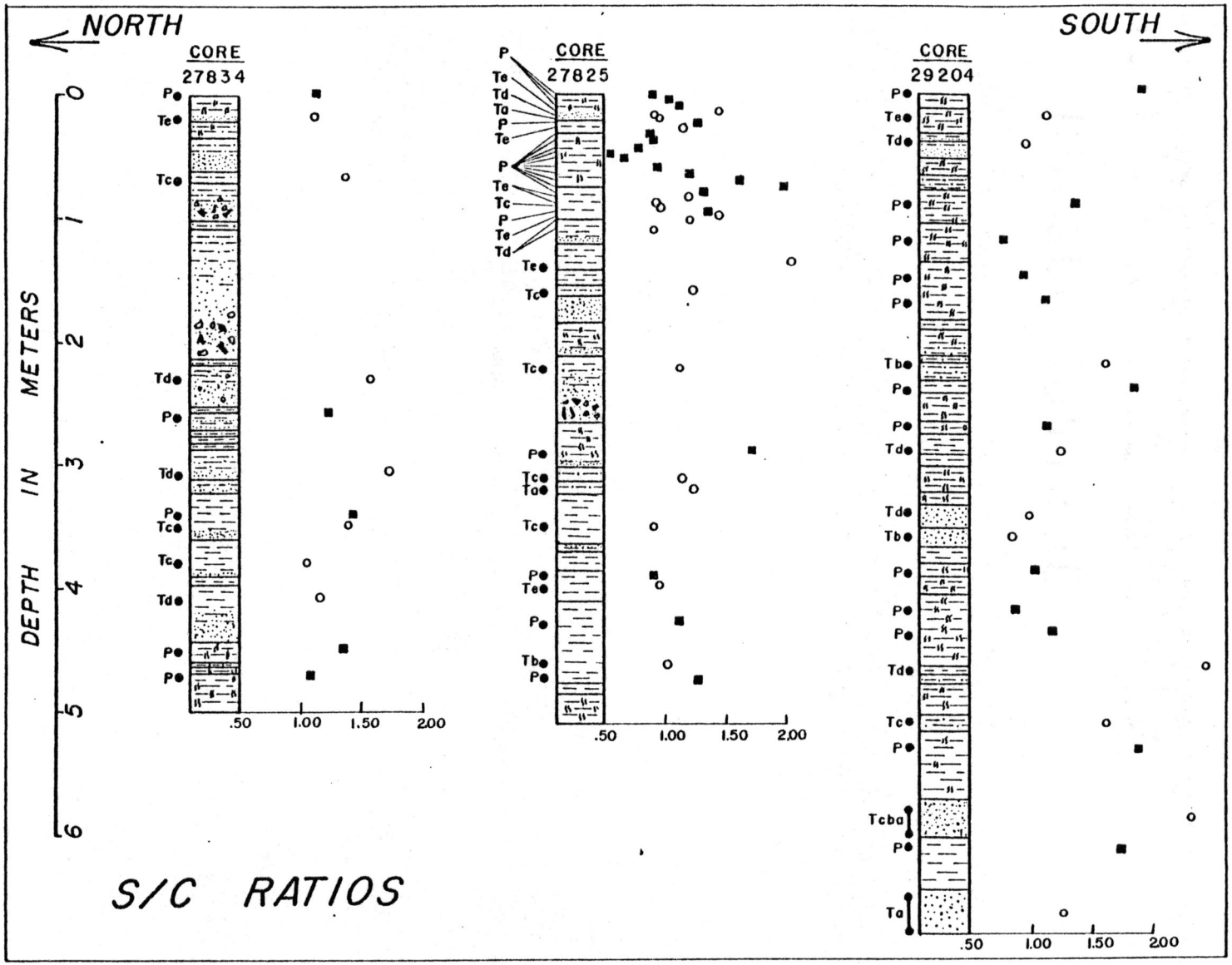

Appendix 6D. S/C ratios of the <2μ samples from the cores. For an explanation of the symbols see the first page of this appendix.

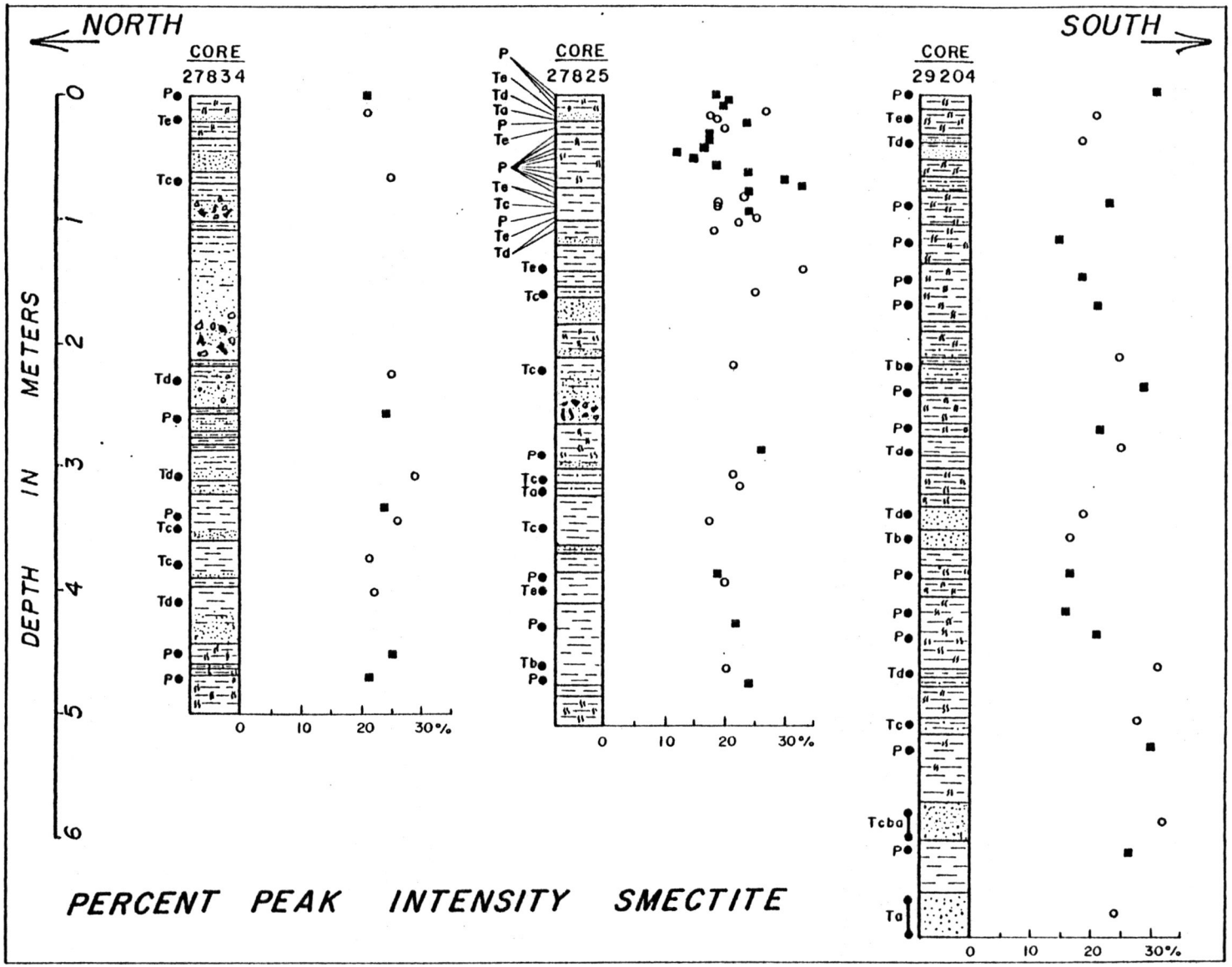

Appendix 6E. Percent peak intensity of smectite in the $<2\mu$ samples from the cores. For an explanation of the symbols see the first page of this appendix.

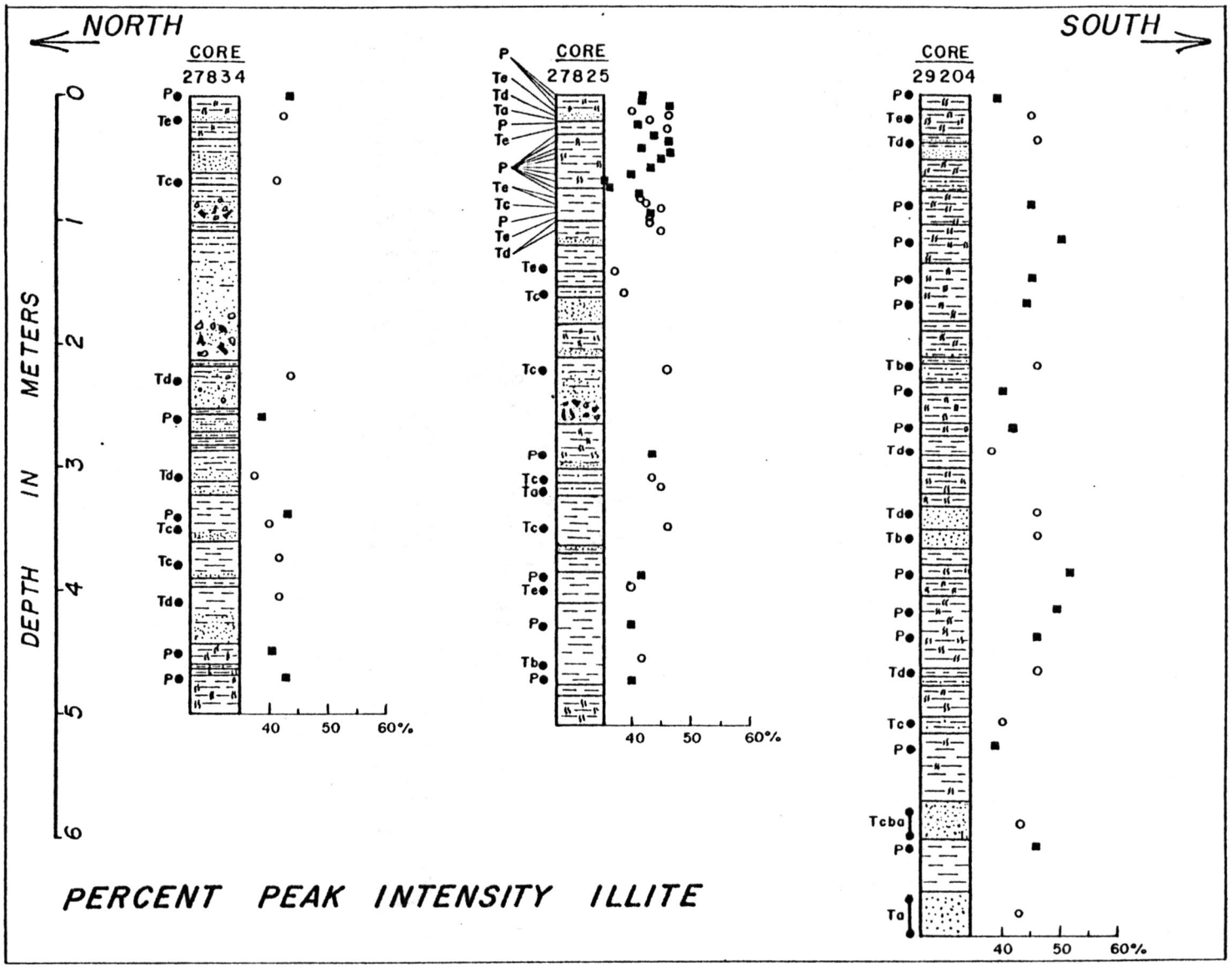

Appendix 6F. Percent peak intensity of illite in the < 2μ samples from the cores. For an explanation of the symbols see the first page of this appendix.

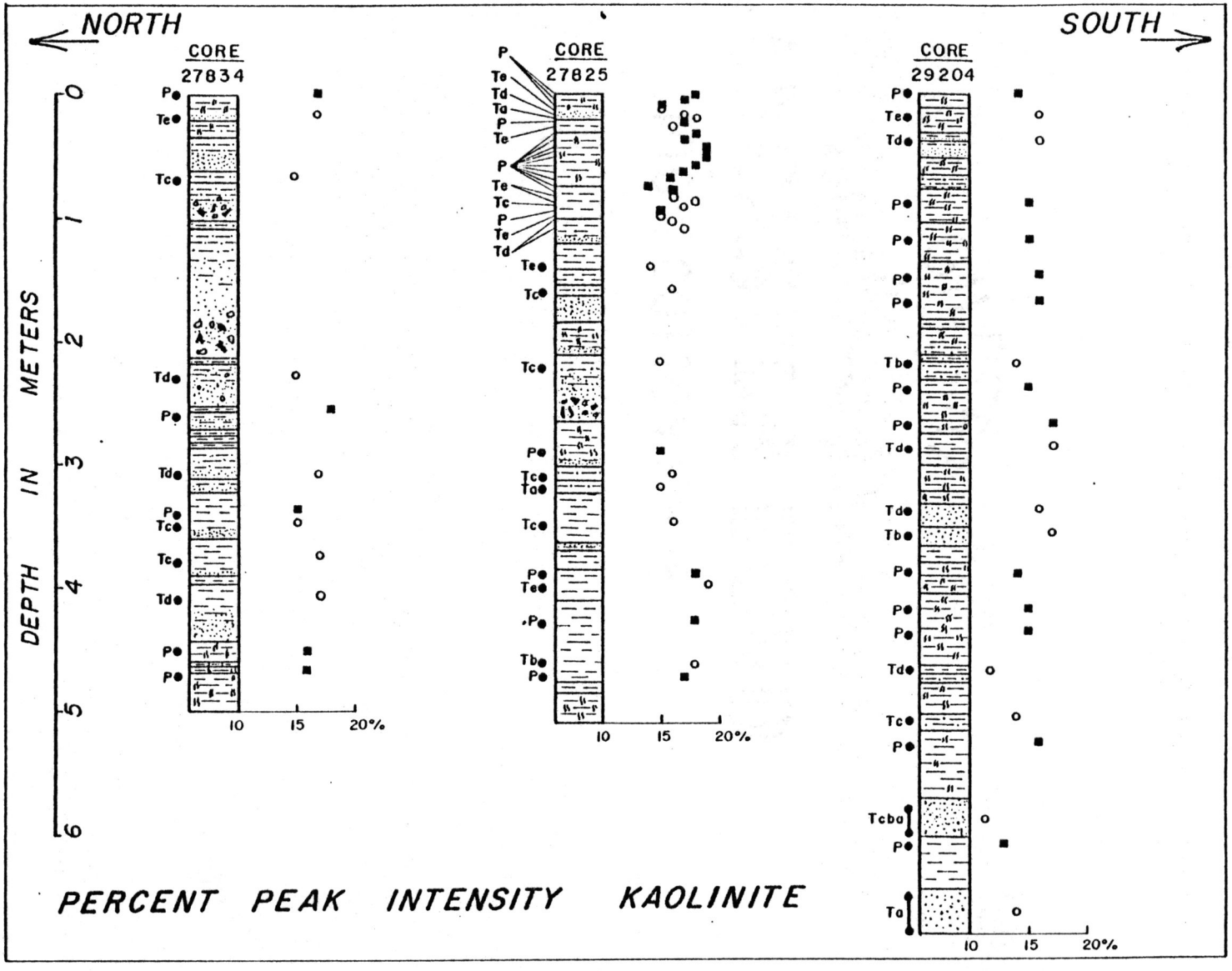

Appendix 6G. Percent peak intensity of kaolinite in the $< 2\mu$ samples from the cores. For an explanation of the symbols see the first page of this appendix.

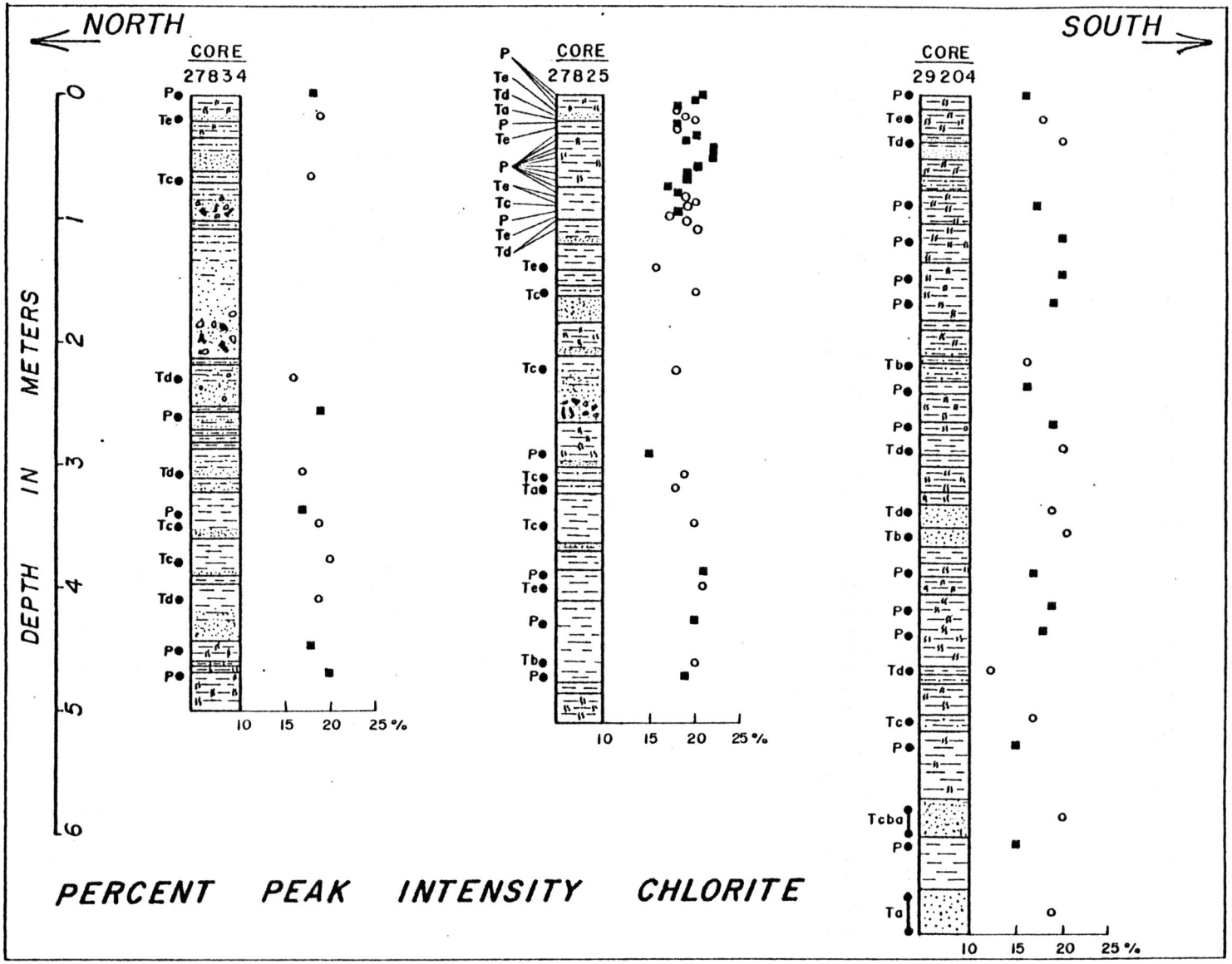

Appendix 6H. Percent peak intensity of chlorite in the <2μ samples from the cores. For an explanation of the symbols see the first page of this appendix.

APPENDIX 7

Composition of whole subsurface samples.

Legend

o	Turbiditic Sample
■	Hemipelagic Sample
T_{A-E}	Turbiditic deposit (with indication of Bouma's sequence)
P	Hemipelagic deposit

Sediment types

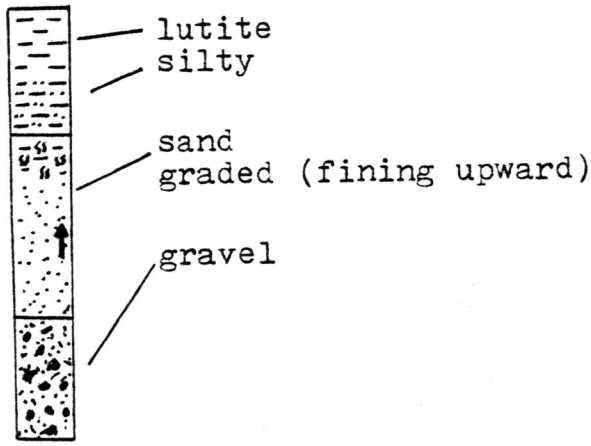

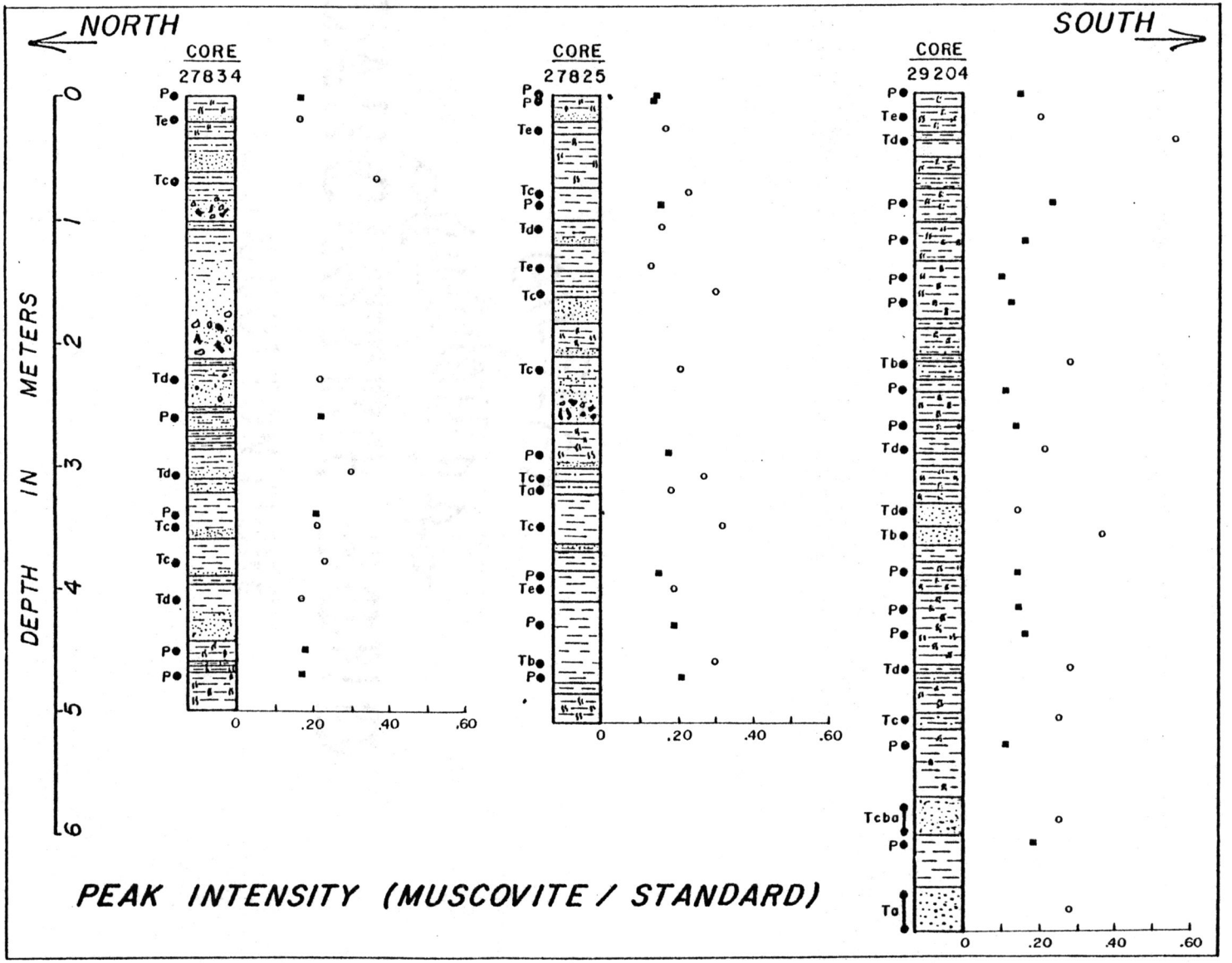

Appendix 7A. The peak intensity of muscovite divided by the peak intensity of the silicon standard (obtained by the whole-sample X-ray analyses of samples from the cores). For an explanation of the symbols see the first page of this appendix.

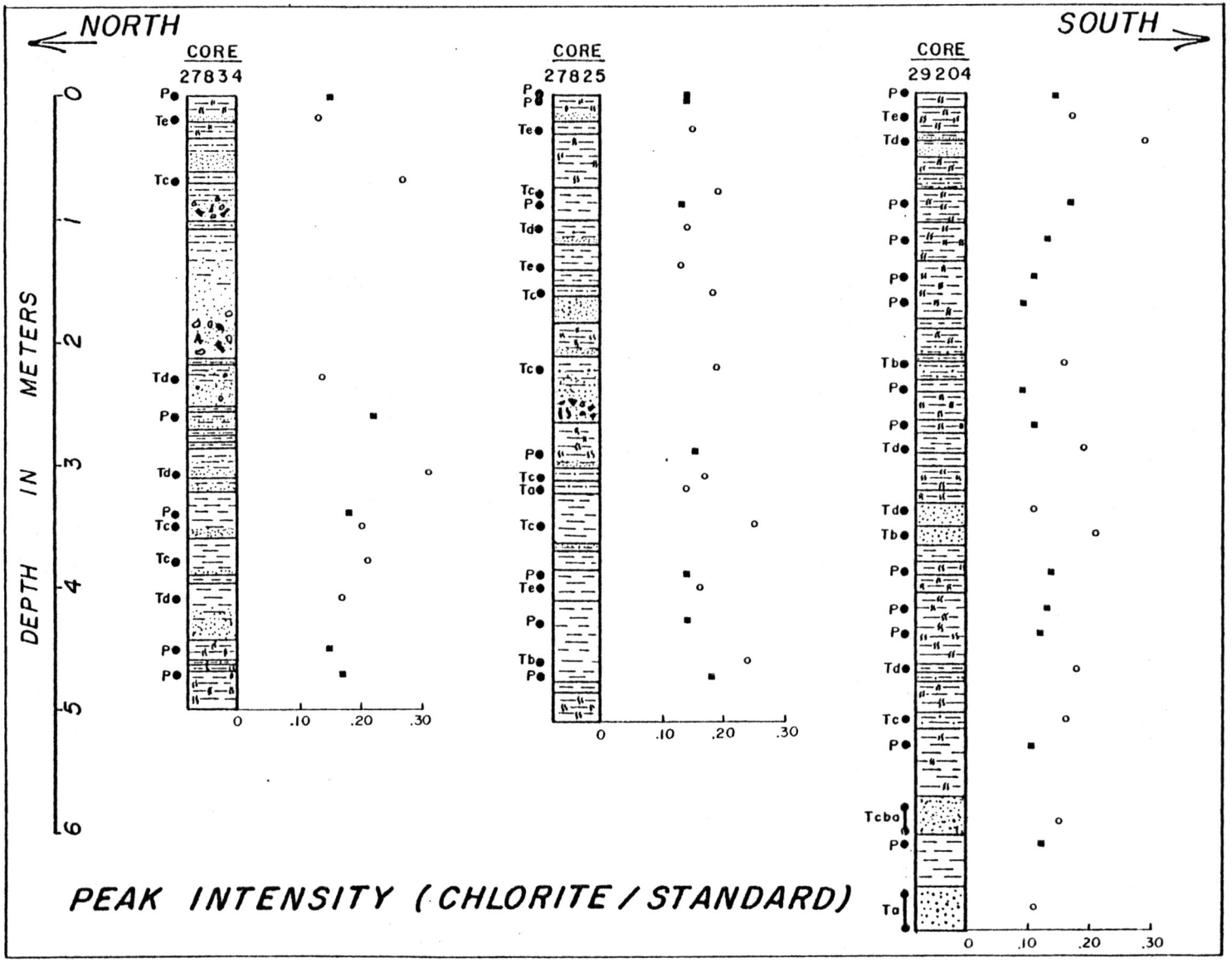

Appendix 7B. The peak intensity of chlorite divided by the peak intensity of the silicon standard (obtained by the whole-sample X-ray analyses of samples from the cores). For an explanation of the symbols see the first page of this appendix.

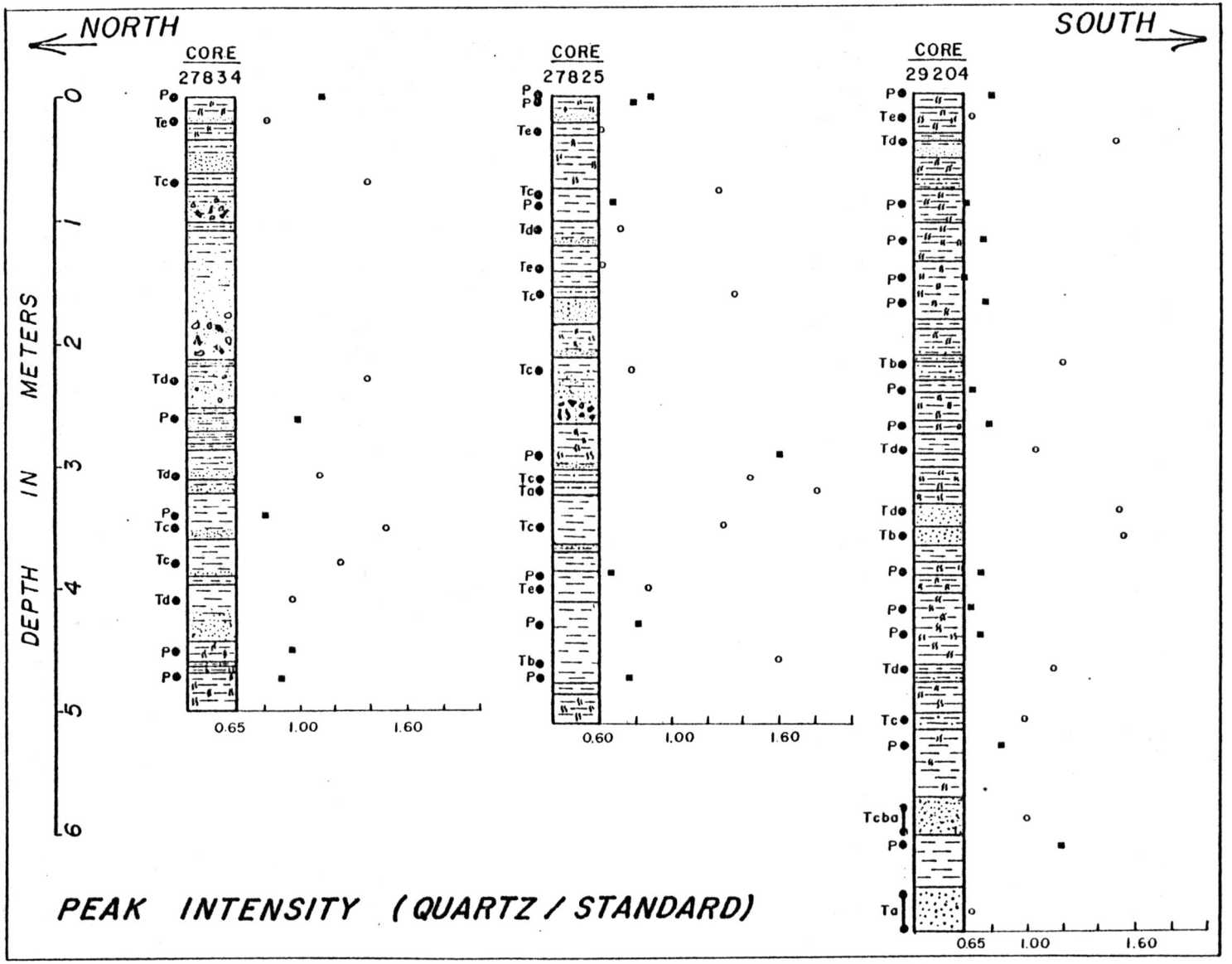

Appendix 7C. The peak intensity of quartz divided by the peak intensity of the silicon standard (obtained by the whole-sample X-ray analyses of samples from the cores). For an explanation of the symbols see the first page of this appendix.

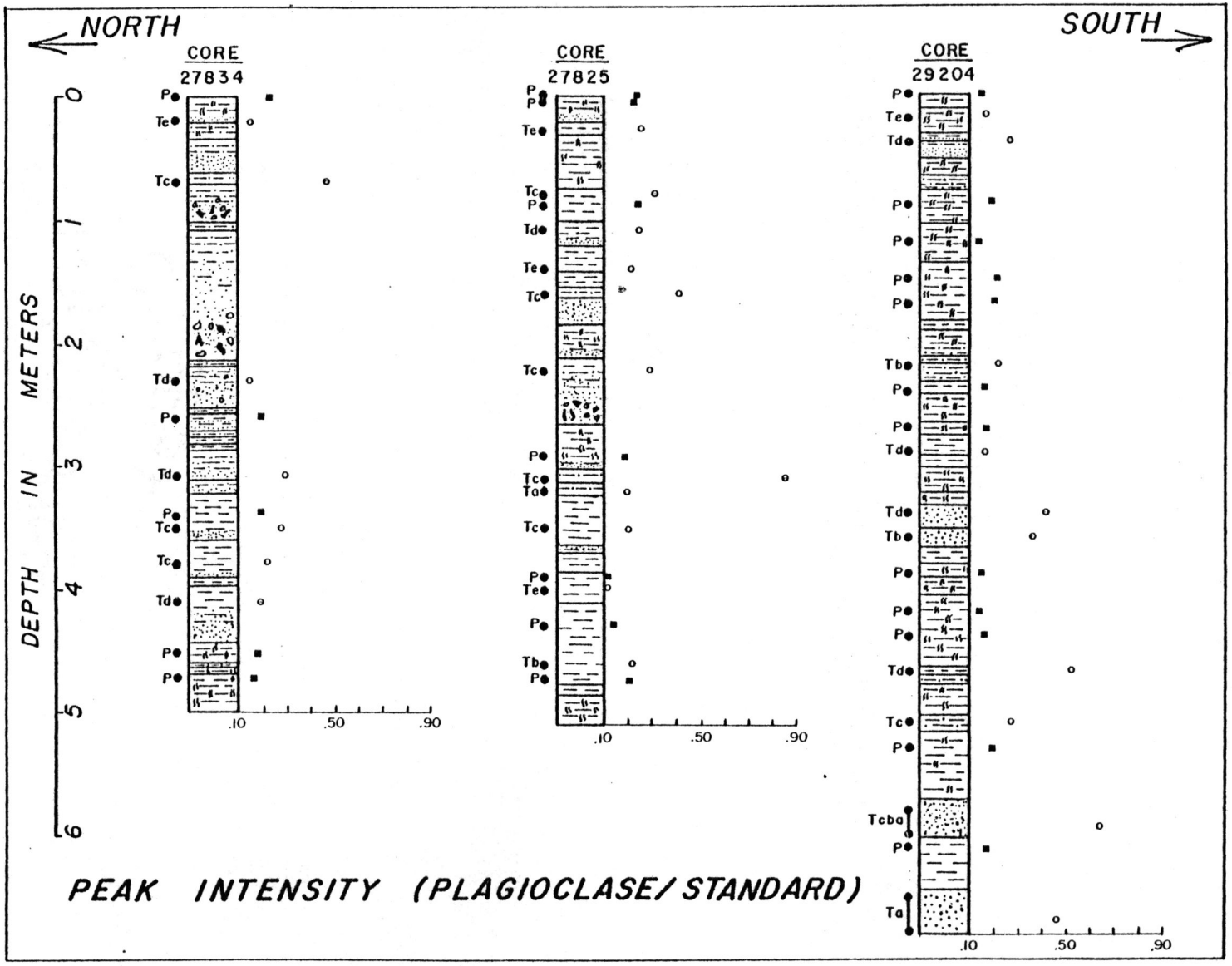

Appendix 7D. The peak intensity of plagioclase divided by the peak intensity of the silicon standard (obtained by the whole-sample X-ray analyses of samples from the cores). For an explanation of the symbols see the first page of this appendix.

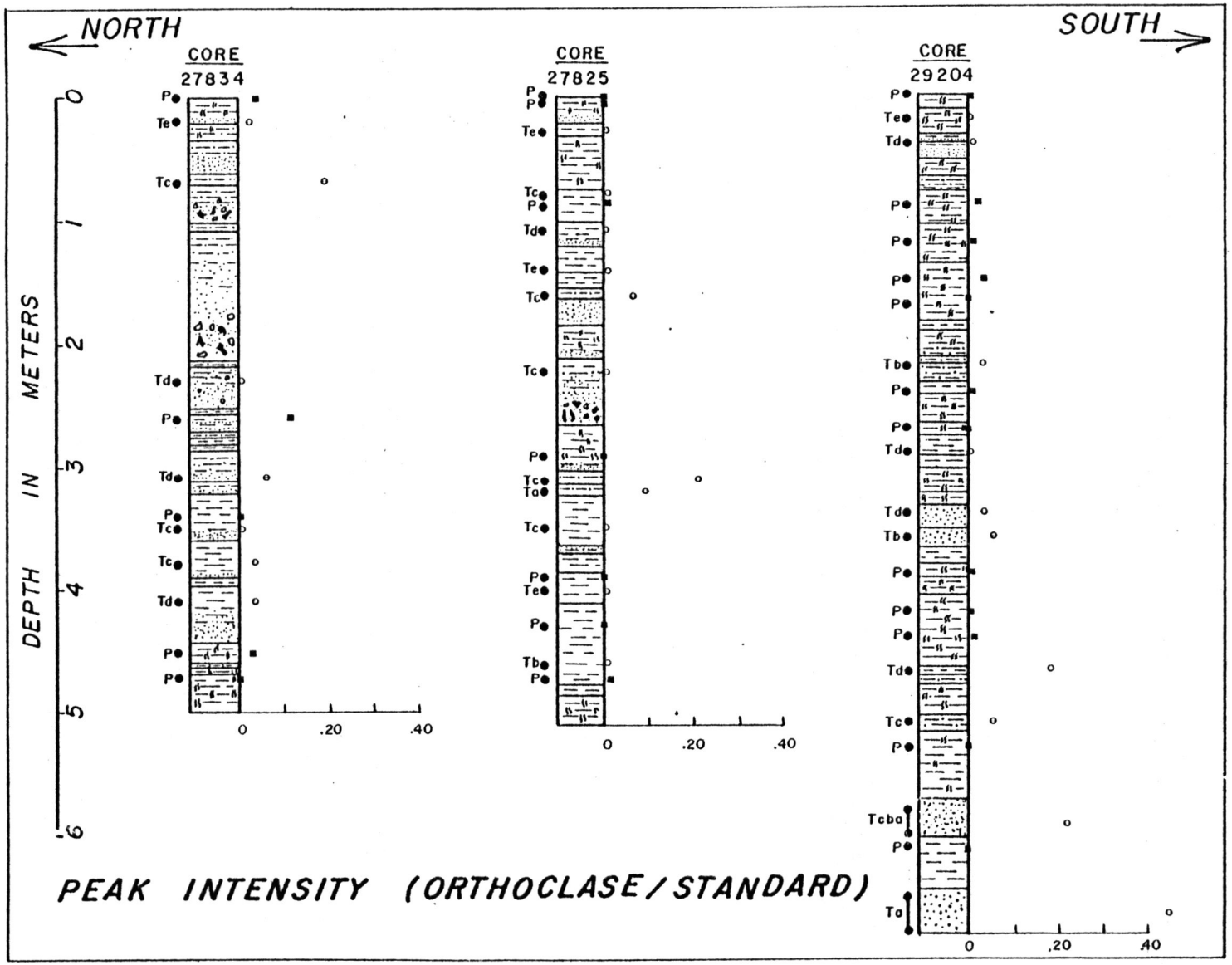

Appendix 7E. The peak intensity of orthoclase divided by the peak intensity of the silicon standard (obtained by the whole-sample X-ray analyses of samples from the cores). For an explanation of the symbols see the first page of this appendix.

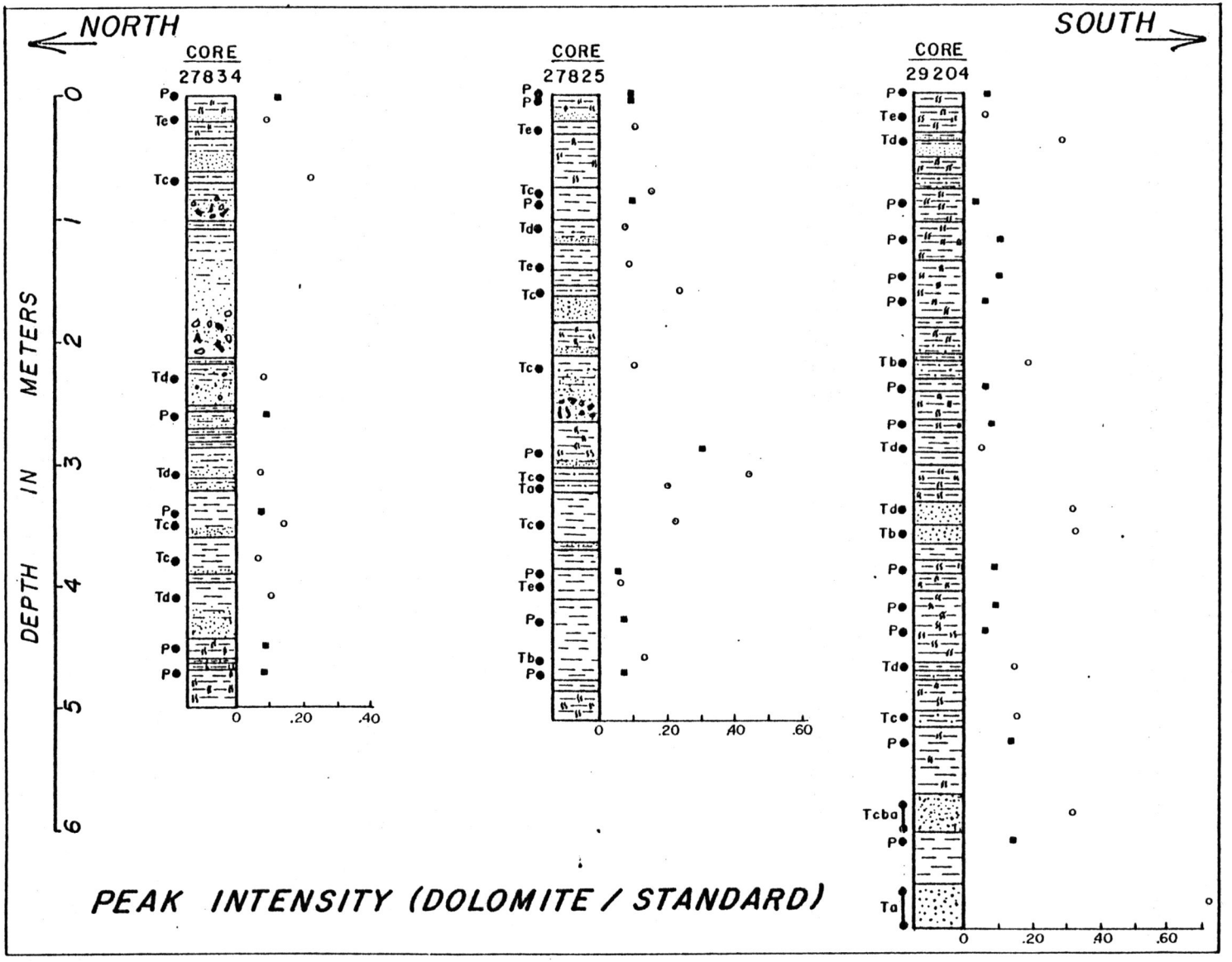

Appendix 7F. The peak intensity of dolomite divided by the peak intensity of the silicon standard (obtained by the whole-sample X-ray analyses of samples from the cores). For an explanation of the symbols see the first page of this appendix.

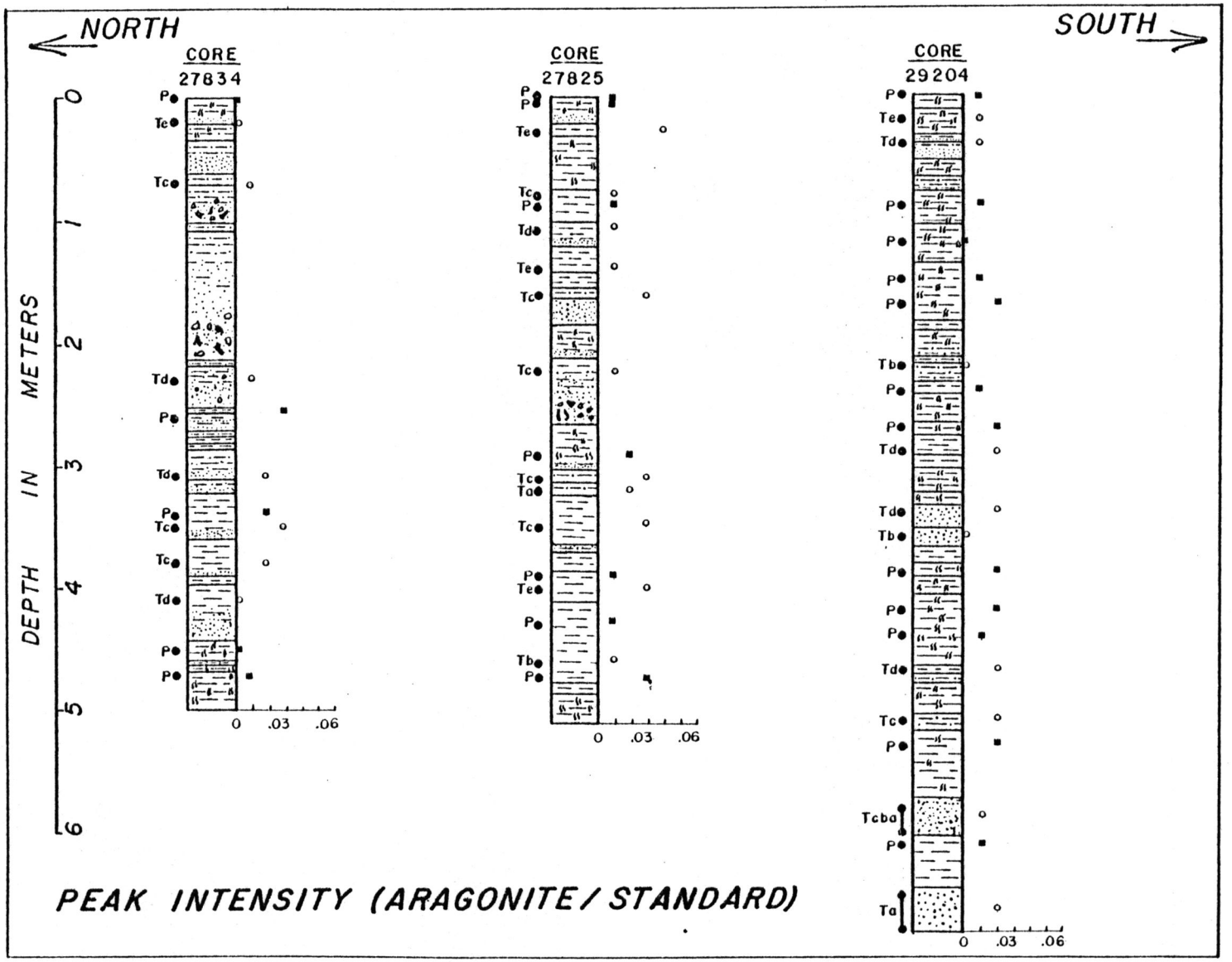

Appendix 7G. The peak intensity of aragonite divided by the peak intensity of the silicon standard (obtained by the whole-sample X-ray analyses of samples from the cores). For an explanation of the symbols see the first page of this appendix.

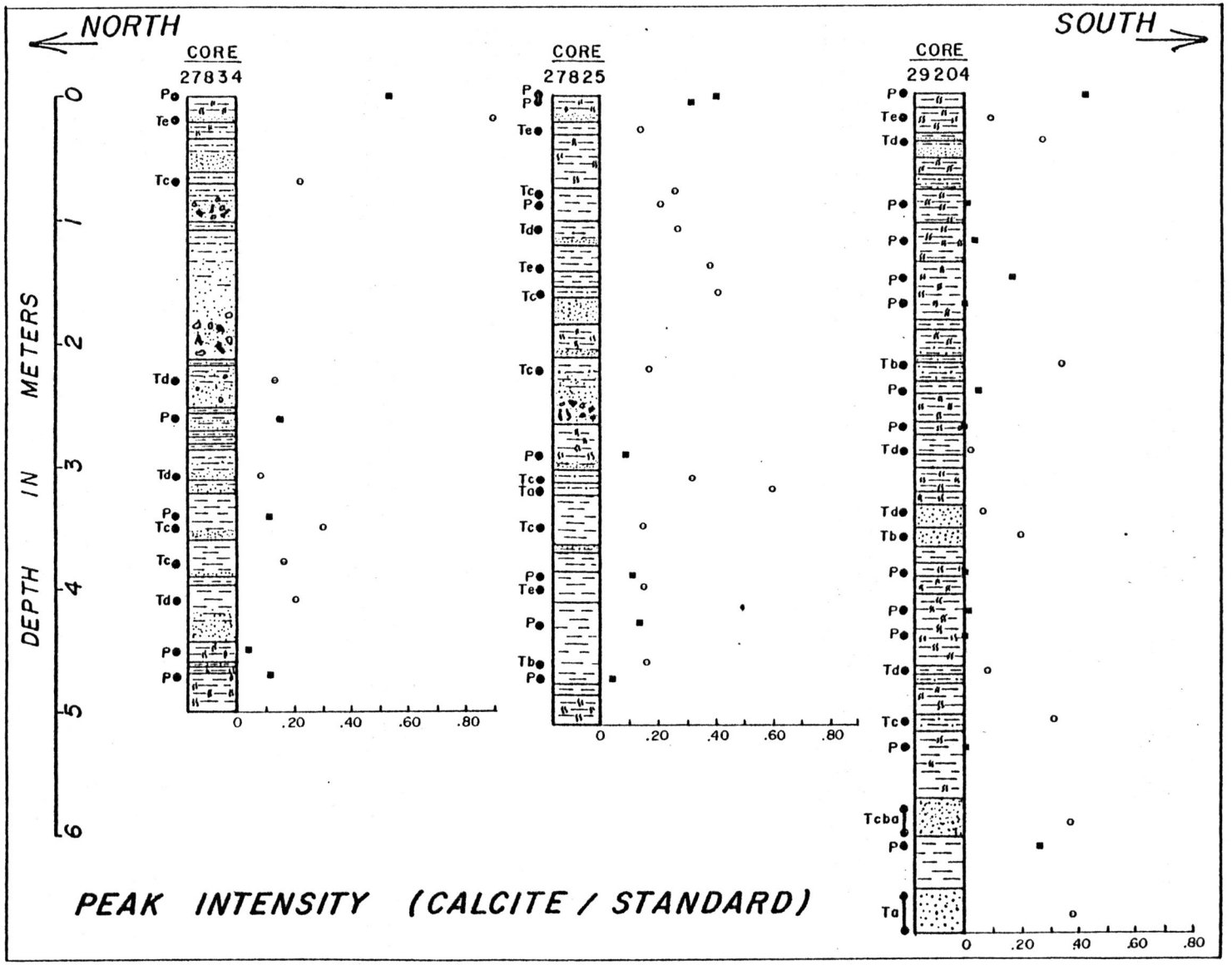

Appendix 7H. The peak intensity of calcite divided by the peak intensity of the silicon standard (obtained by the whole-sample X-ray analyses of samples from the cores). For an explanation of the symbols see the first page of this appendix.

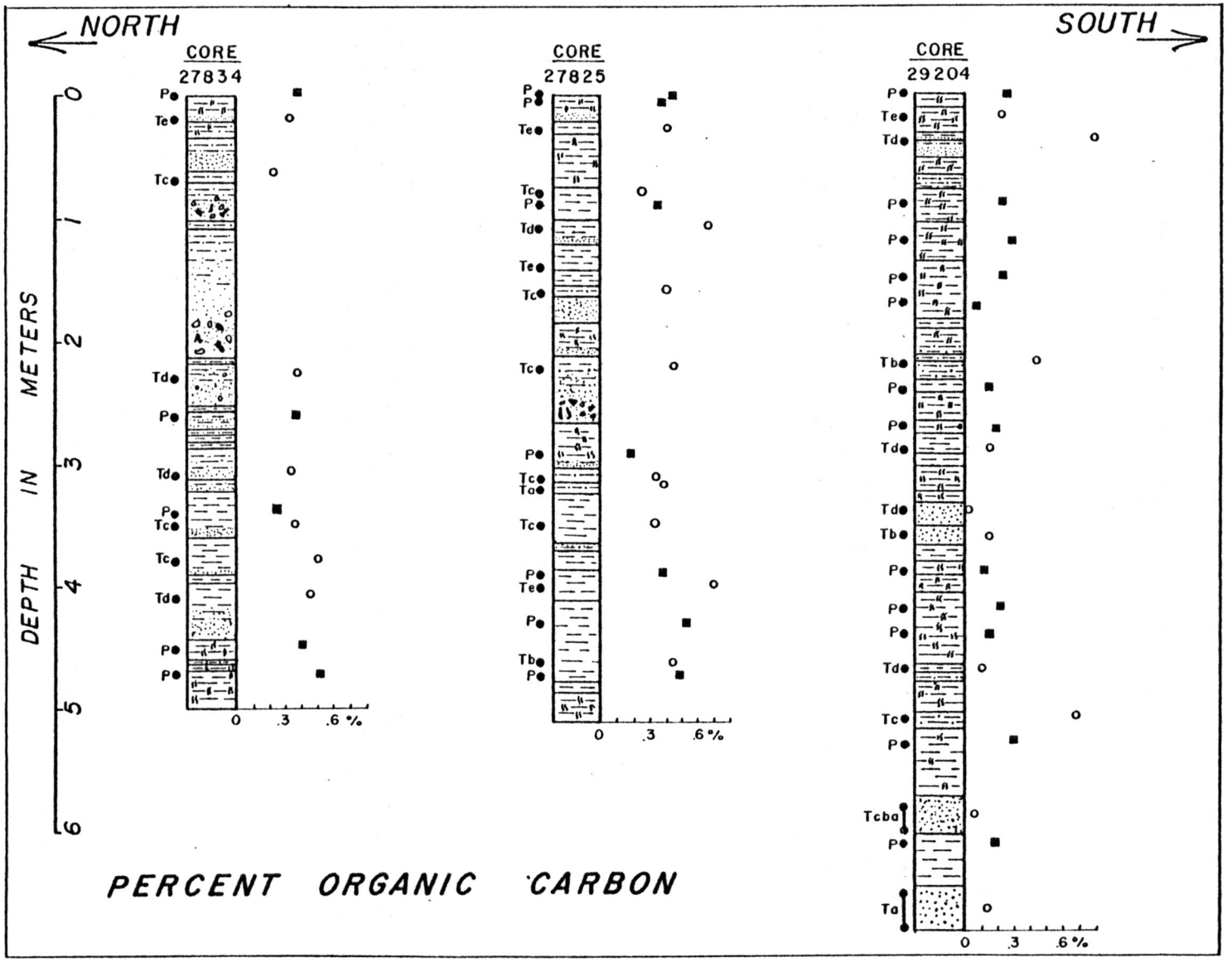

Appendix 7I. Weight percentage of organic carbon in samples from the cores. For an explanation of the symbols see the first page of this appendix.

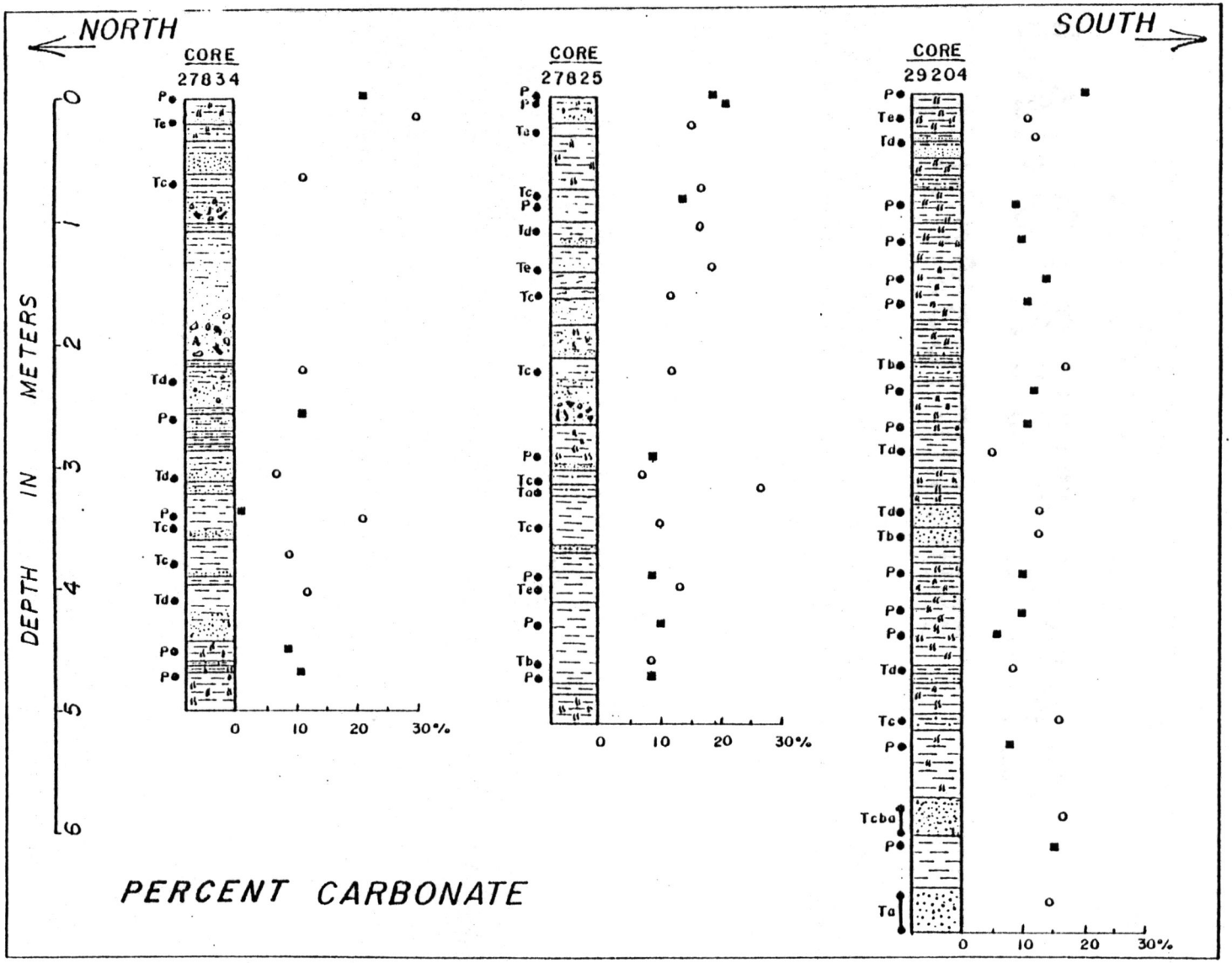

Appendix 7J. Weight percentage of carbonate in samples from the cores. For an explanation of the symbols see the first page of this appendix.

REFERENCES CITED

Allen, J.R.L., 1971, Mixing at turbidity current heads and its geological implications: Jour. Sed. Petrology, v. 41, p. 97-113.

Ayers, M.W., AND W.J. Cleary, Patterns of deposition at the terminus of the Wilmington Canyon System (in preparation).

Beall, A.O., AND A.G. Fischer, 1969, Sedimentology: in Initial Reports Deep Sea Drilling Project, v. 1, p. 521-594.

Biscaye, P.E., 1964, Distinction between kaolinite and chlorite in recent sediments by X-ray diffraction: Am. Mineralogist, v. 49, p. 1281-1289.

_____, 1965, Mineralogy and sedimentation of recent deep-sea clay in the Atlantic Ocean and adjacent seas and oceans: Geol. Soc. America Bull., v. 76, p. 803-832.

_____, 1974, Suspended sediments above the continental margin of the Western North Atlantic: in Gibbs, R.J. (ed.), Suspended Solids in Water, Plenum Press, New York, p. 131-150.

Bouma, A.H., AND C.D. Hollister, 1973, Deep ocean basin sedimentation: in Turbidites and Deep-Water Sedimentation, Soc. Econ. Paleontologists and Mineralogists Pacific Sec., p. 79-118.

Carroll, D., 1970, Clay minerals: a guide to their x-ray identification: Geol. Soc. America Special Paper 126, 80 p.

Cleary, W.J., AND J.R. Conolly, 1974a, The Hatteras Deep Sea Fan: Jour. Sed. Petrology, v. 44, p. 1140-1154.

_____, AND _____, 1974b, Petrology and origin of deep sea sands: Hatteras Abyssal Plain: Marine Geology, v. 17, p. 263-279.

_____, O.H. Pilkey, AND M.W. Ayers, 1977, Morphology and sediments of three ocean basin entry points, Hatteras Abyssal Plain: Jour. Sed. Petrology, v. 47, p. 1157-1170.

Daly, R.A., 1936, Origin of submarine canyons: Amer. Jour. Sci., 5th ser., v. 31, p. 410-420.

Damuth, J.E., 1977, Late Quaternary sedimentation in the Western Equatorial Atlantic: Geol. Soc. America Bull., v. 88, p. 695-710.

_____, AND N. Kumar, 1975, Late Quaternary depositional processes on continental rise of Western Equatorial Atlantic: comparison with Western North Atlantic and implications for reservior-rock distribution: Am. Assoc. Petroleum Geologists Bull., v. 59, p. 2172-2181.

Eittreim, S., M. Ewing, AND E.M. Thorndike, 1969, Suspended matter along the continental margin of the North American Basin: Deep-Sea Research, v. 16, p. 613-624.

Elmore, R.D., 1976, The "Black Shell" Turbidite, Hatteras Abyssal Plain: Duke University, unpubl. M.S. thesis, 107 p.

Emery, K.O., AND E. Uchupi, 1972, Western North Atlantic Ocean: Amer. Assoc. Petroleum Geologists Memior no. 17, 532 p.

Ericson, D.B., M. Ewing, G. Wollin, AND B.C. Heezen, 1961, Atlantic deep-sea sediment cores: Geol. Soc. America Bull., v.72, p. 193-286.

Fritz, S.J., AND O.H. Pilkey, 1975, Distinguishing bottom and turbidity current coarse layers on the continental rise: Jour. Sed. Petrology, v. 45, p. 57-62.

Gibbs, R.J., 1965, Error due to segregation in quantitative clay mineral X-ray diffraction mounting techniques: Am. Mineralogist, v. 50, p. 741-751.

Hathaway, J.C., 1972, Regional clay mineral facies in estuaries and continental margin of the United States East coast: in Nelson, B.W. (ed.), Environmental Framework of Coastal Plain Estuaries, Geol. Soc. America Memoir 133, p. 293-316.

Heezen, B.C., C.D. Hollister, AND W.F. Ruddiman, 1966, Shaping of the continental rise by deep geostrophic contour currents. Science, v. 152, p. 502-508.

_____, AND M. Tharp, 1968, Physiographic diagram, North Atlantic Ocean (revised): Geol. Soc. America, scale 1:1,450,000 1 sheet.

Hollister, C.D., 1967, Sediment distribution and deep circulation in the Western North Atlantic: Columbia University, unpubl. Ph.D. thesis, 464 p.

Horn, D.R., M. Ewing, B.M. Horn, AND M.N. Delach, 1971, Turbidites of the Hatteras and Sohm Abyssal Plains, Western North Atlantic: Marine Geology, v. 11, p. 287-323.

Klasik, J.A., AND O.H. Pilkey, 1975, Processes of sedimentation on the Atlantic continental rise off the southeastern U.S.: Marine Geology, v. 19, p. 69-89.

Middleton, G.V., 1966, Experiments on density and turbidity currents. 1. Motion of the head: Canadian Jour. Earth Sci., v. 3, p. 523-546.

_____, AND M.A. Hampton, 1973, Sediment gravity flows: Mechanics of flow and deposition: in Turbidites and Deep Water Sedimentation, Soc. Econ. Paleontologists and Mineralogists Pacific Sec., p. 79-118.

Neileisel, J., AND C.E. Weaver, 1967, Transport and deposition of clay minerals Southeastern United States: Jour. Sed. Petrology, v. 37, p. 1084-1116.

Pevear, D., 1968, Clay mineral relationships in recent river, nearshore marine, continental shelf, and slope sediments of the Southeastern United States: University of Montana, unpubl. Ph.D. thesis, 163 p.

_____, 1972, Source of recent nearshore marine clays, Southeastern United States: in Nelson, B.W. (ed.), Environmental Framework of Coastal Plain Estuaries, Geol. Soc. America Memoir 133, p. 317-335.

Pierce, J.W., 1971, Clay mineralogy of cores from the continental margin of North Carolina: Southeastern Geology, v. 12, p. 33-51.

Pratt, R.M., 1965, Ocean bottom topography: the divide between the Sohm and Hatteras Abyssal Plains: Science, v. 148, p. 1598-1599.

Rex, R.W., 1969, X-ray mineralogy studies - leg 1. in Initial Reports Deep Sea Drilling Project, v. 1, p. 354-367.

Rona, P.A., 1969, Linear lower continental rise hills off Cape Hatteras: Jour. Sed. Petrology, v. 39, p. 1132-1141.

Rupke, N.A., AND D.J. Stanley, 1974, Distinctive properties of turbiditic and hemipelagic mud layers in the Algero-Baleric Basin, Western Mediterranean Sea: Smithsonian Contributions to Earth Sciences, no. 13, 40 p.

Terlecky, P.M., 1966, The clay minerals of a traverse on the North Carolina continental margin and Bermuda Rise: Southeastern Geology, v. 7, p. 141-150.

Tien, Pei-Lin, 1974, A simple device for smearing clay-on-glass slides for quantitative X-ray diffraction studies: Clays Clay Minerals, v. 22, p. 367-368.

Zemmels, I., H.E. Cooke, AND J.C. Hathaway, 1972, X-ray mineralogy studies - leg X1: in Initial Reports Deep Sea Drilling Project, v. 11, p. 729-790.

Zimmerman, H.B., 1972, Sediments of the New England continental rise: Geol. Soc. America Bull., v. 83, p. 3709-3724.